EPFL

Thèse n° 10 574

Influence of model uncertainty and long term deformations in action effects calculation in reinforced concrete structures

Présentée le 19 avril 2024

Faculté de l'environnement naturel, architectural et construit
Laboratoire de construction en béton
Programme doctoral en génie civil et environnement

pour l'obtention du grade de Docteur ès Sciences

par

Xhemsi MALJA

Acceptée sur proposition du jury

Prof. D. Lignos, président du jury
Prof. A. Muttoni, directeur de thèse
Prof. A. Laaksonen, rapporteur
Prof. P. Castaldo, rapporteur
Prof. D. M. V. Ruggiero, rapporteur

École polytechnique fédérale de Lausanne

2024

"It is clear that our beliefs arise from certain dispositions and experiences which, so far as we know, don't guarantee their truth and are compatible with radical error. The trouble is that we can't fully take on the skepticism that this entails, because we can't cure our appetite for belief, and we can't take on this attitude toward our own beliefs while we're having them. Beliefs are about how things probably are, not just about how they might possibly be, and there is no way of bracketing our ordinary beliefs about the world so that they dovetail neatly with the possibility of skepticism."

The view from nowhere, Thomas Nagel

Foreword

Xhemsi Malja's doctoral thesis deals with several topics relating to the reliability of reinforced concrete structures and the redistribution of internal forces. The first theme concerns the uncertainties associated with the calculation of internal forces in a statically indeterminate reinforced concrete structure. Internal forces are very often calculated assuming linear elastic behaviour, where the concrete is considered to be uncracked and the contribution of the reinforcing steel is neglected. In the verification, these internal forces are compared with the resistance of the cross-sections, often assuming that the concrete is cracked and that the reinforcing steel behaves according to an elastic-plastic law. It is often overlooked that these two assumptions are clearly inconsistent, but studies to investigate the influence of this problem on the reliability of structures are rare. In this context, Xhemsi Malja addresses the issue from the point of view of model uncertainties, an aspect often neglected in reliability analyses and the calibration of partial factors (which should be accounted for in the partial factors for actions).

The second topic concerns the behaviour of concrete close to failure, where non-linear creep in case of sustained loading leads to a reduction in strength. This well-known detrimental effect is accounted for in the standards, which define a concrete strength reduction in case of significant sustained loads. What is overlooked, however, is the fact that non-linear creep has also a beneficial effect since it leads to a significant increase in deformation capacity, with an increased possibility of internal force redistribution at the ultimate limit state. The results of this work are interesting and have been implemented in the 2nd generation of the European standards for concrete structures EN 1992-1-1:2023 and in the latest draft of the international standard for concrete structures fib MC2020 published some months ago. This topic, apparently disconnected from the others, is in fact linked to them, as the deformation capacity plays an important role in the safety of statically indeterminate structures.

The third topic refers to the partial factors to be applied to the self-weight of the structure and other non-load-bearing elements. It has often been suspected that this factor, assumed to be equal to 1.35 for both cases, is overestimated for the self-weight of the structure, while it may be underestimated for the weight of the non-load-bearing elements. The rigorous reliability analysis carried out by Xhemsi Malja confirms these suspicions and proposes more consistent values for the case of bridges.

As described above, the results of the second topic have been implemented in new codes for practice. The results of the other topics can have also a significant influence in the design of new structures and the assessment of existing structures. For these reasons, the outcome of this research, which has been supported by the Swiss Federal Road Administration, has a significant practical relevance.

Lausanne, February 2024, Prof. Aurelio Muttoni

Acknowledgments

The past four and a half years at IBETON have been an invaluable experience both from the professional and human point of view.

First of all, my sincere gratitude goes to Prof. Aurelio Muttoni who gave me the opportunity to pursue my doctoral studies. His passion, energy and expertise have been essential to push the boundaries of research a little further with this thesis. In addition, I would like to thank Prof. Alain Nussbaumer and Prof. Miguel Fernández Ruiz for the collaborations on part of this work and the insightful discussions.

This work would not have been possible without the financial support provided by the Swiss Federal Roads Administration (FEDRO) in the framework of the research project AG BGT 20 02B. The regular meetings and valuable discussions with the research committee chaired by Dr Hans R. Ganz have been highly appreciated.

My gratitude goes also to the members of the jury, namely Prof. Dimitrios Lignos, Prof. Anssi Laaksonen, Prof. Paolo Castaldo and Prof. David Ruggiero, for the interesting comments and discussions which significantly improved this work.

Special thanks go to the laboratory secretaries Yvonne Buehl-Brauch and Jessica Ritzi for the warm welcome at IBETON and for always being there for any kind of difficulty. In addition, I would like to thank Dr Olivier Burdet for his availability, the interesting discussions and the valuable help with programming and beyond; the lab technicians, Gilles, Gérald, Serge, François, Armin and Fréd for their help during the time I spent in the laboratory; the PhD student's representatives and Emma Sorrentino with whom I collaborated sharing interesting thoughts and organizing events; the volunteers of the first aid group at EPFL for their dedication.

I would like to express my sincere gratitude to all my colleagues at IBETON who have contributed to making these past years special. Starting from those with whom I shared most of my stay at EPFL, Diego, Marko, Enrique, Frédéric and Qianhui; the previous generation of PhDs that warmly welcomed me, Patrick, Francesco, Raffaele, Max and Eduardo; all the previous PhDs from IBETON which I had the chance to exchange with in various events, special thanks go to Damien for the many interesting discussions; the exchange students and postdocs, Julia, Xianlin, Mads, Daniel, among whom special thanks go to Andri who was my officemate for his entire stay at EPFL and to Hamid for the collaboration on part of this research.

I would also like to thank all the colleagues and friends from the different labs at EPFL and Unil, among others RESSLab, EESD, LMC, TRANSP-OR, with whom I had the pleasure to share thoughts and discussions, special thanks to Lucas, Colin, Paola and Hisham with whom I collaborated.

Finally, I want to express my deepest gratitude to my parents, my brother Moreno, my partner Beatrice and her parents for the support I have received during all these years. The awareness

that I could always count on them encouraged me to embark on this journey and complete it, especially I would like to thank Moreno for always being there for me and Beatrice for making every day count more. I would also like to thank Ronnie, our dog, for the invaluable emotional support.

Lausanne, February 2024, Xhemsi Malja

Abstract

Most codes of practice adopt a semi-probabilistic design approach for the dimensioning and assessment of structures. Accordingly, structural safety is ensured by performing limit state verifications using design values determined with adequately calibrated Partial Safety Factors. Depending on the type of structure, the analysis performed and the code of practice used, structural verifications can be performed by comparing actions effects to sectional resistances or by comparing the load bearing capacity directly to the actions. Both verification methods lead to the same result for statically determinate structures, but the results can be different for statically indeterminate structures. While extensive studies have been performed to quantify the model uncertainty on the resistance side, the model uncertainties related to the calculation of actions effects and load bearing capacity in statically indeterminate structures have not been properly investigated yet. Thus, the first contribution of this thesis is to quantify this uncertainty for reinforced concrete structures by considering various mechanical models and failure modes. As there is little experimental data available on statically indeterminate systems, to perform statistical analyses, the experimental response of statically indeterminate systems is obtained by using a simple and effective technique. Practical implications are finally discussed on the basis of parametric analyses and case studies.

The second contribution of this thesis is to clarify the influence of high-level sustained loading on the resistance and deformation capacity of reinforced concrete members in compression. While the detrimental effect of high-level sustained loading on the concrete compressive strength is already acknowledged in current codes of practice, its influence in terms of deformation capacity is generally neglected. Besides the uncertainty in calculating the member compressive strength due to a larger activation of the reinforcement, the deformation capacity influences also the calculation of the action effects, which is caused by forces redistribution between elements of the same structural system. On this basis, the effects of high-level sustained loading and its practical consequences are addressed in this thesis on the basis of an experimental programme which consists of 14 prismatic specimens tested under various uniaxial stress rates and a theoretical investigation using a mechanical model. The results allow clarifying the materials responses and validating the mechanical model. Practical implications are discussed based on parametric analyses performed for different concrete ages, reinforcement ratios and materials properties.

The last part of the thesis focuses on updating the partial safety factors for permanent loads in road bridges by means of updated statistical distributions. To accurately estimate the sensitivity factors, in addition to permanent loads, the variability of the resistance calculation, materials strength and traffic loads is investigated. Finally, parametric analyses are performed to calibrate the partial safety factors for permanent loads. Two different partial factors are proposed for structural and non-structural self-weight and, by means of case studies, it is demonstrated that a

sufficient level of safety is ensured, both in absolute terms and when compared to the current partial factors.

Keywords: reinforced concrete, structural reliability, model uncertainty, failure modes, action effects, statically indeterminate, sustained loading, permanent loads, partial factors, materials strength, traffic variability, road bridges

Résumé

La plupart des normes adoptent une approche de vérification structurelle semi-probabiliste pour le dimensionnement et l'évaluation des structures. Sur cette base, la sécurité structurale est assurée en effectuant des vérifications à l'état limite ultime avec des valeurs de calcul obtenues en utilisant des coefficients partiels de sécurité. En fonction du type de la structure, de l'analyse effectuée et de la norme utilisée, les vérifications structurelles peuvent être effectuées en comparant les effets des actions aux résistances sectionnelles ou en comparant la résistance à l'état limite ultime de la structure directement aux charges. Les deux méthodes de vérification amènent au même résultat pour les structures isostatiques, alors que pour les structures hyperstatiques, les deux résultats sont généralement différents. Alors que les incertitudes du modèle du côté de la résistance ont été largement étudiées dans le passé, les incertitudes du modèle pour le calcul des effets des actions dans les systèmes hyperstatiques n'ont pas encore été suffisamment étudiée. Par conséquent, la première contribution de cette thèse est de quantifier cette incertitude pour les structures en béton armé en considérant différents modèles mécaniques et plusieurs modes de rupture. Etant donné que les campagnes expérimentales concernant les systèmes structurels hyperstatique ne sont pas suffisantes pour effectuer des analyses statistiques, la réponse expérimentale de tels systèmes est obtenue à l'aide d'une technique simple et efficace. Les implications pratiques sont discutées sur la base d'analyses paramétriques et des cas d'étude.

Le deuxième objectif de cette thèse est de clarifier l'influence des charges soutenues de haute intensité sur la résistance et la capacité de déformation des éléments en béton armé en compression. Bien que l'effet défavorable des charge soutenues sur la résistance à la compression du béton soit déjà considérée dans plusieurs normes actuelles, son influence en termes de capacité de déformation est généralement négligée. En plus de l'incertitude dans le calcul de la résistance à la compression des éléments due à une activation plus importante de l'armature, la capacité de déformation des éléments influence également le calcul des effets des actions, causés par la redistribution des forces entre les éléments d'un même système. Dans ce contexte, l'influence des charges soutenue de haute intensité et ses implications pratiques sont étudiée dans cette thèse sur la base d'un campagne expérimentale composée de 14 échantillons prismatiques testés avec une charge axiale et différentes vitesses de chargement. Les résultats permettent de clarifier la réponse des matériaux et de valider le modèle mécanique. Les implications pratiques sont ensuite discutées sur la base d'analyses paramétriques réalisées pour différents âges du béton, ratios d'armature et propriétés des matériaux.

La dernière partie de cette thèse se concentre sur la mise à jour des coefficients partiels pour les actions permanentes (poids propre structurel et non structurel) pour les ponts routiers. En plus des charges permanentes, la variabilité du calcul de la résistance sectionnelle, de la résistance des matériaux et des charges de trafic sont étudiées pour estimer les facteurs de sensibilité. Enfin, des analyses paramétriques sont effectuées pour calibrer les coefficients partiels pour les actions

permanentes. Deux coefficients partiels différents sont proposés pour le poids propre structurel et non structurel et, à l'aide de plusieurs cas d'étude, il est démontré qu'un niveau de sécurité suffisant est assuré, à la fois en termes absolus et par rapport aux coefficients partiels de sécurité actuels.

Mots-clefs : béton armé, fiabilité structurelle, incertitude de modèle, modes de rupture, effets des actions, systèmes hyperstatique, charge soutenue, charges permanentes, coefficients partiels, variabilité de la résistance des matériaux, variabilité des charges du trafic

Riassunto

La maggior parte delle norme per le costruzioni adotta un approccio semi-probabilistico per il dimensionamento e la valutazione delle strutture. Di conseguenza, la sicurezza strutturale è garantita mediante verifiche allo stato limite utilizzando valori di progetto, questi valori sono determinati con fattori parziali di sicurezza adeguatamente calibrati. A seconda del tipo di struttura, dell'analisi effettuata e della norma utilizzata, le verifiche possono essere eseguite confrontando gli effetti delle azioni con le resistenze sezionali o confrontando la capacità portante direttamente con le azioni. Entrambi i metodi conducono allo stesso risultato per le strutture isostatiche ma i risultati possono differire per le strutture iperstatiche. Mentre per quantificare le incertezze di modello per il calcolo della resistenza sono stati condotti studi approfonditi, le incertezze di modello relative al calcolo degli effetti delle azioni e della capacità portante delle strutture iperstatiche non sono state ancora studiate adeguatamente. Pertanto, il primo contributo di questa tesi è quello di quantificare questa incertezza per le strutture in calcestruzzo armato, considerando diversi modelli meccanici e modi di rottura. Poiché i dati sperimentali disponibili per sistemi strutturali iperstatici sono scarsi, per poter eseguire analisi statistiche, la risposta sperimentale di tali sistemi si ottiene utilizzando una tecnica semplice ed efficace. Le implicazioni pratiche dei risultati ottenuti sono infine discusse sulla base di analisi parametriche e casi studio.

Il secondo contributo di questa tesi è quello di chiarire l'influenza dei carichi sostenuti di alta intensità sulla resistenza e la capacità di deformazione degli elementi in calcestruzzo armato soggetti a compressione. Mentre l'effetto dannoso di questi carichi sulla resistenza a compressione del calcestruzzo è considerato nelle norme attuali, l'influenza in termini di capacità di deformazione è generalmente trascurata. Oltre all'incertezza nel calcolo della resistenza a compressione degli elementi, dovuta all'ulteriore attivazione dell'armatura, la capacità di deformazione influenza anche il calcolo degli effetti delle azioni, causati dalla ridistribuzione delle forze tra elementi dello stesso sistema strutturale. Su questa base, gli effetti dei carichi sostenuti di alta intensità e le sue conseguenze pratiche sono studiati in questa tesi mediante (1) un programma sperimentale, composto da 14 provini prismatici testati fino a rottura sotto uno sforzo assiale applicato con varie velocità e (2) mediante uno studio teorico utilizzando un modello meccanico. I risultati consentono di chiarire la risposta dei materiali e di validare il modello meccanico. Le implicazioni pratiche sono discusse sulla base di analisi parametriche eseguite per diverse età del calcestruzzo, tassi di armatura e proprietà dei materiali.

L'ultima parte della tesi riguarda l'aggiornamento dei fattori parziali per i carichi permanenti nei ponti stradali mediante distribuzioni statistiche aggiornate. Per stimare accuratamente i fattori di sensibilità, oltre ai carichi permanenti, viene studiata anche la variabilità del calcolo della resistenza, della resistenza dei materiali e la variabilità dei carichi dovuti al traffico. Infine, vengono eseguite delle analisi parametriche per calibrare i fattori parziali per i carichi permanenti. Sono proposti due diversi fattori parziali per il peso proprio strutturale e non

strutturale e, attraverso casi studio particolari, si dimostra che un livello di sicurezza strutturale sufficiente è raggiunto, sia in termini assoluti che rispetto ai fattori di sicurezza attuali.

Parole chiave: strutture in calcestruzzo armato, affidabilità strutturale, incertezza di modello, effetti delle azioni, capacità portante, sistemi iperstatici, analisi non lineari, carico sostenuto, scorrimento viscoso del calcestruzzo, ridistribuzione degli sforzi, variabilità dei carichi permanenti, variabilità della resistenza dei materiali, variabilità del carico da traffico, modi di rottura;

Zusammenfassung

Die meisten Regelwerke verwenden für die Bemessung und Überprüfung von Bauwerken einen semiprobabilistischen Ansatz. Die Tragsicherheit wird mit Bemessungswerten in verschiedenen Grenzzuständen nachgewiesen, die mit hierfür kalibrierten Teilsicherheitsbeiwerten bestimmt werden. Je nach Art des Tragwerks, der durchgeführten Analyse und des angewandten Regelwerks können Tragsicherheitsnachweise durch den Vergleich von Auswirkungen mit Querschnittswiderständen oder durch den Vergleich der Tragfähigkeit mit den Einwirkungen durchgeführt werden. Bei statisch bestimmten Tragwerken führen beide Nachweismethoden zum selben Ergebnis, bei statisch unbestimmten Tragwerken können die Ergebnisse jedoch unterschiedlich ausfallen. Es wurden bereits umfangreiche Studien zur Quantifizierung der Modellunsicherheit auf der Widerstandsseite durchgeführt, während die Modellunsicherheiten im Zusammenhang mit der Berechnung der Auswirkungen und der Tragfähigkeit in statisch unbestimmten Tragwerken noch nicht ausreichend untersucht worden sind. Der erste Beitrag der vorliegenden Dissertation besteht darin, diese Unsicherheiten für Stahlbetonkonstruktionen unter Berücksichtigung verschiedener mechanischer Modelle und Versagensarten zu quantifizieren. Da für eine statistische Analyse statisch unbestimmter Systeme nur wenige experimentelle Daten zur Verfügung stehen, wird ihr Verhalten mit Hilfe einer einfachen und effektiven Prozedur ermittelt. Die für die Praxis relevanten Schlussfolgerungen Auswirkungen werden anhand von parametrischen Analysen und Fallstudien erörtert.

Der zweite Beitrag dieser Arbeit betrifft die Klärung des Einflusses hoher Dauerbelastungen auf den Widerstand und das Verformungsvermögen von gedrückten Stahlbetonbauteilen. Während die nachteilige Wirkung hoher Dauerlasten auf die Betondruckfestigkeit in den aktuellen Regelwerken bereits anerkannt ist, wird ihr Einfluss auf das Verformungsvermögen im Allgemeinen vernachlässigt. Neben der Unsicherheit bei der Berechnung der Bauteildruckfestigkeit aufgrund der grossen Aktivierung der Bewehrung beeinflusst die Verformung auch die Berechnung der Einwirkungen, die durch die Umverteilung der Kräfte zwischen verschiedenen Elementen desselben Tragwerkssystems verursacht werden.

Entsprechend werden in dieser Arbeit die Auswirkungen hoher Dauerbelastungen und ihre praktischen Folgen anhand eines Versuchsprogramms untersucht, bestehend aus 14 prismatische Probekörper. Diese wurden unter verschiedenen einachsigen Beanspruchungsraten getestet und mit Hilfe eines mechanischen Modells theoretisch untersucht. Die Ergebnisse ermöglichen eine Klärung des Materialverhaltens und die Validierung des mechanischen Modells. Auf der Basis parametrischer Analysen, die für verschiedene Betonalter, Bewehrungsgrade und Materialeigenschaften durchgeführt wurden, werden praktische Auswirkungen diskutiert.

Der letzte Teil der Dissertation befasst sich mit der Aktualisierung der Teilsicherheitsbeiwerte für ständige Lasten im Fall von Straßenbrücken mit Hilfe von aktualisierten statistischen Verteilungen. Um die Sensitivitätsfaktoren genau abzuschätzen, werden neben den ständigen

Lasten auch die Variabilität in der Widerstandsberechnung, Materialfestigkeit und den Verkehrslasten untersucht. Schließlich werden parametrische Analysen durchgeführt, um die Teilsicherheitsbeiwerte für ständige Lasten zu kalibrieren. Es werden zwei verschiedene Teilsicherheitsbeiwerte vorgeschlagen, für strukturelles und nicht-strukturelles Eigengewicht. Anhand von Fallstudien wird gezeigt, dass hiermit ein ausreichendes Sicherheitsniveau gewährleistet ist, sowohl absolut als auch im Vergleich zu den derzeit verwendeten Teilsicherheitsbeiwerten.

Schlagwörter: Stahlbeton, Strukturzuverlässigkeit, Modellunsicherheit, Versagensarten, Einwirkungseffekte, statisch unbestimmt, Dauerbelastung, ständige Lasten, Beiwerte, Materialfestigkeit, Verkehrsvariabilität, Straßenbrücken

Resumen

La mayoría de códigos estructurales adoptan un enfoque semiprobabilístico para el dimensionamiento y la verificación de estructuras. En consecuencia, la seguridad estructural se garantiza realizando verificaciones de los estados límite utilizando valores de diseño determinados con Factores Parciales de Seguridad adecuadamente calibrados. Dependiendo del tipo de estructura, del análisis realizado y del código utilizado, las verificaciones estructurales pueden realizarse comparando los efectos de las acciones con las resistencias seccionales o comparando la capacidad portante directamente con las acciones. Ambos métodos de verificación conducen al mismo resultado para estructuras isostáticas, pero los resultados pueden ser diferentes para estructuras hiperestáticas. Mientras que amplios estudios se han realizado para cuantificar la incertidumbre del modelo del lado de la resistencia, las incertidumbres del modelo relacionadas con el cálculo de los efectos de las acciones y la capacidad portante en estructuras hiperestáticas aún no se han investigado adecuadamente. Así, la primera contribución de esta tesis consiste en cuantificar esta incertidumbre para estructuras de hormigón armado considerando varios modelos mecánicos y modos de fallo. Debido a la escasez de datos experimentales de sistemas hiperestáticos, se ha utilizado una técnica simple y efectiva para obtener la respuesta experimental de sistemas hiperestáticos de cara a realizar los análisis estadísticos. Por último, se explican las implicaciones prácticas a partir de análisis paramétricos y estudios de casos prácticos.

La segunda contribución de esta tesis es aclarar la influencia de cargas sostenidas elevadas en la resistencia y la capacidad de deformación de elementos de hormigón armado en compresión. Mientras que el efecto desfavorable de cargas sostenidas elevadas en la resistencia a compresión del hormigón ya se recoge en los códigos estructurales, su influencia en términos de capacidad de deformación es generalmente despreciada. Además de la incertidumbre en el cálculo de la resistencia a la compresión del elemento debido a una mayor activación de la armadura, la capacidad de deformación influye también en el cálculo de los efectos de las acciones por la redistribución de esfuerzos entre elementos del mismo sistema estructural. Sobre esta base, los efectos de cargas sostenidas elevadas y sus consecuencias prácticas se abordan en esta tesis mediante un programa experimental compuesto por 14 probetas prismáticas ensayadas bajo distintos niveles de compresión uniaxial y una investigación teórica mediante un modelo mecánico. Los resultados permiten identificar la respuesta de cada material y validar el modelo mecánico. Se exponen también las implicaciones prácticas basadas en análisis paramétricos, realizados para diferentes edades del hormigón, tasas de armado y propiedades de los materiales.

La última parte de la tesis se centra en la actualización de los factores parciales de seguridad para cargas permanentes en puentes de carretera mediante distribuciones estadísticas actualizadas. Para estimar con precisión los factores de sensibilidad, se investigan la variabilidad del cálculo de la resistencia, la resistencia de los materiales y las cargas de tráfico además de las cargas permanentes. Por último, se realizan análisis paramétricos para calibrar los factores

parciales de seguridad para las acciones permanentes. Se proponen dos factores parciales diferentes para el peso propio de los elementos estructurales y para la carga muerta y, mediante casos prácticos, se demuestra que se garantiza un nivel de seguridad suficiente, tanto en términos absolutos como en comparación con los factores parciales actuales.

Palabras clave: hormigón armado, fiabilidad estructural, incertidumbre del modelo, modos de fallo, efectos debidos a las acciones, hiperestático, carga sostenida, cargas permanentes, factores parciales, resistencia de materiales, variabilidad del tráfico, puentes de carretera.

Contents

Chapter 1

Introduction

1.1 Context and motivation

Starting in the second half of the last century, for the dimensioning and assessment of structures, most codes of practice adopted a semi-probabilistic design approach, the so-called Partial Safety Factor Format (PSFF). Accordingly, to ensure structural safety, limit state verifications are performed by means of design values, which are determined using adequately calibrated Partial Safety Factors (PSFs), see Figure 1.1. However, only in recent years some effort was made to establish a standard probability modelling framework [CEN02]. In fact, although the notion of probabilistic structural safety was already introduced at the beginning of the last century, the representative values and the partial safety factors were initially calibrated to ensure a similar level of safety to that obtained using previous standards or empirical rules [CEB59, CEB64]. Reliability analyses for calculating and updating the partial safety factors were introduced at a later stage [CEB74]. Nevertheless, each partial safety factor was calibrated independently from the others, e.g. the partial safety factor for the resistance was calibrated without considering the uncertainty related to the calculation of action effects, which is considered on the actions side. The current definition of the PSFF, with the partial factors calibrated using First and Second Order Reliability Method Analyses (FORM and SORM) as well as Monte-Carlo analyses (MC) was later introduced by [Cor69, Has74, Der91].

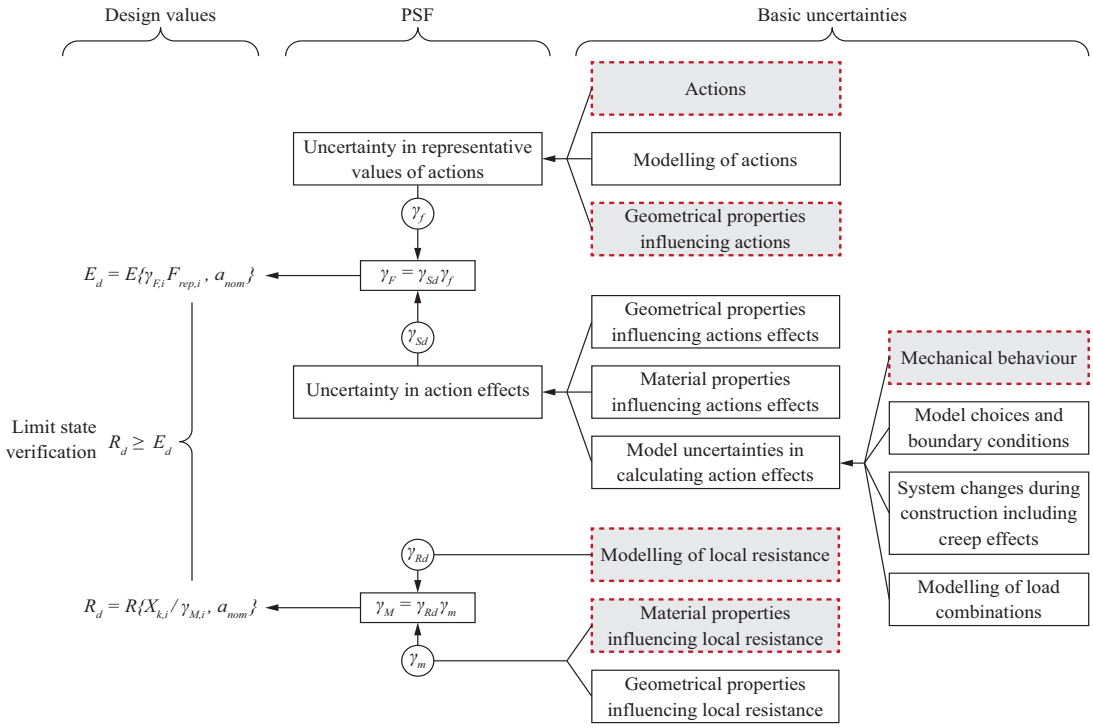

Figure 1.1: Basic uncertainties and corresponding partial safety factors (PSFs). Figure adapted from [CEN02] and [Yu21], notation consistent with [CEN22]. The uncertainties investigated in this thesis are highligheted.

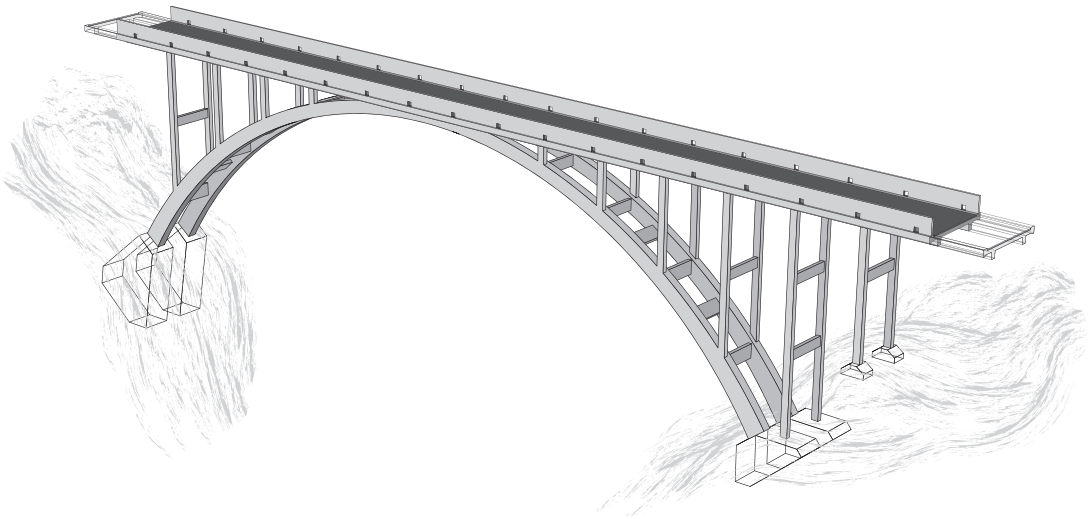

Figure 1.2: Illustration of a reinforced concrete arch bridge with most of the elements working in compression. Inspired from the work of Alexandre Sarrasin in canton Valais, Switzerland during the first half of the 20th century.

Still nowadays, the sources of uncertainties covered by each partial factor are a matter of discussion in the scientific community since they are not clearly defined in codes of practice and the related background documents. To clarify this subject, Figure 1.1 presents on overview of the current partial factors based on the comprehensive literature review performed by [Yu21] and the information available in [CEN02] and the new generation [CEN22].

It is important to note that the statistical distributions of the basic random variables are assumed according to the best knowledge at a specific time. As knowledge evolves, technological advancement progresses and more data is available, these statistical data should be updated and lead to either a confirmation or an update of the partial safety factors. The fact that some of the partial safety factors do not have a solid scientific base might lead to insufficient levels of safety in different scenarios (type of structures, failure modes, materials etc.), or, in some cases, lead also to excessively expensive structures (too safe). In addition, an adequate knowledge of the basic uncertainties covered by each partial factor is fundamental to improve decision-making when dealing with existing structures. Within this context, to design safe and more cost-effective structures, the main uncertainties covered by each partial safety factor need to be clarified and updated according to newly available data.

For the dimensioning and assessment of structures, it is common practice for designers to compare action effects with sectional resistances. To calculate actions effects in statically indeterminate structures, engineers assume a linear-elastic uncracked mechanical behaviour of the structure, neglecting both cracking of concrete and the influence of the reinforcement on the stiffness, see Figure 1.3. On the other hand, the sectional resistance is generally calculated considering cracking of concrete and non-linear behaviour of materials, assuming that each

section or member can reach its design resistance. This assumption, while not consistent with the one related to the stiffness, is certainly true if all sections have a sufficient deformation capacity, nonetheless, a premature failure of the system can occur if this is not the case.

While model uncertainties on the resistance side have been extensively investigated in the past, the model uncertainty in the calculation of action effects in statically indeterminate systems has not been properly investigated yet. Currently the statistical distribution recommended by the Joint Committee of the Structural Safety report (JCSS) is used to account for this uncertainty [JCS01], though, as stated in part 3, section 3.9.3, to estimate this uncertainty "… *a more or less standard structural Finite Element Model has been kept in mind*" without specifying the adopted mechanical behaviour. It is assumed that the values are determined using a linear elastic model.

Regarding codes of practice, in EN1990:2002 [CEN02], the model uncertainty in action effects is implicitly covered by the partial factors for permanent and variable actions, see Figure 1.1. For particular verifications, the designer is allowed to decouple this uncertainty, however, the recommended values are based on the prescriptions originally proposed by [CEB59] to consider uncertainties related to the calculation methodology and tools ("*moderately careful or uncertain studies and calculations*", in French *"études et calculs moyennement soignés ou incertains"*), while statically indeterminate systems were not explicitly mentioned.

One can note that the approach used by current codes of practice, PSF for calculation of action effects considered on the action side, does not allow to account for the type of system failure. Nonetheless, FprEN1990:2022 [CEN22] specifies that the partial factors on the load side may be used for both linear and non-linear calculation, although the verifications are generally different: sectional verifications for linear analyses (local) and load bearing verifications for non-linear analyses (global). In this context there is a need to quantify the model uncertainty in action effects and load-bearing capacity for different mechanical behaviours and clarify whether the failure mode of the system has an influence.

For reinforced concrete structures which rely on members working in compression, the calculation of the load bearing capacity is strictly related to the calculation of the compressive strength of the members, see Figure 1.2. If failure of the structure occurs due a member failing in compression under high intensity sustained loading, the detrimental effect on the concrete strength is already acknowledged in most of current codes of practice but the increased deformation capacity, which can be beneficial, has not been properly investigated yet. This enhancement of the deformation capacity influences both the uncertainty in calculating the resistance of the member, since it influences the activation of the reinforcement, and the uncertainty in calculating the action effects in different members since it allows redistribution between members of the system. Therefore, a deeper investigation in this field is necessary to clarify the redistribution of forces within the same member and provide the tools to quantify the redistribution between different members part of the same structural system.

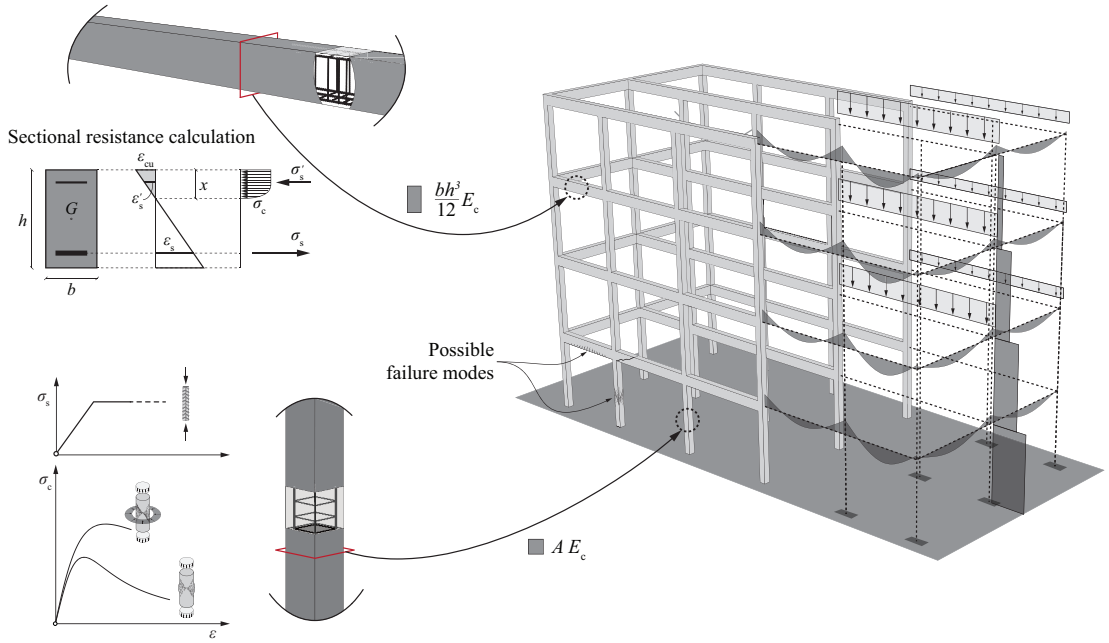

Figure 1.3: Illustration of the approach used by designes to perform structural verifications:, a linear-elastic uncracked mechanical behaviour of the members is used to calculate actions effects in statically indeterminate structures (right) while the sectional resistance is calculated considering cracking of concrete and non linear behaviour of materials (left).

Within the context of the PSFF, it is not correct to refer to an individual PSF; instead, one must consistently consider a set of PSFs. In fact, in addition to the variability of each random variable, the extent to which these quantities contribute to the limit state function, which separates the safe structural domain from the unsafe one, must be considered. For instance, in the First Order Reliability Analysis Method (FORM), this contribution is represented by the sensitivity factors (refer to the following section). According to EN 1990:2002 [CEN02]) the sensitivity factors on the resistance and action side are assumed $\alpha_R = 0.8$ and $\alpha_E = -0.7$. While this assumption simplifies considerably the calibration of the partial factors, allowing to calibrate the PSFs on the resistance and action side separately, it also makes the strong simplification that these values are constant and do not depend on the failure scenario and the structure considered. Due to the wide range of scenarios covered, such simplification requires the choice of conservative values. In the case of EN 1990:2002 [CEN02], this can be observed by the fact that the sum of the squares of the sensitivity factors α_R and α_E is 1.13, however, per definition, for a specific failure scenario and structural system the sum of the squares of all the sensitivity factors must be 1.0 [Sch17]. Nowadays, with increasing computational power and data availability it is fundamental to verify the suitability of the above-mentioned assumptions. This is especially significant in road bridges where, for instance the variability of the traffic is very large and it is not clear whether the values presented above are suitable. Further investigation on this topic not

only allows the design of safe structures but also cost-effective and environmentally sustainable, with more conscious and rational use of materials. That is especially true for existing structures, in fact, in the near future a large number of bridges and structures will reach the end of their design life and will require an adequate evaluation of the structural safety to improve decision-making concerning rehabilitation interventions.

1.2 Reliability analyses

The general formulation of the probability of failure P_f calculation is formulated as in Eq. (1.1), where:

- $\boldsymbol{X}$ is the transposed vector containing the random variables, which are assumed continuous and represent uncertain structural quantities, e.g., material properties, geometry of the members, loads, and models,
- $f_{\boldsymbol{X}}(\boldsymbol{x})$ is the joint probability density function of $\boldsymbol{X}$,
- $g(\boldsymbol{X})$ is the so-called limit state function specific to that scenario and is formulated in such a way that $g(\boldsymbol{X}) > 0$ and $g(\boldsymbol{X}) < 0$ represent respectively the survival and the failure of the structure.

$$P_f = P\left[g(\boldsymbol{X}) \leq 0\right] = \iiint\limits_{g(\boldsymbol{X})<0} f_{\boldsymbol{X}}(\boldsymbol{x})\, d\boldsymbol{x} \quad \text{with} \quad \boldsymbol{X} = \left[X_1 \dots X_n\right]^T \tag{1.1}$$

Typically, for structural reliability the function $g(\boldsymbol{X})$ may be difficult to evaluate and, although $g(\boldsymbol{X})$ could be easily calculated and $f_{\boldsymbol{X}}(\boldsymbol{x})$ is known, the computation of high dimensional integrals is very difficult [Sch17]. Thus, the approaches mentioned in the previous section, FORM, SORM and MC, were developed to overcome these challenges and allow calculating the P_f.

According to the FORM approach, the limit surface is approximated by a plane and the probability of failure is calculated using the First Order Reliability Index β [Mad06], which is calculated as in Eq. (1.2) with Φ being the reversed cumulative distribution function of the standard normal distribution. The reliability index is the minimum distance from the origin to the failure surface in a normalized space. This assumption is based on the fact that the value of $f_{\boldsymbol{X}}(\boldsymbol{x})$ becomes negligible with increasing distance from the origin of the normalized space. The closest point on the failure surface to the origin is the so-called *design point*. Using this approach, a valuable information can be obtained by computing the partial derivatives of the limit state function in the design point. This value is the so-called FORM sensitivity factor (α) and represents the weight of each variable for the calculation of the reliability index β.

$$P_f \approx \Phi(-\beta) \tag{1.2}$$

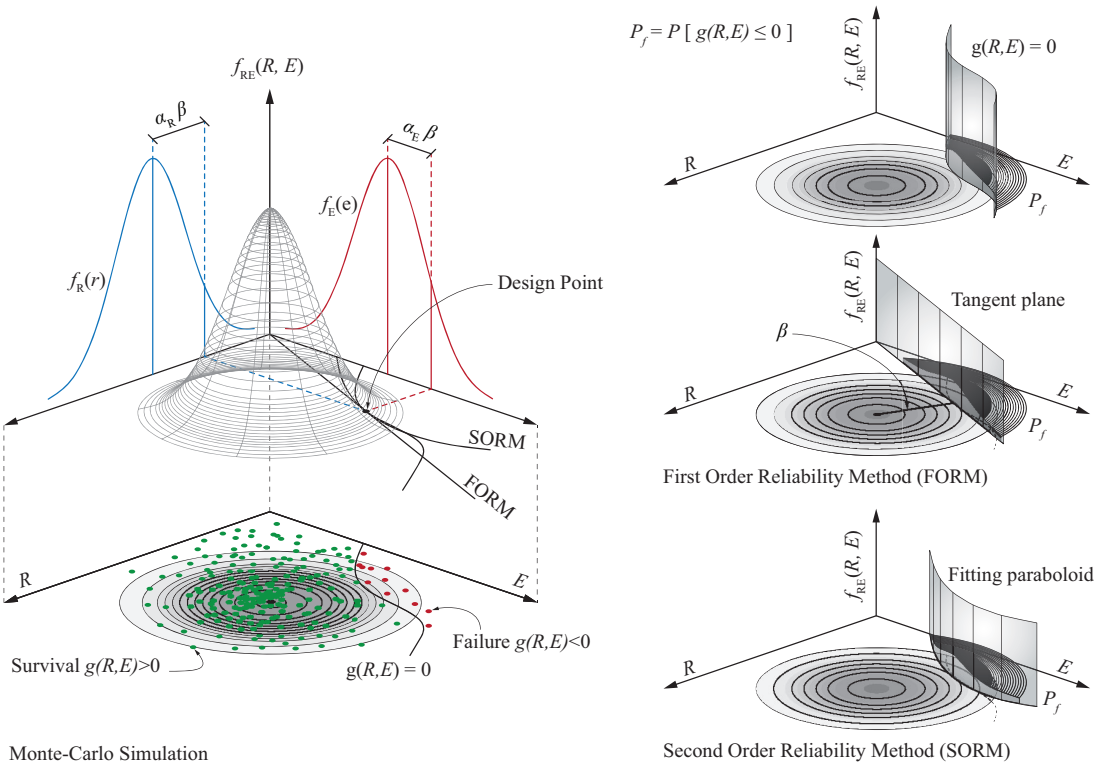

Figure 1.4: Illustration of the approaches used for calculating the probability of failure P_f: FORM, SORM and MC.

In the SORM approach, the failure surface is approximated using a paraboloid instead of a plane, which leads generally to better estimations of the failure probability [Der91].

Besides approximating the limit surface, the probability of failure P_f can also be calculated using numerical simulation methods. To this purpose, in the Crude-Monte-Carlo (CMC) method the limit state function is evaluated multiple times with a set of random variables resulting from a random sampling. For each evaluation, by means of an indicator function $I(\boldsymbol{x})$, it is recorded if structural failure occurs. The probability of failure is then calculated as the ratio between the simulations leading to structural failure and the overall number of simulations. These concepts are formulated in Eq. (1.3) and (1.4). The main drawback of this method is related to the large amount of simulations necessary to obtain an accurate estimation of P_f. In fact, to estimate accurately a probability of failure of 10^{-n}, the number of simulations required ranges from 10^{n+2} to 10^{n+3}. Figure 1.4 illustrates these approaches for a limit state function formulated in the classical form $g(R, E)$ where R is the resistance and E is the action effect. To simplify the illustration both probability density functions of R and E are assumed normally distributed.

To reduce the number of simulations required to estimate P_f, a commonly used variation of the CMC method is the Importance Sampling Monte Carlo method (MC-IS). In this case, the random sampling for evaluating the limit state function is performed around a predefined point

which generally corresponds to the design point calculated using the FORM method. To account for the biased sampling of the random variables the Eq. (1.4) is modified by introducing a weighting factor which depends on the selected point.

$$P_f = \int_{g(\boldsymbol{X})<0} f(\boldsymbol{x})\, d\boldsymbol{x} = \int_{g(\boldsymbol{X})<0} I(\boldsymbol{x}) \cdot f(\boldsymbol{x})\, d\boldsymbol{x} = E(I(\boldsymbol{x})) \tag{1.3}$$

$$I(\boldsymbol{x}) = \begin{cases} 1 & \text{if} \quad g(\boldsymbol{X}) \le 0 \\ 0 & \text{if} \quad g(\boldsymbol{X}) > 0 \end{cases} \qquad E(I(\boldsymbol{x})) = \frac{1}{N}\sum_{i=1}^{N} I(\boldsymbol{x}) \tag{1.4}$$

1.3 Objectives

Within the context introduced in the previous section, the main objectives of this thesis can be summarized as follows:

- quantify the model uncertainty in action effects and load-bearing capacity calculations of reinforced concrete structures for various mechanical models,
- clarify whether the failure mode has an influence on the model uncertainty in action effects and load-bearing capacity calculations,
- investigate stress redistributions in reinforced concrete members under uniaxial compressive load accounting for linear and nonlinear creep strains,
- clarify if the compressive strength of reinforced concrete members can be enhanced by using higher reinforcement grade steel,
- estimate the value of the sensitivity factors on the load and resistance side for a wide range of scenarios,
- update the partial safety factors for permanent loads in road bridges to provide a constant level of safety and better reflect the basic uncertainties covered,
- clarify how the uncertainties related to structural system change are considered and which are the uncertainties are covered by the partial factors for permanent loads.

1.4 Structure of the thesis

This thesis is structured in three main parts accompanied by this introduction and a general conclusion resumed as follows:

- Chapter 1: Introduction

  The research context, the need to pursue this work and the main objectives are elaborated.

- Chapter 2: Model uncertainties in action effects and load bearing capacity calculation in statically indeterminate reinforced concrete structures

  In this chapter the model uncertainties in actions effects and load bearing capacity calculation are investigated and results are discussed along with practical implications.

- Chapter 3: Influence of sustained loading on resistance and deformation capacity of reinforced concrete members in compression

  In this chapter the influence of high-level sustained loading on reinforced concrete members under compression is investigated by means of an experimental and theoretical work, the detrimental and beneficial effects are discussed along with practical implications.

- Chapter 4: Recalibration of partial safety factors for permanent loads in road bridges

  In this chapter the partial safety factors for permanent loads, within the context of the partial safety factor format are calibrated using updated statistical distributions. A new set of partial safety factors is proposed and the basic uncertainties covered by each partial factor is clarified.

- Chapter 5: Conclusion and Outlook

  The conclusions of each chapter are resumed and the outlook for potential future research is discussed.

As the present thesis is a compilation of journal articles, it must be noted that chapters 2, 3 and 4 include their own abstract, introduction, conclusion and notation. The bibliography is unique and can be found at the end of the thesis.

1.5 Scientific contributions

Details on the contributions of each chapter can be found at the beginning of the chapter. A general, non-exhaustive summary given below:

- comprehensive literature review for each of the investigated topics,
- collection of detailed databases (including force displacement relationship) regarding experimental tests on reinforced concrete beams and columns,
- implementation of algorithms for analysis and visualisation of large amounts of data for the model uncertainty in action effects and load bearing capacity calculation,
- recommendations for implementation of the results concerning the model uncertainty in codes of practice,
- experimental programme consisting of 14 specimens with various reinforcement ratios tested under a wide range of uniaxial stress rates,
- proposition of a mechanical model to account for the reinforcement contribution in reinforced concrete members under high-level sustained loading,
- practical recommendations concerning the use of high strength grades reinforcement steel in reinforced concrete members under compression,
- investigation of structural and non-structural self-weight of actual bridges,
- collection and analysis of databases for reinforcement steel and concrete properties used in Switzerland,
- quantification of the sectional resistance variability of reinforced concrete members,
- recommendation of new partial safety factors for permanent loads in bridges.

1.6 Limitations of the thesis

Chapter 2 is limited to the investigation of linear reinforced concrete elements; however, the methodology can be generalised and applied to other structural elements (i.e. slabs, walls, etc.). When referring to the modelling assumptions made by engineers, the standard practice in several European countries is generally taken as a reference (constant stiffness independently of cracking). Also, this investigation focuses on models that are most likely to be used in practice, additional models can be investigated using the same methodology.

The experimental programme presented in Chapter 3 is limited to the investigation of members failing under variable loading rate, different loading patterns should be investigated to further validate the mechanical model for reinforced concrete members as already performed for plain concrete specimens [Tas18]. Concerning the parametric analyses for concrete loaded at older ages, no tests are available for comparison, an experimental programme should be designed to this purpose.

Chapter 4 is limited to the investigation of reinforced concrete and mixed (steel-reinforced concrete) bridges. Additional research should be performed to investigate the variability of structural and non-structural self-weight for various structures and additional materials.

1.7 List of publications

The research was conducted at the Structural Concrete Laboratory (IBETON) of the Swiss Institute of Technology of Lausanne (École Polytechnique Fédérale de Lausanne, EPFL). The following publications have been published, submitted or will be submitted in the near future:

- **Malja X., Muttoni A.**, *Evaluation of the model uncertainty of action effects in statically indeterminate systems*, 14th fib International PhD Symposium in Civil Engineering, pp. 895-902, Rome, Italy, 2022.
- **Malja X., Motlagh H.R.E., Fernández Ruiz M., Muttoni A.**, *Influence of sustained loading on resistance and deformation capacity of reinforced concrete members in compression*, Structural Concrete, Vol. 24.3, pp. 3656-3673, 2023. https://doi.org/10.1002/suco.202200571
- **Malja X., Nussbaumer A., Muttoni A.**, *Model uncertainty in action effects and load bearing capacity calculation in statically indeterminate reinforced concrete structures*, (Submitted in January 2024)
- **Malja X., Nussbaumer A., Muttoni A.**, *Recalibration of partial safety factors for permanent loads in road bridges*, (to be submitted in 2024).

This page intentionally left blank.

Chapter 2

Model uncertainties in action effects and load bearing capacity calculation in statically indeterminate reinforced concrete structures

This chapter is the pre-print version of the following paper submitted in January 2024:

Malja X., Nussbaumer A., Muttoni A., *Model uncertainties in action effects and load bearing capacity calculation in statically indeterminate reinforced concrete structures*.

The work is performed by Xhemsi Malja under the supervision of Prof. Aurelio Muttoni and Prof. Alain Nussbaumer.

The main contributions of Xhemsi Malja are the following:

- comprehensive literature review,
- collection of a detailed database of experimental tests,
- implementation of the mechanical models available in literature,
- implementation of an algorithm to perform simulations of the assembled systems,
- implementation of an algorithm to perform parametric reliability analyses,
- interpretation of the results,
- design recommendations,
- elaboration of the figures and tables,
- writing of the manuscript.

Abstract

For the dimensioning and assessment of structures, it is common practice to compare action effects with sectional resistances. Extensive studies have been performed to quantify the model uncertainty on the resistance side. However, for statically indeterminate systems, the model uncertainty in the calculation of action effects has not been properly investigated yet. The aim of this work is to contribute in quantifying the model uncertainty in action effects and load-bearing capacity calculations for reinforced concrete structures, accounting for the type of mechanical model used and for various failure modes. To collect a sufficient amount of data and perform statistical analyses, the experimental response of statically indeterminate systems is obtained with a simple and effective technique which allows using experimental results available in literature. Finally, on the basis of a parametric analysis and case studies, practical implications are discussed and recommendations are given concerning the implementation in the Partial Safety Factor Format.

Keywords: reinforced concrete, structural reliability, model uncertainty, action effects, load-bearing capacity, statically indeterminate systems, redistribution, non-linear analysis

2.1 Introduction

The typical design process of reinforced concrete structures consists of three main steps. First, the structure is conceived considering the constrains and requirements. Experience and empirical rules (e.g., span/depth ratios) govern this phase, which results in the definition of the structural members geometry. Second, the relevant load cases are identified and the action effects are calculated by means of idealised models. Finally, with the geometry and the action effects for each section, the reinforcement is designed and dimensioned so that the sectional resistance is larger than the action effects. If the initial geometry of the structure is not suitable, the process can be repeated.

To calculate actions effects in statically indeterminate structures, engineers assume a linear-elastic uncracked mechanical behaviour of the structure, neglecting the influence of the reinforcement on the stiffness. The main advantages of these assumption are that the stiffness of the members does not depend on the load level and consequently no iteration is required. Thus, the process is direct and the results are easily obtainable, making these assumptions suitable for practical applications. However, for statically indeterminate systems (Figure 2.1a and 2.1b), a linear-elastic uncracked behaviour does not provide a completely realistic prediction of the action effects. In fact, because cracking is neglected, so is the ensuing redistribution of internal forces.

In spite of that, the sectional resistance is generally calculated considering cracking of concrete and non-linear behaviour of materials, assuming that each section or member can reach its design resistance. This assumption, while not consistent with the one related to the stiffness, is certainly true if all sections have a sufficient deformation capacity. However, a premature failure of the system can occur if this is not the case. To illustrate this scenario, Figure 2.1c shows the evolution of the bending moment (in absolute value) in the sagging and hogging section of a continuous beam under a distributed load q (see Figure 2.1a [Mut89]). Several regimes can be observed: (1) uncracked behaviour; (2) cracking in the hogging region, with the hogging moment increasing less than the sagging moment; (3) cracking of the sagging region, with the hogging moment increasing again more rapidly and (4) plastic regime with reinforcement's yielding in the hogging region. In the presented case, after some plastification of the reinforcement in the hogging region, due to insufficient deformation capacity (failure of the compression zone or of the reinforcement in tension), the sagging section is unable to reach its design resistance, leading to failure of the system for a load $q^* < q_d$, which is the theoretical failure load predicted assuming an elastic uncracked mechanical behaviour. Compared to the predicted linear elastic behaviour (dashed lines in Figure 2.1c), not only the actual load-bearing capacity can be underestimated ($q^* < q_d$), but also in terms of actual internal forces, deviations can be expected (differences between continuous lines and dashed lines). These deviations are one of the components contributing to the uncertainty in calculating action effects.

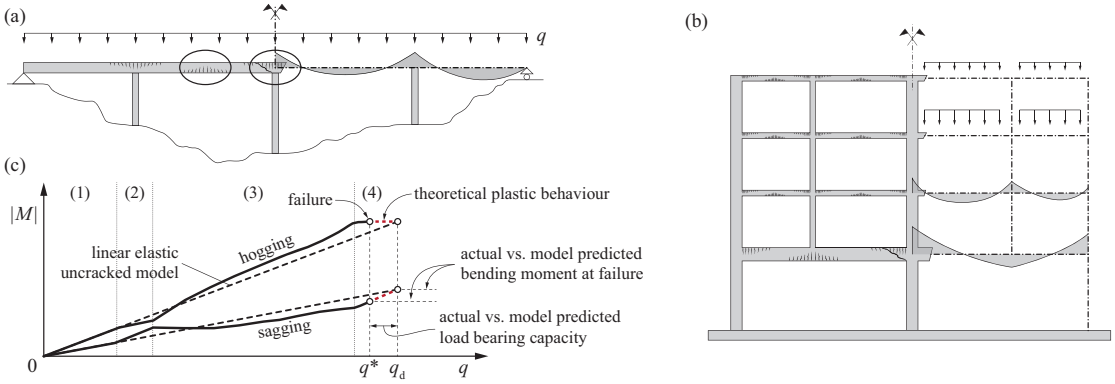

Figure 2.1: Redistribution of forces: (a) continuous beam, (b) frame system; (c) bending moment redistribution between the hogging and the sagging section of a continuous beam with regimes (1)-(4) (see explanation in the text) and premature failure of the hogging section.

To ensure structural safety, most current codes of practice adopt a semi-probabilistic design approach. Accordingly, limit state verifications are performed by means of design values and adequately calibrated Partial Safety Factors (PSFs), which cover uncertainties related to geometry, materials, actions effects and models, as shown in Figure 2.2. Regarding the uncertainty in model assumptions (idealization of the actual structure), previous research was mainly focused in investigating the model uncertainty related to the sectional resistance, while little effort was put in investigating the uncertainty in action effects. Depending on the type of

action, for the ratio of the actual internal force to the calculated value, the JCSS Probabilistic Model Code [JCS01] recommends a log-normal distribution with mean equal to 1.0 and CoV between 0.05 and 0.2. However, the origin of this recommendation is not clear. As stated in the JCSS Probabilistic Model Code (part 3, section 3.9.3), to obtain those values "… *a more or less standard structural Finite Element Model has been kept in mind"* without specifying the adopted mechanical behaviour. The authors assume that the recommended values are based on a linear elastic uncracked mechanical behaviour.

Regarding codes of practice, in EN1990:2002 [CEN02], the model uncertainty in action effects is implicitly covered by the partial factors for permanent and variable actions (γ_G and γ_Q). However, for particular verifications, the designer is allowed to decouple the model uncertainty in action effects, γ_{Sd}, from the uncertainty in the representative values of actions, γ_g and γ_q. In those cases, the recommended value for γ_{Sd} is between 1.05 and 1.15, consistent with the prescriptions of the first codes dealing with the topic, which proposed a factor γ_{Sd} equal to 1.15 [CEB59]. This value was originally proposed to consider uncertainties related to the calculation methodology and tools ("*moderately careful or uncertain studies and calculations*", in French *"études et calculs moyennement soignés ou incertains"*, [CEB59]), while statically indeterminate systems and redistribution of forces were not explicitly mentioned. Additional literature review on this topic can be found in [Yu21]. In the latest available draft of FprEN1990:2022 [CEN22], the model uncertainty in action effects is still covered by the partial safety factor for permanent and variable actions, presented with slightly different notation ($\gamma_F = \gamma_f \cdot \gamma_{Sd}$). It is also specified that γ_F may be used for both linear and non-linear calculation, although the different verifications types may differ: local verifications for linear analyses, global verifications for non-linear analyses. In FprEN1990:2022 [CEN22], except for some specific design cases, no recommended values of γ_{Sd} are specified. It is worth noting that one of the possible disadvantages of considering γ_{Sd} on the actions side is the impossibility to consider the mode of failure of the system (brittle vs. ductile), as it depends on the sectional resistance model.

Interestingly, the approach of codes of practice nowadays does not account for the type of system in terms of uncertainties in modelling and determination of action effects. For statically determinate systems, the calculation of action effects is only influenced by equilibrium and geometry, whereas the stiffness and the mechanical behaviour have no influence on the results, provided that second order effects can be neglected. For statically indeterminate systems, however, additional phenomena and basic uncertainties contribute to the uncertainty in action effects, as can be schematically observed in Figure 2.2, adapted from [Yu21] and [CEN02], notation consistent with [CEN22]. As shown in Figure 2.1, one of the main components influencing the calculation of action effects is modelling of the mechanical behaviour. Indeed, any model is a simplification of the actual structure and leads to a different degree of accuracy and precision. Generally, more complex models lead to more precise but not necessarily more accurate results and they require additional parameters and calculation time, often involving iterative processes and more complex interpretation of results. Also, time-dependent

deformations due to creep can influence the uncertainties in action effects. Another phenomenon that can increase the uncertainty in action effects, is the system change during construction (casting of concrete parts which constitute a statically indeterminate structure at different times time or/and assembly of precast members). Generally, in the design process, the model of the structure is generated as a whole and the totality of the load is applied at once, including self-weight. In actual structures, however, self-weight is applied according to construction stages, permanent load is incrementally applied after construction and live loads are applied sporadically. In statically indeterminate systems, this sequential application of the loading can lead to internal force redistributions, increasing the uncertainty in action effects. In addition, the internal forces are affected by the uncertainties related to the actual creep behaviour, the age of concrete at system change and the time at activation of self-weight (removal of propping or scaffolding). Finally, combinations of different actions, which is generally a task left to the designer, can lead to further uncertainties in calculating action effects.

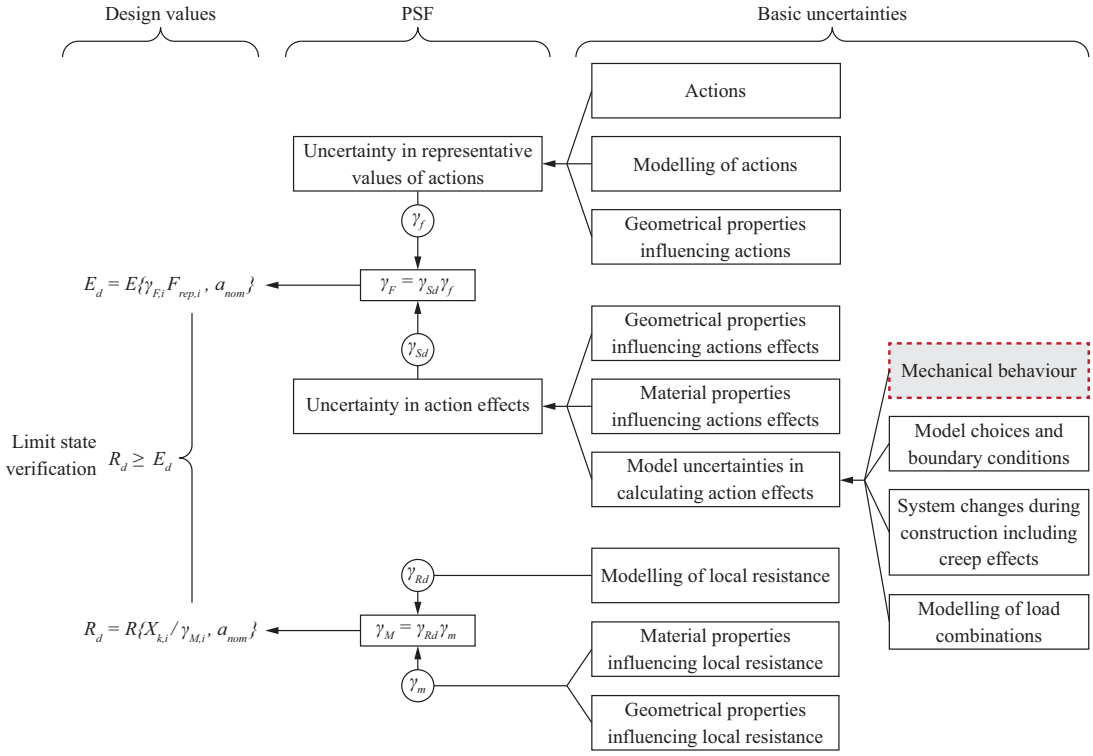

Figure 2.2: Basic uncertainties and corresponding partial safety factors (PSFs), figure adapted from [CEN02] and [Yu21], notation consistent with [CEN22]

As numerical models evolve, they are becoming more and more complex, giving designers many options to model a structure. For instance, the modelling of boundary conditions, the type of elements, the interaction between different element types and the adopted solver can influence the calculated action effects. As there is no standard for modelling structures, these choices are

left to the discretion and the experience of the designer, leading to further uncertainties in the value of action effects.

The aim of this work is to contribute to quantifying the model uncertainty in action effects and load-bearing capacity calculations of reinforced concrete structures and clarify whether the failure mode of the system influences this uncertainty. This investigation focuses on uncertainties related to the mechanical behaviour of the structure, see highlighted box in Figure 2.2, by comparing tests results and calculated values. Uncertainties related to geometrical variability effects on model uncertainties and system changes are not considered. Based on updated distributions, the partial safety factor γ_{Sd} is calculated by means of parametric analyses and case studies. Finally, uncertainties covered by γ_{Sd} are clarified and practical implications are discussed.

2.2 Investigated structural system and practical relevance

Since there is little experimental data available on statically indeterminate systems, it cannot be used to perform statistical analyses. To overcome these difficulties, the experimental response of statically indeterminate systems is obtained by assembling the response of simply supported beams tested in a 3-point bending setup. This technique has already been used by [Yu21] with structural members exhibiting brittle failure modes. It is also applicable to reinforced concrete systems where both brittle and ductile failure modes can occur. The deformability of supports is also considered by supporting beams on reinforced concrete columns tested under concentric uniaxial load.

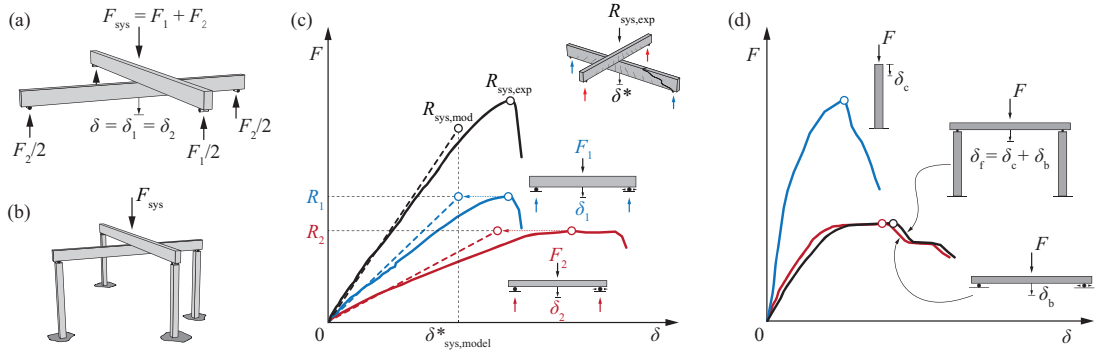

Figure 2.3: (a) Assembled system with beams on infinitely rigid supports and (b) supported by columns; (c) experimental response of the system (black) assembled with beams (red and blue) and linear-elastic uncracked model prediction (dashed); (d) Force-deflection (F-δ) response of a beam tested in a 3-point bending setup (red), a column tested in compression (blue) and a beam supported by two columns (black).

For the case presented in Figure 2.3a, the response of the assembled system in terms of force-displacement relationship (F-δ) is obtained by combining the response of various beams crossing at midspan. For compatibility reasons, the force applied to the system for a given displacement is the sum of the forces required to produce that same displacement in each of the beams composing the system, see Figure 2.3c. For the statically determinate systems with a beam supported on columns, which constitute the indeterminate system shown in Figure 2.3b, the displacement at midspan is obtained by adding the displacement of both members as shown in Figure 2.3d.

The theoretical response predicted by the model is obtained by using the same technique, where the F-δ response of each beam is calculated using several models. As an example, Figure 2.3c shows the experimental F-δ response of a system composed of two beams and the response of a linear elastic model. It is important to note that the model uncertainty related to the sectional resistance calculation is not considered. For this reason, the predicted resistance of each beam is equalled to the experimental resistance (in Figure 2.3c $R_{1,\mathrm{mod}} = R_{1,\mathrm{exp}}$ and $R_{2,\mathrm{mod}} = R_{2,\mathrm{exp}}$). With this assumption, the load-bearing capacity predicted by the elastic model for the system presented in Figure 2.3c is lower than the experimental one ($R_{\mathrm{sys,exp}}$), which results from the superposition of the two experimental load-displacement curves.

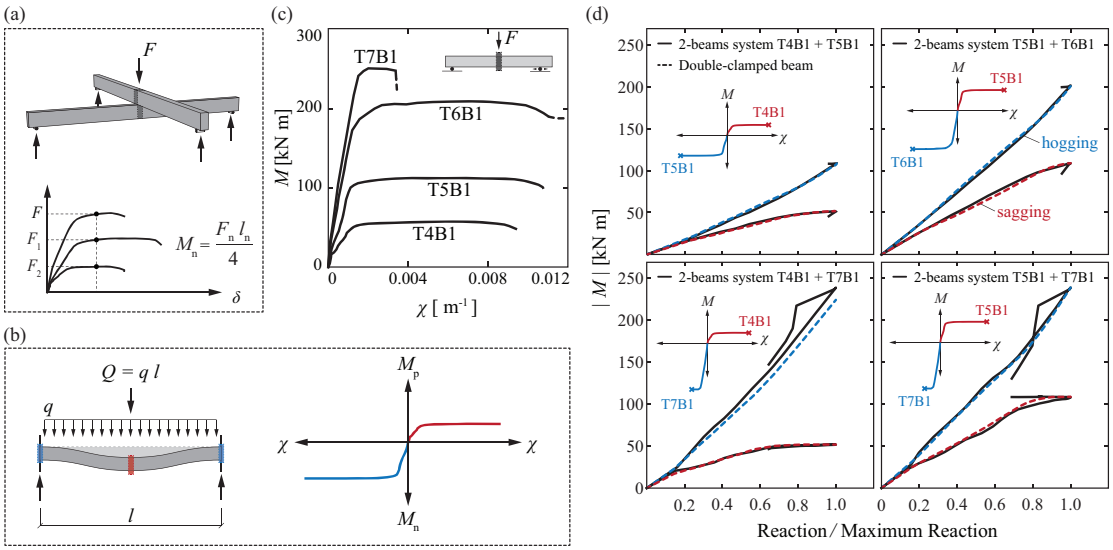

Figure 2.4: (a) F-δ response of an assembled 2-beams system; (b) double-clamped beam and assumed M-χ relationship; (c) experimental M-χ relationships of beams used in the comparison; (d) comparison of bending moment evolution as a function of the load for the 2-beams system (continuous curves) and the double-clamped beam (dashed curves).

To assess whether the assembled 2-beams system (Figure 2.4a) is representative of redistributions occurring in a continuous beam (Figure 2.4b), action effects in each beam of the system are compared with those in a double-clamped beam in the sagging and hogging sections. The double-clamped beam is subjected to both a distributed load q and a concentrated force at midspan $Q = q \cdot l$. All beams used in the comparison have been tested by [Bos93], have the same cross section ($b \times h = 200 \times 400\ mm$) and variable longitudinal reinforcement ratios ($0.4\% < \rho_l < 1.8\%$). The moment-curvature (M-χ) relationships (measured over a length equal to the effective depth of the corresponding beam) are shown in Figure 2.4c. In the double-clamped beam, the sagging and hogging bending moment are calculated using the measured M-χ relationship to fulfil equilibrium and compatibility. The shear deformations are neglected.

Figure 2.4d shows the bending moments at midspan of the 2-beams system as well as the sagging and hogging bending moments in the double-clamped beam as a function of the normalized load. It can be observed that the bending moment at midspan of each beam in the 2-beams system (continuous curves) closely follows the bending moment in the double-clamped beam (dashed red at midspan and dashed blue at the clamped end). For the case shown in the bottom left of Figure 2.4d (system T4B1 + T7B1), the resistance of the midspan section of the double-clamped beam is extremely under-designed and its deformation capacity is not sufficient to allow the clamped section to reach its designed resistance. Overall, except for cases where sections are extremely under-designed, the redistribution of forces in the assembled system is a good approximation of the redistributions occurring in a continuous beam. Even when sections are under-designed, Figure 2.4d shows that the redistribution of internal forces between the 2-beam system and the continuous beam is very similar up to failure. Thus, the assembled 2-beams system is representative of several practical cases, including double-clamped beams and continuous beams.

2.3 Definitions

2.3.1 Random variables

Depending on the type of analysis performed and the code of practice used, structural verifications can be performed by comparing action effects to sectional resistances (approach typically used in the design of new structures) or by comparing the load-bearing capacity directly to the actions (approach often used in the assessment of existing structures). In the present work, these two approaches are defined as *local* and *global verification methods*. For statically determinate structures, both methods lead to the same result, whereas for statically indeterminate structures, the results are typically different. The local verification method is typically used in combination with linear elastic analyses (or analyses with partial redistribution of internal

forces) whereas the global verification method is used with non-linear analyses or calculations based on limit analysis.

To cover both cases, two random variables are defined in this work. The global random variable θ_G is defined in Eq. (2.1), where $R_{sys,exp}$ is the experimental load-bearing capacity of the 2-beams assembled system and $R_{sys,mod}$ is the theoretical load-bearing capacity predicted by the model, see Figure 2.5a.

$$\theta_G = \frac{R_{sys,exp}}{R_{sys,mod}} \tag{2.1}$$

The local random variable θ_E is defined in Eq. (2.2), where $E_{j,mod}$ is the theoretical action effect in each member of the system (predicted by the model) and $E_{j,exp}$ is the experimental action effect for the theoretical load-bearing capacity ($R_{sys,mod}$). The random variables are graphically illustrated in Figure 2.5a. The action effects (E_j) are proportional to the force carried by each beam (F_j) at each load step where j is the index of the beam used to assemble the system.

$$\theta_{E,j} = \frac{E_{j,exp}}{E_{j,mod}} = \frac{F_{j,exp}}{F_{j,mod}} \qquad \text{with} \qquad j=[1,2] \tag{2.2}$$

As already mentioned, the aim of the present work is to investigate the model uncertainty in action effects related to the modelling of the mechanical behaviour. The model uncertainty related to calculation of the sectional resistance is not considered, in fact, it is removed by equalling the theoretical predicted resistance of each member of the system to the experimental value.

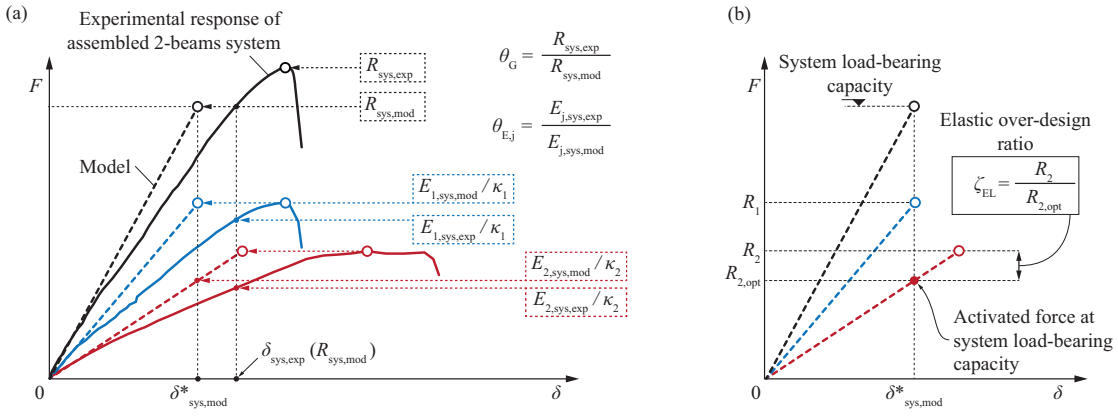

Figure 2.5: (a) Global and local random variable definition, respectively θ_G and θ_E, for the shear force at the support $\kappa_1 = \kappa_2 = 0.5$ and for the bending moment at midspan $\kappa_1 = 4/l_1$ and $\kappa_2 = 4/l_2$; (b) elastic over-design ratio definition, ζ_{EL}

2.3.2 Elastic over-design ratio

Overdesign of a section can result from several sources. Generally, structures are dimensioned by considering the envelope of action effects calculated using a linear elastic uncracked model for the relevant load combinations. As failure can occur for a specific load combination, this leads to some sections being over-designed with respect to others. Another source is often related to detailing and serviceability requirements (like minimal reinforcement ratio, limitation of deformations and cracking control) or fatigue and fire requirements. In addition, the effective amount of reinforcement provided is often slightly larger than calculated, to accommodate commercially available reinforcement bars and convenient spacings. Sometimes, simplicity of construction leads to uniform reinforcement diameters, leading to possible over-design. Finally, if various failure modes are involved, the uncertainty of the resistance model could also lead to over-design of some sections. To account for these effects, the *elastic over-design ratio*, defined in Eq. (2.3) is introduced to investigate the model uncertainty for action effects.

$$\zeta_{EL} = \frac{R_j}{R_{j,opt}} \tag{2.3}$$

This ratio is graphically represented in Figure 2.5b and, by definition, cannot be lower than 1 as it is calculated on members that do not cause the failure of the system.

2.4 Database and considered models

A database of 93 beams and 75 columns was collected. Tables 2.1 and 2.2 shows details of the beams and columns database. All beams and columns used in the simulations have well documented F-δ experimental responses, including the post-peak branch and well as documented material and geometrical properties. For beams, only 3-points bending tests are considered.

Among the beams included in the database, 46 failed in flexion and 47 in shear. Because one of the aims of this work is to clarify whether a brittle or a ductile mode of failure influences the model uncertainty, the deformation capacity is determined from the reported load-deformation relationships. To this aim, the indicator of the deformation capacity of each beam is calculated as the ratio between the deformation at 90% of the experimental post-peak branch δ_R and the predicted elastic uncracked ultimate displacement δ_y, see Figure 2.6a for a graphical representation.

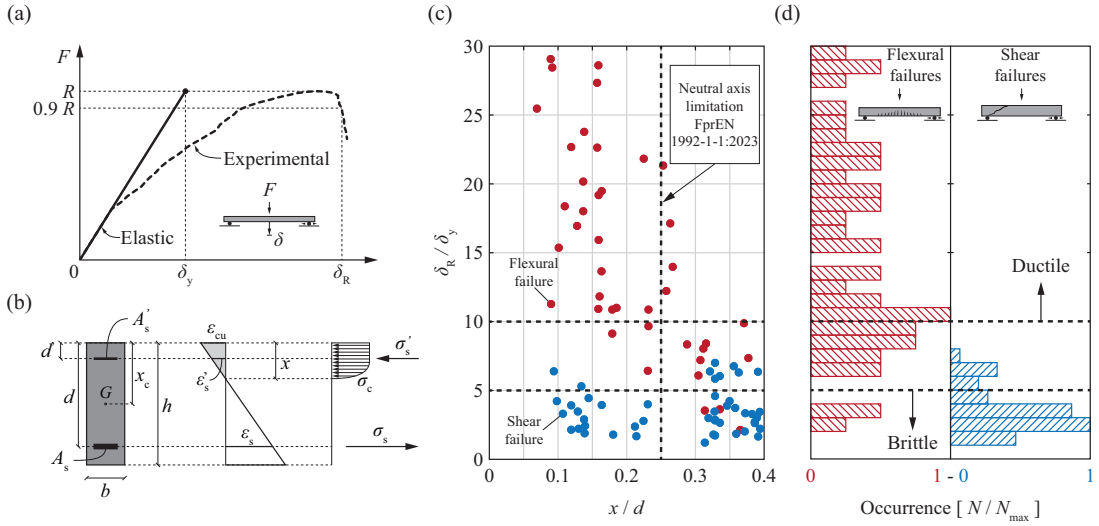

Figure 2.6: *(a) F-δ response of a beam tested in a 3-point bending setup with definition of δ_y and δ_R; (b) strain profile of a RC beam section at Ultimate Limit State (ULS); (c) beams grouped based on their deformation capacity ratio at failure, failure modes and the neutral axis depth; (d) histogram of the deformation capacity ratio by failure mode (bending in red and shear in blue).*

Table 2.1: Database of beams tested in a 3-points bending setup

Reference	Number of tests	Span l_b [mm]	Effective depth d [mm]	Long. reinf. ratio ρ_l [%]	Shear reinf. ratio ρ_w [%]	f_c [MPa]	f_y [MPa]
[Hug82]	5	1600-2700	175	0.32-2.29	0.15-0.26	44.4	460
[Bos93]	21	2000-6000	176-565	0.13-1.94	0.13-0.38	30.9	587-595
[Big93]	2	2000	170	0.30-1.22	0	34.4-35.3	562-573
[Shi99]	11	645-1075	215	3.77	0.45-1.81	52.0	414
[Ang99]	8	5400	875-925	0.50-1.75	0-0.08	21.0-38.0	550
[Yos00]	1	10800	1890	0.74	0	33.6	455
[Vec04]	12	3600-6840	457	1.72-3.46	0-0.20	22.6-43.5	440-445
[Saa09]	3	3000	372	1.51	0-0.21	55.2	464
[Fuj09]	2	1400	210	2.46	0.5	42.0	418-426
[Lau10]	3	4200	340-348	0.23-2.10	0.36	35.3-45.9	336-507
[Lee11]	6	1175-1952	235-244	3.29-3.60	0.22-0.32	37.0-42.2	402-436
[Fuj14]	6	1400	160-210	0.84	0-0.19	40.3	510-520
[Cav15]	4	2800-7700	556	0.89	0	32.6-35.6	713
[Adh15]	6	1600	140-210	0.80-1.6	0-0.20	39.9	520
[Zha17]	3	3000-5000	460	1.37	0.09-0.19	23.8-27.0	495

Table 2.2: Database of columns tested under uniaxial compression

Reference.	Number of tests	Width b_c [mm]	Slenderness ratio λ_G	ρ_l [%]	f_c [MPa]	f_y [MPa]
[She80]	24	305	4.0	1.72-3.66	31.3-40.0	372-438
[Li16]	19	200-600	3.0-4.5	1.50-2.50	33.2	247-475
[Du17]	6	267-600	3.0	0.28	42.8	458-494
[Jin17]	26	267-600	3.0	0.28	42.8	458-494

The failure is assumed to be ductile if the deformation capacity ratio is larger than 10 and brittle if it is smaller than 5 (intermediate behaviour for $5 \leq \delta_R / \delta_y \leq 10$). Figure 2.6c shows the deformation capacity ratio plotted against the depth of the neutral axis calculated according to FprEN1992-1-1:2023 [Eur23] (see definition in Figure 2.6b). It can be observed that beams that fail in bending and respect the condition imposed by FprEN1992-1-1:2023 for performing plastic analyses ($x/d \leq 0.25$) [Eur23], generally exhibit a ductile behaviour. As shown in Figure 2.6c and in the histograms of Figure 2.6d, shear failures lead to brittle or intermediate behaviour.

All columns included in the database have a square cross section (width b_c between 250 and 600 mm) and a geometrical slenderness ratio of the specimen λ_G, (defined as the ratio of the height of the column over the width b_c) between 3 and 4. None of the columns exhibit a buckling failure.

2.4.1 Moment-curvature relationships and calculation models

Besides the Linear Elastic Uncracked model (LEU), five additional models are considered to evaluate the model uncertainty in action effects. An overview of the models is given in Table 2.3 and the corresponding M-χ relationships are shown in Figure 2.7a.

For the LEU model, the flexural stiffness is calculated according to Eq. (2.4). In the Linear Elastic Fully-Cracked model (LEFC), and all sections are assumed to be fully cracked before applying the load, the flexural stiffness is calculated according to Eq. (2.5) where the location of the neutral axis is calculated according to Eq. (2.6).

$$EI_{LEU} = E_c \cdot \frac{b \cdot h^3}{12} \tag{2.4}$$

$$EI_{LEFC} = b \cdot d^3 \cdot E_c \cdot \left[\frac{1}{3} \cdot \left(\frac{x}{d} \right)^3 + n \cdot \rho_l \cdot \left(1 - \frac{x}{d} \right)^2 + n \cdot \rho_l' \cdot \left(\frac{d'}{d} \cdot \frac{x}{d} \right)^2 \right] \tag{2.5}$$

$$x = d \cdot (\rho + \rho') \cdot n \cdot \left(\sqrt{1 + 2 \cdot \frac{\rho + \rho' \cdot \frac{d'}{d}}{n \cdot (\rho + \rho')^2}} - 1 \right) \quad \text{with} \quad \rho = \frac{A_s}{b \cdot d} \qquad \rho' = \frac{A'_s}{b \cdot d} \tag{2.6}$$

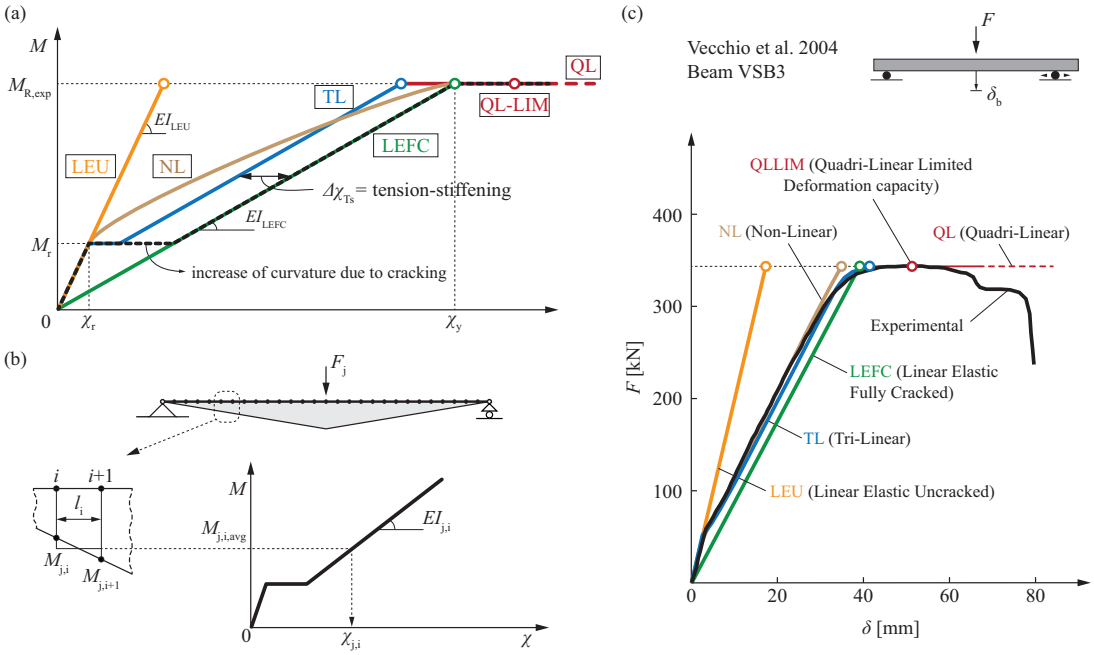

*Figure 2.7: (a) Assumed M-χ relationships for the various models; (b) computation of the deflection; (c) example of the experimental and predicted F-δ responses for beam VSB3 [*Vec04*].*

Where $n = E_s/E_c$ is the ratio between elastic moduli of steel and concrete. In the Tri-Linear model (TL), the section is uncracked until the cracking moment M_r acacording to Eq. (2.7) is reached. For cracked sections, tension stiffening is accounted for by shifting the M-χ line by a value equal to $\Delta\chi t_s$, calculated according to Eq. (2.8), as shown in Figure 2.7a, see [Mut08]. The Quadri-Linear model, with and without limitation of the deformation capacity, respectively QL and QL-LIM, is identical to the TL model up to the level of the resisting moment M_R. Thereafter, the M-χ relationship has an infinite plastic plateau in the QL model while in the QL-LIM model, the curvature is limited to match the experimental displacement at peak load. Finally, the behaviour of the Non-Linear model (NL), in brown in Figure 2.7a, is obtained by discretizing the section in fibres, with each concrete fibre having a uniaxial stress-strain response calculated according to FprEN1992-1-1:2023 [Eur23] for the compression zone and an elastic-brittle behaviour in tension. The reinforcement is modelled by fibres with an elastic-perfectly plastic stress-strain response.

$$M_r = f_{ct} \cdot \frac{EI_{LEU}}{E_c \cdot (h - x)} \tag{2.7}$$

$$\Delta\chi_{Ts} = \frac{3}{8} \cdot \frac{1}{n \cdot \rho_T} \cdot \chi_r \qquad \rho_T = \rho \cdot \frac{5 \cdot d}{h} \qquad \chi_r = \frac{M_r}{EI} \tag{2.8}$$

Figure 2.7b shows the methodology used for calculating the force-displacement relationship of the simply supported beams for the TL model. At each load step, the beam is discretized and the displacement is calculated by updating the flexural stiffness of each element based on the calculated bending moment. For beams without shear reinforcement, the displacement due to shear deformations is calculated using the mechanical model proposed by [Can22], which is based on [Cav15]. For beams contain shear reinforcement, the model proposed by [Col78] is used. Figure 2.7c shows the experimental *F-δ* response of a simply supported beam (in black, beam VSB3 by [Vec04]) and the theoretical response predicted by the various models.

Table 2.3: Implemented models for beams

Model	Abbreviation	M-χ	Section	Shear deformation	Tension stiffening	Concrete σ-ε	Steel σ-ε
Linear Elastic Uncracked	LEU	Linear	Uncracked	No	No	Elastic	Elastic
Linear Elastic Fully-Cracked	LEFC	Linear	Fully-cracked	No	No	Parabola-rectangle [Eur23]	Elastic
Tri-Linear	TL	Tri-Linear	Uncracked / Fully-cracked	Non-linear	Yes	Parabola-rectangle [Eur23]	Elastic / Plastic
Quadri-Linear	QL	Quadri-Linear	Uncracked / Fully-cracked	Non-linear	Yes	Parabola-rectangle [Eur23]	Elastic / Plastic
Quadri-Linear-Limited	QL-LIM	Quadri-Linear	Uncracked / Fully-cracked	Non-linear	Yes	Parabola-rectangle [Eur23]	Elastic / Plastic
Non-Linear	NL	Non-Linear	Variable	Linear	No	Parabola-rectangle [Eur23]	Elastic / Plastic

The *F-δ* response of the columns is modelled using either a linear elastic model (LE) or a non-linear model (NL). In the LE model, both concrete and the reinforcement constitutive laws are assumed linear-elastic, Figure 2.8a. In the non-linear model (NL), the constitutive law of concrete proposed by Guidotti et al. 2011 [Gui11] is used, and the increase of strength and deformation capacity due to transverse reinforcement is considered according to [Fer07]. The reinforcement is modelled by an elastic-perfectly plastic stress-strain behaviour. Figure 2.8b shows the experimental *F-δ* response of a column tested under uniaxial compression (column CAM1 by [Du17]) and the theoretical response predicted by the two models.

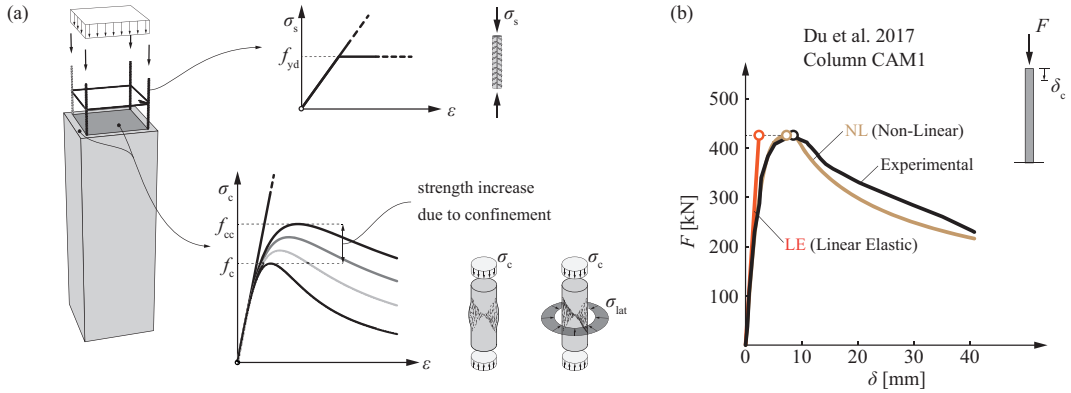

Figure 2.8: *(a) Materials stress-strain for linear elastic and non-linear model; (b) example of the experimental and predicted F-δ responses for column CAM1 [Du17].*

2.4.2 Examples of two-beams assembled systems

Figure 2.9 shows the experimental and theoretical response, as predicted by the Linear Elastic Uncracked model, of three characteristic systems. In Figure 2.9a, the failure of the system is controlled by beam 1 in the experimental response and by beam 2 in the model prediction. Due to concrete cracking, the relative decrease of flexural stiffness for beam 2 is larger than for beam 1 and, since beam 1 fails in a brittle manner, so does the assembled system. This cannot be predicted by the LEU model, that in this case leads to an unsafe prediction (load-bearing capacity larger than the experimental value, $\theta_G < 1$). A slightly larger theoretical load-bearing capacity with respect to the experimental is also observed in Figure 2.9b, where both beams have a relatively ductile behaviour, but their peak resistance occurs for significantly different displacements. A rather different result is shown, however, in Figure 2.9c, where the experimental peak resistance is reached for a similar displacement in both beams, leading to a experimental load-bearing capacity of the 2-beams system which is larger than the value predicted by the model. It must be noted that the examples in Figure 2.9 are for illustrative purposes and are not exhaustive.

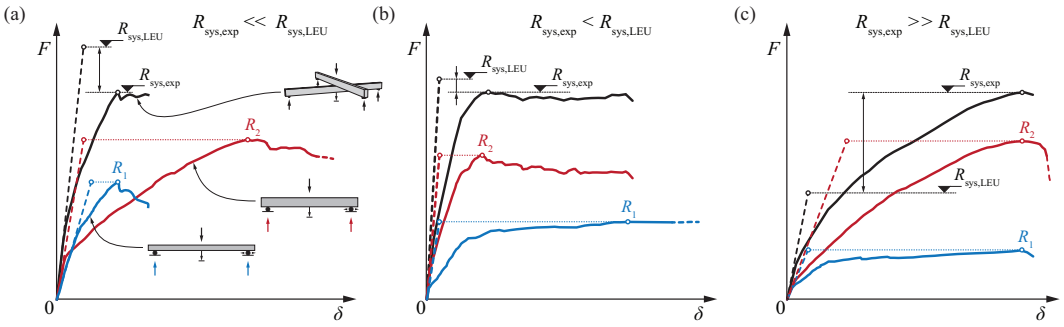

Figure 2.9: Examples of theoretical (Linear Elastic Uncracked model) and experimental response of 2-beams assembled systems: (a) beam DB0530M [Ang99] and S130 [Lee11]; (b) beam DR572 [Adh15] and T1A1[Bos93]; (c) beam DR382[Adh15] and VSC2[Vec04].

2.5 Results and distribution fitting

The combination of the 93 beams described in Table 2.1 allows to produce up to 4278 two-beams systems with the corresponding experimental behaviours. For all assembled systems, the internal forces and the theoretical load-bearing capacities have been determined according to the models defined above. Figure 2.10a shows the log-normal probability-plot of θ_E defined in Eq. (2.2) where the internal forces $E_{j,mod}$ are calculated using the linear elastic uncracked model (LEU). the logarithm of the random variable (x-axis) is plotted against the normal quantile in terms of standard deviation σ (y-axis). The red, blue and green distributions correspond respectively to ζ_{EL} smaller than 1.1, 1.25 and 5 while the continuous line represents the fitting LN distribution. This type of graphical representation allows to graphically verify if a LN distribution is a good fit for a random variable. In fact, data lying on a straight line indicate an exact LN distribution and the slope corresponds to the coefficient of variation (CoV). Whether a LN distribution is suitable to represent the tail of the distribution has already been discussed in the past. According to [Dit94], to compare different propositions, a simple fitting criterion with an arbitrary choice of the distribution is practically non-verifiable and there is a need to have standardized distribution types to perform adequate comparisons. The present Chapter accounts for these considerations and, accordingly, a LN distribution is adopted to describe θ_E and θ_G. In fact, besides being a good fit for the distribution of θ_E as shown in Figure 2.10, the comparison with the recommendations of [JCS01] is facilitated.

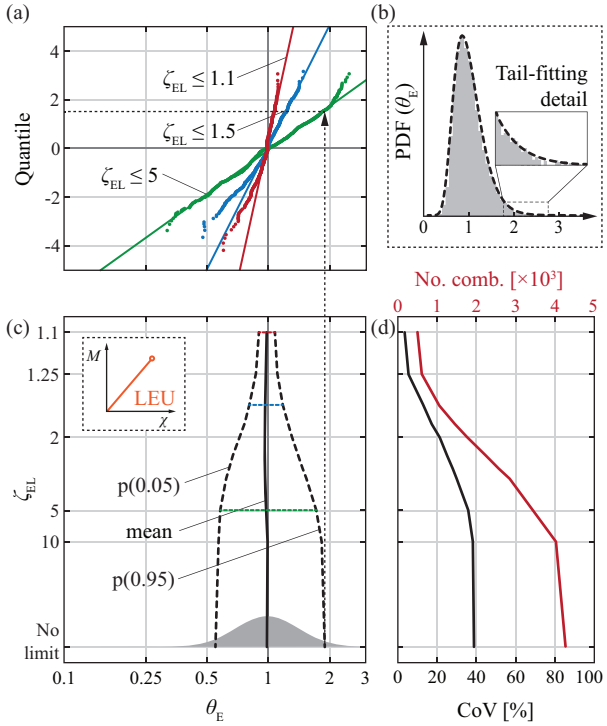

Figure 2.10: *(a) Probability plot of θ_E using a Linear Elastic Uncracked model and (b) detail of the tail fitting; (c) graphical representation of the distribution parameters with varying elastic over-design ratio; (d) CoV (black) and number of combinations (red).*

It can be observed that the LN distribution is a good fit for the distribution, including the tail regions. Figure 2.10b shows the histogram of θ_E and the detail of the upper tail fitting. Because θ_E is defined as the ratio between the experimental action effect and the calculated one, the values in the upper tail region are the unsafe cases where $E_{exp} > E_{mod}$. The dashed line in Figure 2.10a represents the fitting of the data with a LN distribution (fitting performed using a linear least-squares fitting algorithm, tail values larger than the 95th percentile of the data are weighted by a factor equal to 2).

Figure 2.10c shows the distribution parameters of θ_E (mean, 5th and 95th percentile) with varying elastic over-design ratio (ζ_{EL}). If one of the beams is largely over-designed compared to the other (large ζ_{EL}), redistribution of the force is more likely to occur, resulting in a larger uncertainty in determining action effects and leading to an increase of the coefficient of variation of θ_E, see Figure 2.10d. However, as shown in Figure 2.4d, if the elastic over-design ratio is very large ($\zeta_{EL} > 2$), the assembled system is not necessarily representative of a practical case. In Figure 2.10c, it can be observed that the mean of the distribution is always close to unity. This is due to the fact that, if the action effect is overestimated in one member, it is generally underestimated in the other. The red line in Figure 2.10d shows the number of systems that is

possible to assemble for a given limit of ζ_{EL}. At least 500 systems are analysed for each ζ_{EL} value, which is sufficient to perform statistical analyses.

2.5.1 Discussion of the results

Using the same format proposed in Figure 2.10, Figure 2.11a shows the distribution parameters of θ_E (mean, 95th percentile and CoV) for the LEU, LEFC, TL and NL models (the results of the LEU model are already discussed in the previous section, they are presented again to allow for a comparison). For the LEFC model, very large CoVs can be observed. This is due to the fact that the flexural stiffness can be largely underestimated. For instance, if the failure of the system occurs with limited cracking in one of the beams (actual experimental behaviour), the action effect can be considerably underestimated considering the beam fully cracked. The probability for this scenario to occur is larger for large values of ζ_{EL} since the system has a higher probability to fail with one member still in the uncracked state. On the other hand, for the tri-linear (TL) and the non-linear model (NL), ζ_{EL} has a limited influence on the distribution of θ_E. In fact, for these models, the flexural stiffness depends on the load level, leading to a satisfactory prediction of the displacement and the internal forces for each load step. Since non-linear shear deformations and tension stiffening are considered in the tri-linear model (TL), but not in the non-linear model (NL), displacements are generally better predicted for the former and lead to a smaller CoV. Figure 2.11b shows the distribution of θ_E using the LEU model for systems exhibiting brittle and ductile failure modes (for details about the failure mode classification see Figure 2.6). Since the LEU model better describes the behaviour of brittle systems (uncracked section), for a given ζ_{EL} smaller CoVs are obtained for brittle systems than for ductile systems (see Figure 2.11b).

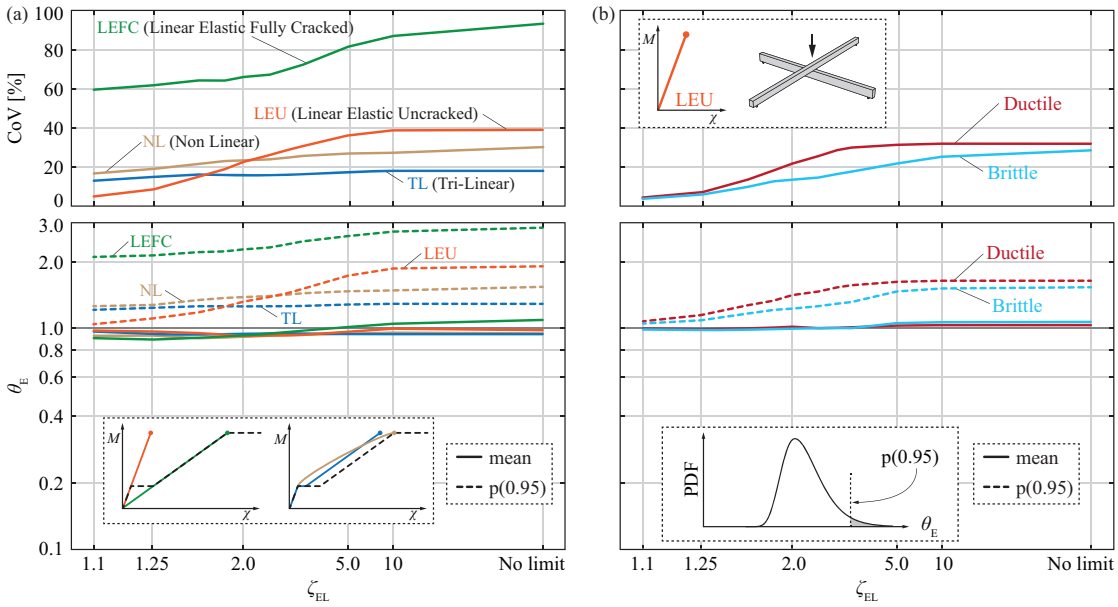

Figure 2.11: CoV (top) and distribution parameters (bottom) of θ_E: (a) for various models and (b) for the Linear Elastic Uncracked model with various ductility degrees.

Figure 2.12 shows the CoV and the distribution parameters of θ_G according to Eq. (2.1) (ratio between the experimental and calculated load-bearing capacities, mean, 5th percentile and CoV) for the various models. Unlike θ_E, for which the values in the upper tail region are the less safe, for θ_G the unsafe values are located in the lower tail ($\theta_G < 1$), where the experimental load-bearing capacity (R_{exp}) is smaller than the one predicted by the model (R_{mod}). As for θ_E, ζ_{EL} does not influence the distribution of θ_G for the TL and NL models. On the other hand, it does for the LEU and LEFC models, but this influence is less pronounced than for θ_E. Two major trends can be identified: (1) the mean value of θ_G tends towards unity with increasing refinement of the model (see continuous lines in the bottom of Figure 2.12); (2) the CoV decreases with increasing refinement of the model (top of Figure 2.12). The combination of these two phenomena leads to a 5th percentile of the distributions which is almost constant ($p(0.05) \sim 0.95$-0.98 for all the analysed models) despite the fact that the complexity and the calculation time for refined models increases considerably. A good compromise for estimating the load-bearing capacity of the system is achieved by using the LEFC model which does not require an iterative process for the assessment of an existing structure, but for which the reinforcement needs to be known in each section to determine the fully cracked flexural stiffness (this means that for designing a new structure, an iteration is needed).

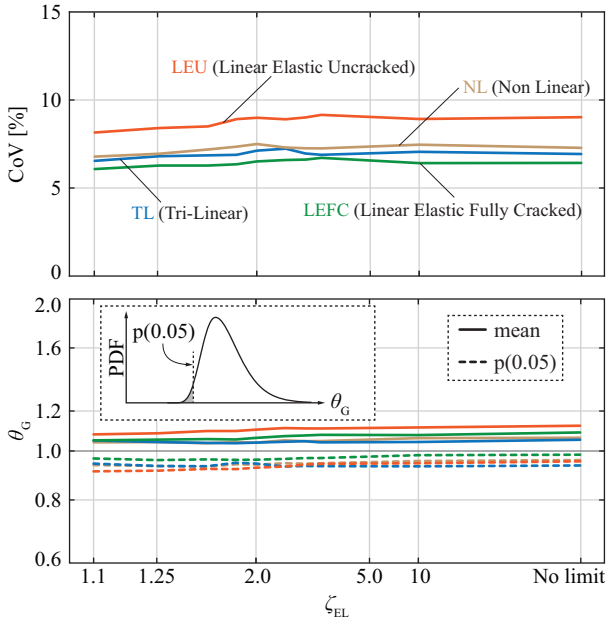

Figure 2.12: CoV (top) and distribution parameters (bottom) of θ_G for various models

Figure 2.13 shows the statistical values of θ_G for brittle and ductile systems using the LEU and the TL models. As already mentioned, ζ_{EL} only influences the results of the distribution of θ_G for the LEU model whereas it has no influence for the TL model. For both models, brittle systems exhibit a larger CoV compared to ductile systems (see Figure 2.13, top). Also, due to the redistribution of forces, the mean value of the distribution is larger for ductile systems. In fact, both the TL and the LEU model do not consider plastic deformations, thus underestimating on average the load-bearing capacity for ductile systems and leading to a larger safety margin ($R_{sys,exp} > R_{sys,mod}$). This does not occur for brittle systems that do not undergo plastic deformations, leading to mean values closer to unity. The combination of these two effects leads to a larger 5th percentile of θ_G for ductile systems (~ 1.00) compared to brittle systems (~ 0.90).

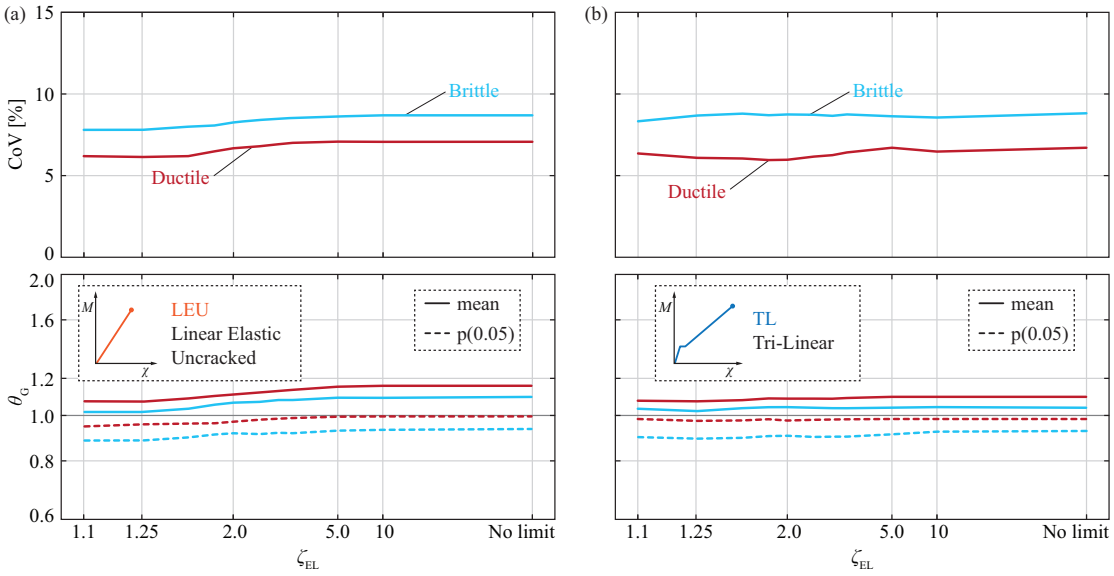

Figure 2.13: CoV (top) and distribution parameters (bottom) of θ_G for ductile and brittle systems: (a) using the LEU (Linear Elastic Uncracked) model and (b) using the TL (Tri-Linear) model.

2.5.2 Plastic models

If a quadrilinear model (Quadri-Linear, QL) with a plastic plateau without deformation limit is used, the results will be identical to a rigid plastic investigation according to limit analysis. In this case, the random variable θ_G cannot be larger than one. In fact, the theoretical load-bearing capacity ($R_{sys,mod}$), is always equal to the sum of the single resistances of the individual beams. For the experimental load-bearing capacity of the system ($R_{sys,exp}$), this scenario occurs only if the experimental peak resistance of the individual beams in the 2-beams assembled system is reached for the same displacement, as shown in Figure 2.9c. The CoV of the θ_G values for the QL model are shown in Figure 2.14a. The QL model allows for unlimited redistribution between the members of the 2-beams system. However, the beams included in the database exhibit both brittle and ductile failure modes, thus, redistribution in the assembled 2-beams system can be limited. This leads to large values of CoV for the QL model (see Figure 2.14a). As an example, the probability-plot of θ_G for $\zeta_{EL} \leq 2$ is presented in Figure 2.14c. It must be noted that the mean value of the log-normal distribution it is not meaningful for the cases where the maximum value is limited (i.e. to 1 for the QL model). In fact, in these cases, a log-normal distribution is not suitable to represent the whole distribution but only the lower-tail, see Figure 2.14c for the QL model. However, this choice allows performing comparisons between the different models.

If the deformation capacity of the beams is limited to the experimental displacement at peak resistance, as in the QL-LIM model, the CoV of θ_G decreases and does not depend on ζ_{EL}, see

Figure 2.14a. Moreover, the 5th percentile of the distribution is closer to unity than for the QL model. Also, since the deformation capacity is the same as the experimental one, the predicted load-bearing capacity is not necessarily equal to the sum of the single members resistance and the value of θ_G is not limited to 1.0 as can be observed in Figure 2.14c. If the QL model is used for systems assembled with beams failing in bending and complying with the requirements according to FprEN1992-1-1:2023 [Eur23] (QL-LIM-REQ model), the CoV of θ_G reduces considerably with respect to the QL and QL-LIM models and the 5th percentile is very close to unity, see Figure 2.14a. The limitations mentioned above for the QL-LIM-REQ model are shown in Figure 2.14b and include the depth of the neutral axis according to [Eur23] ($x/d \leq 0.25$, Figure 2.6b) and the relative resistance of the critical sections ($0.5 \leq R_1/R_2 \leq 2$).

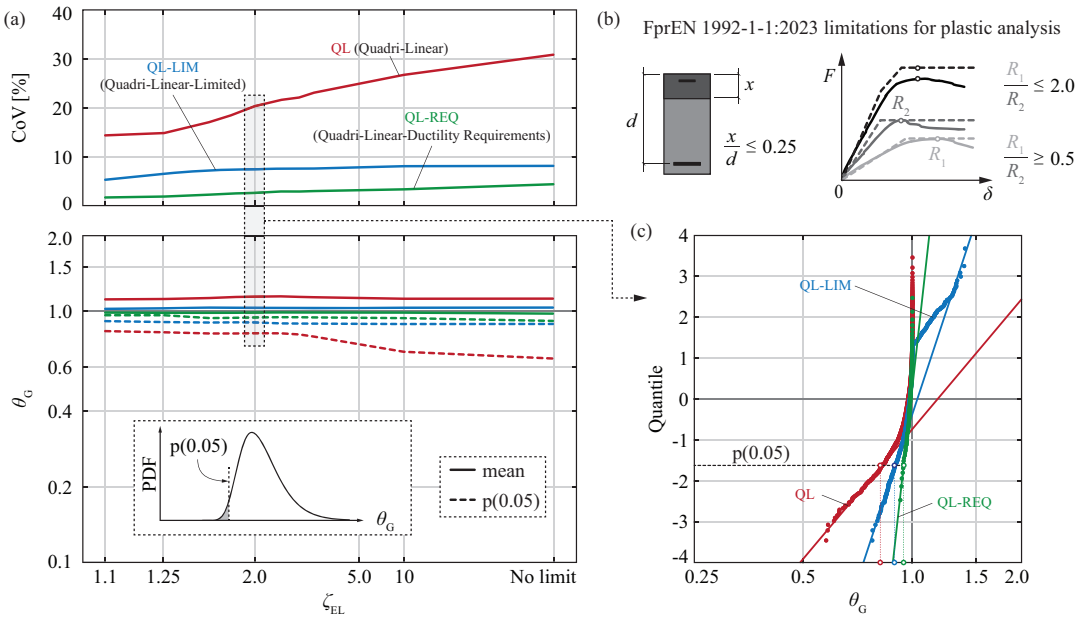

Figure 2.14: *(a) CoV (top) and distribution parameters of θ_G for a Quadri-Linear model with a plastic plateau (QL in red), a Quadri-Linear model with limitation of the deformation capacity (QL-LIM in blue) and a Quadri-Linear model with a plastic plateau used for beams respecting the requirements of FprEN 1992-1-1:2023 (QL-REQ in green); (b) requirements according to FprEN 1992-1-1:2023 [*Eur23*] to perform plastic analyses without explicit checks on the deformation capacity (QL-REQ model); (c) probability plots for the presented models with $\zeta_{EL} = 2$*

2.5.3 Deformability of supports

Figure 2.15 shows the comparison of the 2-beams system investigated above with the same system supported on columns (see insert in Figure 2.15a). A slenderness ratio $\lambda_G = 10$ is

considered for all columns without accounting for 2nd order effects and only cases where column resistance is not governing are considered. The load-deformation relationships are produced with the methodology presented in Figure 2.3d. The results are presented in Figure 2.15 in terms of CoV and mean values of θ_E and θ_G (case with $\zeta_{EL} = 1.1$). Regardless of the model considered, the CoV of θ_E shows a decrease of 1 to 3% while the mean values of θ_E also decrease. With respect to θ_G defined as in Eq. (2.1), a reduction of the mean values and the CoV can also be observed (minor reduction in the case of the CoV). These results can be explained by the fact that the deformability of supports leads to an increased redistribution of forces.

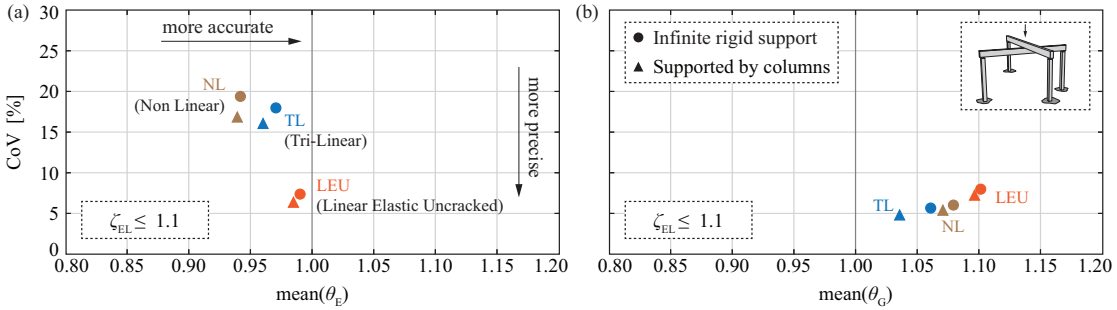

Figure 2.15: CoV and mean values of the of (a) θ_E and (b) θ_G for the 2-beams system on infinitely rigid supports and supported by columns (slenderness ratio $\lambda_G = 10$)

2.6 Case study: reinforced concrete frame

As already mentioned, the model uncertainties related to the calculation of action effects are usually covered by the partial factors for permanent and variable actions (γ_G and γ_Q). In FprEN1990:2022 [CEN22], γ_G and γ_Q are obtained by multiplying γ_{Sd} with γ_g and γ_q, which cover respectively the model uncertainty in action effects and the uncertainty in the representative values of the actions, see Figure 2.2. To estimate the value of γ_{Sd} based on the distribution parameters of θ_E, reliability analyses are performed on the 1st floor beam of the RC frame, shown presented in Figure 2.16. To account for various ratios between structural and non-structural self-weight, the spacing between frames, s, is varied between 4 and 12 m, see Figure 2.16b. The building is designed for a design life of 50 years and for various intended uses. For each intended use, design loads are assumed according to [Eur02]. Only gravity actions are considered, wind and seismic actions are assumed to be carried by a bracing system. In all case studies, action effects are calculated using a linear elastic model with uncracked sectional stiffness (LEU).

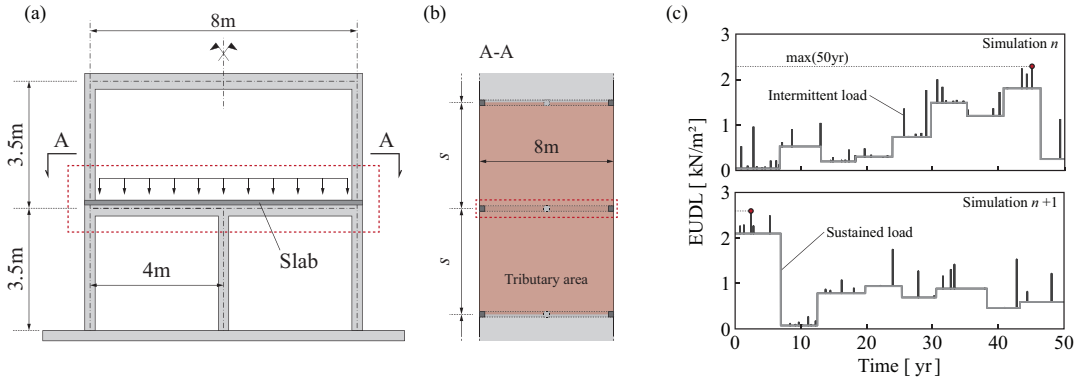

Figure 2.16: (a) Elevation and (b) plan view of the investigated office building; (c) simulations of 50 year live load for s=6 m

The variability of the structural self-weight, denoted by G_1, is modelled considering the geometrical and the specific weight variability according to [JCS01]. For non-structural self-weight, G_2, a general model is not available since it largely depends on the types of building and on common construction practices of different countries. In this work, the variability of G_2 is modelled using a discrete choice model to consider a large number of possible combinations of screed, insulation, flooring, ceiling and partition walls. For each of the above components, mean values and CoV are defined based on experience on similar buildings in Switzerland. Figure 2.17a shows the normal probability-plot of G_1 and G_2 distribution resulting from 10'000 simulations. Besides showing that a normal distribution is a good fit for G_1 and G_2, it can be observed that the CoV of G_2 is much larger that of CoV of G_1, which reflect the large variability of non-structural self-weight in buildings. These results refer to a building with an intended use as an office and a spacing s equal to 6 m. The live load, Q, is modelled according to part 2 of the JCSS report [JCS01] with the tributary area assumed as shown in Figure 2.16b (shaded red area). Each simulation lasts 50 years and leads to a maximum value of EUDL (Equivalent Uniform Distributed Load) as shown in Figure 2.16c. Figure 2.17b shows the log-normal probability-plot of the live load distribution, Q, resulting from 10'000 simulations. It confirms that a LN distribution is a good fit for the distribution of Q. Besides the office space, the other investigated uses are: residence, hotel, lobby, retail and classroom. The same methodology described above and shown in Figure 2.16c is used to determine the distribution of Q for each intended use and spacing of the frame, s.

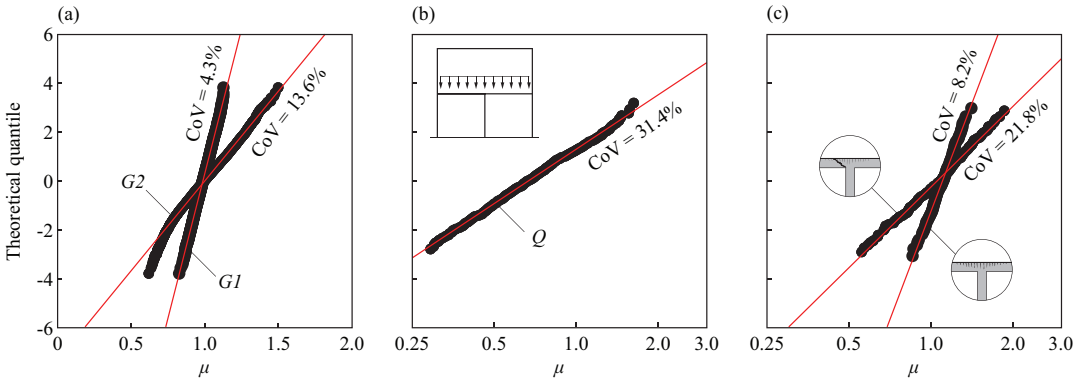

Figure 2.17: (a) Normal probability-plot of G_1 and G_2; (b) log-normal probability-plot of Q; (c) log-normal probability plot of the sectional resistance R for flexural failure and shear failure; s=6m, intended use as office, design life of 50 years.

Table 2.4 presents the characteristic load values and the distribution parameters as a function of the spacing *s* for an intended use as office space. The representative value of the non-structural self-weight is calculated considering the mean values of the discrete choice model. It has to be noted that, according to EC1 [Eur02] linear load of partition walls cannot exceed 3 kN/m to assume the load uniformly distributed. This threshold is satisfied in the discrete choice model used for calculating the distribution of G_2.

Table 2.4: Characteristic value and distribution parameters of G_1, G_2 and Q for an intended use of the building as office space and increasing spacing (s) between frames

s [m]	G_{1k} [kN/m]	G_{2k} [kN/m]	Q_k [kN/m]	G_{1k}/G_{2k}	G/Q	Distributions G_1 [kN/m]		G_2 [kN/m]		Q [kN/m]	
						Mean	CoV [%]	Mean	CoV [%]	Mean	CoV [%]
4	17.43	12.4	12	1.41	2.49	0.99	4.48	12.88	13.59	0.79	35.00
5	24.15	15.5	15	1.56	2.64	0.99	4.42	16.10	13.59	0.73	32.73
6	31.88	18.6	18	1.71	2.80	0.99	4.34	19.32	13.59	0.69	31.41
7	40.38	21.7	21	1.86	2.96	0.99	4.29	22.54	13.59	0.66	30.23
8	48.03	24.8	24	1.94	3.03	0.99	4.27	25.76	13.59	0.63	29.38
9	58.28	27.9	27	2.09	3.19	0.99	4.23	28.98	13.59	0.61	28.71
10	67.18	31	30	2.17	3.27	0.99	4.21	32.20	13.59	0.60	27.84
11	79.18	34.1	33	2.32	3.43	0.99	4.18	35.42	13.59	0.59	27.90
12	92.25	37.2	36	2.48	3.60	0.99	4.15	38.64	13.59	0.57	27.59

The shear resistance and resisting bending moment, denoted respectively with R_{Shear} and R_{Flex}, are calculated according to Chapter 8 of FprEN1992-1-1:2023 while their variability is calculated using the statistical distributions of materials strength, geometric and models variabilities according to annex A of FprEN1992-1-1:2023 [Eur23], see background documents

[Mut23] for details. Figure 2.17c shows that a log-normal distribution is a good fit for both resisting moment and shear resistance calculation variabilities. It can also be observed that the CoV of the shear resistance calculation is much larger than the resisting moment calculation. This is mainly due to the large uncertainty in the model uncertainty for the calculation of the shear resistance for members with shear reinforcement, see [Pej22].

Table 2.5: Statistical parameters of the random variables used to perform reliability analysis for the investigated case studies. If a range is given, the value varies for buildings with different spacing s and intended use.

Variable	Distribution	μ	V [%]
E_{G1}	Normal	0.98-1.00	4.1-4.9
E_{G2}	Normal	1.00	13.6
E_{Q}	Log-normal	0.55-0.80	19.1-58.3
$R_{Flex.}$	Log-normal	1.09-1.12	8.1-8.4
R_{Shear}	Log-normal	1.07-1.14	20.4-22.9
θ_E	Log-normal	1.00	6.5

Table 2.5 presents the distribution parameters of the random variables used to perform the reliability analyses for all the investigated case studies. The limit state function is formulated in the classical form as shown in Eq. (2.9). The uncertainty in calculating action effects is considered as an independent random variable that multiplies the action effects calculated using the adopted mechanical model. In the presented case studies, a Linear Elastic Uncracked (LEU) model is adopted, and each section is designed so that $R/E = 1$. Therefore, the distribution of θ_E is assumed for a LEU mechanical behaviour considering $\zeta_{EL} \leq 1.1$ as shown in Table 2.5, see Figure 2.11.

$$g(R,E) = R - E = R - (E_{G1} + E_{G2} + E_Q) \cdot \theta_E \tag{2.9}$$

$$\gamma_{Sd} = \mu_{\theta E} \cdot \exp(\alpha_{\theta E} \cdot \beta_{tgt} \cdot V_{\theta E}) \qquad \text{with} \qquad V_{\theta E} < 20\% \tag{2.10}$$

Sensitivity factors α, are calculated for each variable using the FORM (First Order Reliability Method) analysis. Based on the sensitivity factor relative to the model uncertainty in action effects ($\alpha_{\theta E}$), the partial safety factor γ_{Sd} is calculated using Eq. (2.10) where $\beta_{tgt,50y}$ is assumed equal to 3.8 according to FprEN1990:2022 [CEN22]. The choice of β_{tgt} depends on the level of risk acceptance at the societal level and is not treated in this work. For details regarding the FORM analysis and the derivation of the partial safety factors, refer to [Sch17]. In addition to the case studies described above, a parametric study was performed to investigate the influence of V_Q, V_R and G/Q on γ_{Sd}. In particular, V_Q is varied between 15 and 70%, V_R is varied between 5 and 25% and G/Q is assumed equal to 1.5 and 3.5, where $G = G_1 + G_2$.

Figure 2.18a and 2.18b present the results of the parametric analysis while Figure 2.18c and 2.18d present the results of the investigated case studies. For all plots two axis labels are

provided, on the left axis indicating the value of $\alpha_{\theta E}$, on the right indicating the corresponding value of γ_{Sd} calculated using Eq. (2.10).

Figure 2.18a shows the variation of $\alpha_{\theta E}$ and γ_{Sd} as a function of V_Q for various values of V_R while Figure 2.18b shows the variation of $\alpha_{\theta E}$ and γ_{Sd} for two selected values of V_R with G/Q equal to 1.5 and 3.5. Generally, results from the parametric analyses show that $\alpha_{\theta E}$, and consequently γ_{Sd}, decrease with increasing values of V_R and V_Q. Also, the ratio G / Q has no influence if V_R is large, on the other hand, if V_R is small, an increase of γ_{Sd} is observed for larger values of G/Q. Figures 2.18c and 2.18d show that the results obtained from the investigated case studies are within the boundaries found with the parametric analyses.

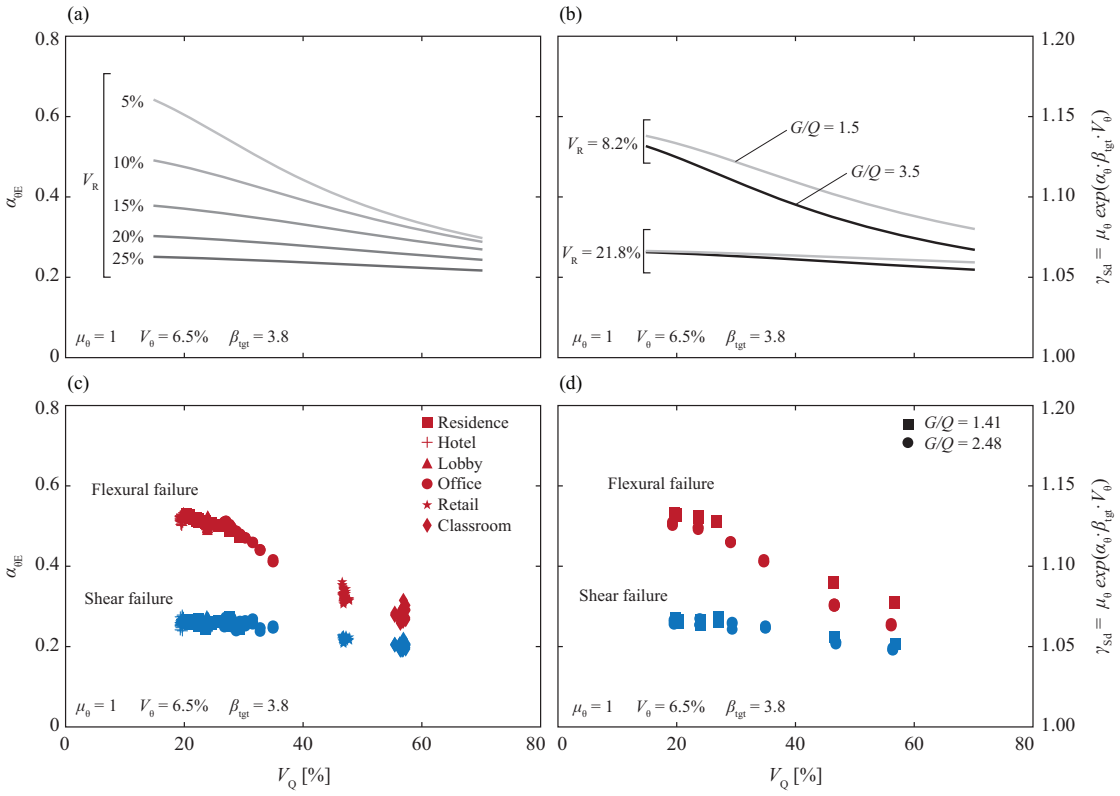

Figure 2.18: $\alpha_{\theta E}$ and corresponding γ_{Sd} as a function of V_Q resulting from: (a) parametric analysis for various V_R; (b) parametric analysis for two selected V_R and G/Q = 1.5 and 3.5; (c) case studies for various V_R; (d) case studies for two selected V_R and G/Q = 1.5 and 3.5

These results can be explained considering that the sensitivity factors, α, represent the weight of each random variable for a defined limit state function and the sum of their square is equal to unity by definition. Thus, if the weight of one variable increases in the limit state function, the weight of the other variables must decrease. This explains the finding that for flexural failures (with lower CoVs of the resistance model), the required γ_{Sd} factor is larger than for shear failures (where the CoV of the resistance model is significantly larger). Nevertheless, this influence can

be compensated by the fact that for flexural failures, which are typically more ductile than shear failures (see Figure 2.6), the load-bearing capacity shows smaller uncertainties (smaller CoV and higher mean value of ratio θ_G as shown in Figure 2.13). In other words, underestimating an action effect when the behaviour is ductile behaviour has typically smaller consequences then when it is brittle.

Based on the results of the parametric analysis, the performed simulations and the obtained distributions of θ_E, it is reasonable to assume a value of γ_{Sd} between 1.05 and 1.15 as initially specified by [CEB59] but based on significantly different motivations. It is important to note that the model uncertainty related to changes of the structural system during construction (including the redistributions due to creep) is not covered by the estimation of the factor γ_{Sd} presented in this Chapter. This means that for structural systems subjected to significant system changes (e.g. high-rise buildings), a sensitivity analysis should be performed to determine the most relevant parameters influencing the calculation of action effects and load bearing capacity.

It is a matter of fact that the model uncertainty related to the action effects significantly depends on the complexity and the level of statical indeterminacy of the structure. In fact, only the influence of geometrical uncertainties can have an influence in statically determinate structures, whereas the uncertainties can increase for highly indeterminate complex structures. In addition, for complex structures, additional uncertainties can be expected with respect to the models implemented in commercial analysis software tools and the choices by the designer in modelling the structures. This applies for linear elastic calculations, but also to a larger extent for nonlinear analyses. These considerations, which were not the aim of the present work, deserve to be investigated in the future also accounting for the increasing complexity of the analysis tools used nowadays.

2.7 Conclusions

This Chapter investigates the model uncertainty in action effects and load-bearing capacity calculations for statically indeterminate concrete structures accounting for the type of mechanical model used and for various failure modes. Based on the presented investigations, the main conclusions are:

1. Compared to more refined models, the Linear Elastic Uncracked model leads to larger CoV of model uncertainty in load bearing capacity calculation (θ_G); however, the mean of the distribution is larger, leading to similar tail's distribution, thus, similar safety margin;
2. For Linear Elastic Uncracked models, an over-design of one or more components of a statically indeterminate system influences the CoV of the model uncertainty in action effects calculation (θ_E);

3. Refined calculation models lead to more accurate results and generally to lower CoV of the internal forces ratio θ_E and the load bearing capacity ratio θ_G;
4. The failure mode influences the model uncertainty in load bearing capacity calculation but it does not influence the model uncertainty in action effects calculation. Larger CoVs of θ_G are observed for brittle systems, independently of the calculation model;
5. Plastic calculation models with unlimited deformation capacity, if performed without ductility requirements (QL), lead to very large CoV and can lead to unsafe results. Limiting the deformation capacity, or verifying that ductility requirements are met reduces considerably the CoV.
6. Considering supports deformability allows larger redistribution of forces and leads to slightly smaller CoV.
7. Parametric analyses and investigated case studies show that the partial factor γ_{Sd} to cover the uncertainties of the internal force calculation ranges between 1.05 and 1.15. It must be noted that the estimated γ_{Sd} factor does not account for uncertainties related to structural system variations during construction or structural modelling of complex structures. These additional uncertainties, which deserve to be investigated more in detail, significantly depend on the complexity of the structure, the construction method, the tools used tools and the experience of the designer.

Notation

***Acronyms*:**

RC:	Reinforced Concrete
PSF:	Partial Safety Factor
CoV:	Coefficient of Variation
LE:	Linear Elastic
LEU:	Linear Elastic Uncracked
LEFC:	Linear Elastic Fully-Cracked
NL:	Non-Linear
QL:	Quadri-Linear with plastic plateau
QL-LIM:	Quadri-Linear Limited deformation capacity
QL-REQ:	Quadri-Linear with plastic plateau and ductility requirements
TL:	Tri-Linear

***Variables*:**

F:	Force
δ:	Displacement
δ_y:	Displacement at maximum load predicted with a linear elastic uncracked model
δ_R:	Displacement at 90% of the F-δ post-peak branch
R:	Load-bearing capacity
R_{exp}:	Experimental load-bearing capacity
R_{mod}:	Theoretical predicted load-bearing capacity
M:	Bending moment
M_r:	Cracking bending moment
M_R:	Resisting bending moment
χ:	Curvature
χ_r:	Curvature at the cracking bending moment
χ_R:	Curvature at the resisting bending moment
θ_G:	Global random variable

θ_E: Local random variable

E_{exp}: Experimental action effect

E_{mod}: Theoretical predicted action effect

l_c: Column height

λ_G: Geometrical slenderness of a column (height / width)

l_b: Beam span

b: Width of the section

b_c: Square column section width

d: Effective depth of a cross section

c: Concrete cover

x: Neutral axis depth

x_c: Center of gravity of the concrete section

ρ_l: Bottom longitudinal reinforcement ratio

ρ'_l: Top longitudinal reinforcement ratio

ρ_w: Shear reinforcement ratio

f_c: Concrete compressive strain (uniaxial)

f_{ct}: Concrete tensile strength

f_y: Steel yielding strength

E_c: Concrete elastic modulus

E_s: Steel elastic modulus

n: E_s / E_c

EI: Flexural stiffness

$\Delta\chi_{Ts}$: Decrease of curvature due to tension stiffening

q: Distributed load

Q: Concentrated force

ζ_{EL}: Elastic over-design ratio

γ_F: Partial factor for actions including model uncertainties [CEN22]

γ_f: Partial factor for action values [CEN22]

γ_G: Partial factor for permanent actions including model uncertainties [CEN02]

γ_g:	Partial factor for representative values of permanent actions [CEN02]
γ_Q:	Partial factor for variable actions including model uncertainties [CEN02]
γ_q:	Partial factor for representative values of variable actions [CEN02]
γ_{Sd}:	Partial factor covering uncertainty in action effects (model uncertainty)
γ_M:	Partial factor for the material including model and geometrical uncertainties
γ_m:	Partial factor for material properties
γ_{Rd}:	Partial factor covering uncertainty in the resistance model
F_{rep}:	Representative value of action variables
X_k:	Characteristic value of material strength
a_{nom}:	Nominal value of geometrical variables
E_d:	Design value of actions
R_d:	Design value of resistance
σ:	Standard deviation
α:	Sensitivity factors

This page intentionally left blank.

Chapter 3

Influence of sustained loading on resistance and deformation capacity of reinforced concrete members in compression

This chapter is the post-print version of the following paper:

Malja X., Motlagh H.R.E., Fernández Ruiz M., Muttoni A., *Influence of sustained loading on resistance and deformation capacity of reinforced concrete members in compression*, Structural Concrete, Vol. 24.3, pp. 3656-3673, 2023. https://doi.org/10.1002/suco.202200571

The work presented in this publication was performed by Xhemsi Malja and Hamid Reza Ebrahimi Motlagh under the supervision of Prof. Aurelio Muttoni and Prof. Miguel Fernández Ruiz.

Hamid Reza Ebrahimi Motlagh performed the experimental programme. The main contributions of Xhemsi Malja to this article and chapter are the following:

- comprehensive literature review,
- post-processing of the experimental results,
- interpretation, analysis and discussion of the tests results,
- proposition of a consistent mechanical model,
- design recommendations,
- elaboration of the figures and tables,
- writing of the manuscript.

Abstract

As acknowledged explicitly or implicitly in most of current design codes, a high level of sustained loading has a detrimental effect on the concrete compressive strength. However, its beneficial effect in terms of deformation capacity is neglected in most cases. This latter topic and its practical consequences are addressed in the present work on the basis of an experimental and theoretical investigation. In particular, the development of nonlinear creep strains in structural concrete members is investigated, clarifying the internal redistribution of forces between concrete and the reinforcement. The results of an experimental programme with refined measurements are presented to better understand the phenomenon and to verify the predictions of a mechanical model developed by the authors on the time-dependent response of concrete. The experimental programme consists of 14 prismatic specimens with different reinforcement ratios tested under a wide range of uniaxial stress rates. The results allow clarifying the material response and validating the mechanical model, both in terms of strength reduction and enhancement of deformation capacity. Finally, the results of parametric analyses, performed considering different concrete ages, reinforcement ratios and materials properties are presented to evaluate the practical implications of the findings.

Keywords: reinforced concrete, sustained loading, deformation capacity, strength reduction, stress redistribution, non-linear creep strain

3.1 Introduction

Sustained loading effects on reinforced concrete (RC) structures has attracted many research efforts in the past. The first works focused on low levels of sustained loading, typically below 50% of the compressive concrete strength [Fab28, Wil28, Dav31, Nev55, Flu58]. Such researches were followed by more comprehensive loading levels and patterns, investigating higher levels of sustained loading [Sha49, Rüs56]. Following these works, the term "*sustained loading strength*" was introduced to account for the detrimental effect of sustained loading on the concrete compressive strength. Such value was defined as the maximum stress level at which concrete can be permanently loaded without leading to failure and was set to approximatively 75% of the short-term concrete strength, see Figure 3.1a (a detailed review is available in [Tas18]). Also, the development of creep strains with time and the level of load was investigated [Hog51, Vie56, Rüs60], showing a significant increase of the ultimate strains for long loading durations. Despite the potentially beneficial implications of such increase of deformation capacity, most studies in the following decades still focused primarily on the concrete strength reduction [Sel59, Dia71].

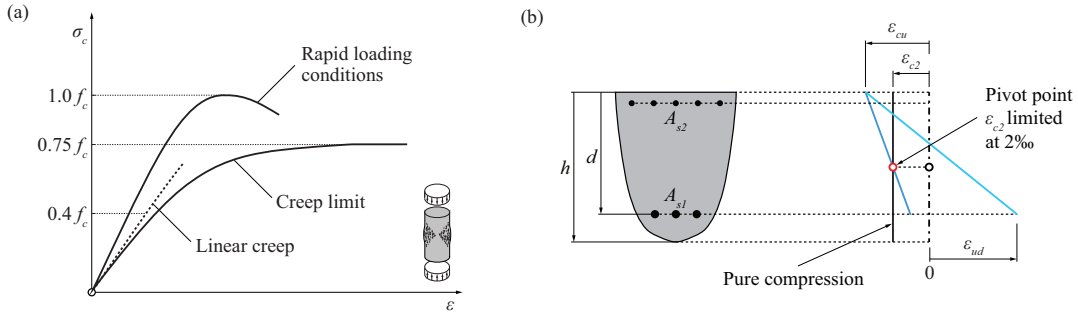

Figure 3.1: Stress redistributions due to creep in reinforced concrete members: (a) short-term and long-term longitudinal stress-strain diagrams for plain concrete; (b) compressive strain limit according to EN 1992-1-1:2004 [EN104]

Concrete long-term response at high levels of load has traditionally been investigated for plain concrete specimens [Stu65, Sha70, Nga80, Sma85, Mae04, Fer07, Sur13]. However, some researches focused on RC elements, observing a redistribution of internal forces between concrete and the reinforcement [Vie56, Dry71, Mic92]. The first extensive research was performed in the 1930s [Ric31, Ric32]. As part of a large experimental programme, 26 RC and 6 PC (plain concrete) columns ($Ø \times h \approx 0.2 \times 1.5$ m) were kept under sustained loading for six years [Ric38]. Later, Troxell [Tro58] investigated creep and shrinkage deformations in 36 spirally-reinforced RC cylinders (longitudinal reinforcement ratio, $\rho = A_s/A$, between 1.9% and 5%). In both cases, the applied level of sustained load was lower than 30% of the short-term concrete strength. Other studies aimed at investigating the role of creep in buckling of RC columns [Mau63, Dry71]. It was observed that creep can significantly reduce the strength and increase the deformation capacity in the compression zone. These results were later confirmed by an experimental programme performed at the University of New South Wales [Gil91, Mic92] on 15 RC columns with square section (150×150 mm^2).

With respect to squat RC columns subjected to high levels of load, 120 specimens with variable eccentricities were tested at the University of Illinois [Hog51]. Failure occurred within 1 hour in most of the tests while time-delayed effects of sustained loading were investigated in 44 specimens [Vie56]. In this programme, specimens with small eccentricity (where failure occurred by crushing of concrete in compression) showed large strain values in the compression zone due to the development of non-linear creep strains (up to 6-8‰). Following these experimental results [Hog51, Vie56], as well as those of other researchers at the time [Tro58, Mau63, Dry71], it was acknowledged the significance of nonlinear creep strains on the global response of columns and compressed members, particularly for slender ones. This issue was subsequently considered in codes of practice as discussed in [Gil91].

It can be noted that research on the phenomena of creep strains at high levels of stress is of large practical relevance. For instance, in RC columns, nonlinear creep strains lead to redistributions of internal forces, reducing the stresses in concrete and increasing them in the reinforcement.

Such phenomenon is potentially beneficial for the overall structural resistance, as the most critical and brittle component (concrete) is partly unloaded. In addition, high-strength reinforcement grades (requiring large strains to yield) could be fully activated in compression. With this respect, the post-peak response of concrete as well as the region where strain localization occurs [Sha87, Sig95, Jan97] considering also its time-dependent response at high levels of load, are of particular relevance. Some works have been performed in the past on this topic (refer for instance to El-Kashif1 and Maekawa [El-04] for a general finite-element based approach). However, there are still scanty simple models to predict how loading rates affect the structural response both in terms of strength and deformation capacity at ULS (particularly in view of their implementation into codes of practice, [Tas19]). Such lack of consistent models, as well as too simplistic and safe design approaches, can hide several beneficial influences and not lead the engineer to adopt suitable design choices. For instance, with respect to RC members in compression, the strain limits considered in many cases do not allow yielding of the reinforcement. This can be observed in Figure 3.1b where the pivot diagram for sections subjected to combined bending and axial force is shown according to EN1992-1-1:2004 [EN104], limiting the maximum strain under pure axial compressive force to 2‰. This contradicts experimental evidence [Vie56] and does not allow taking advantage of the enhancement in terms of strength when high reinforcement grades are used.

Within this context, the present Chapter investigates the stress redistributions in RC members accounting for linear and nonlinear creep strains. To that aim, centrically loaded squat columns are used as a representative case study for the response of reinforced structural concrete in compression. The phenomenon is investigated by means of an experimental programme on columns with different reinforcement ratios and tested under varying loading rates. Advanced measurement techniques, such as FOM (Fibre Optic Measurements) and DIC (Digital Image Correlation) are used, which allow obtaining detailed information on the reinforcement and concrete strains. The results are then investigated on the basis of the mechanical model developed for plain concrete by Fernández Ruiz et al. [Fer07] and Tasevski et al. [Tas18]. The model shows sound agreement with the experimental results and is eventually used to perform parametric analyses aimed to derive practical design recommendations.

3.2 Experimental programme

The experimental programme includes 14 prismatic specimens (cross section of 150 × 150 mm^2 and height equal to 500 mm, including the end steel plates) tested under uniaxial compression. The longitudinal reinforcement is arranged in the form of one bar centred in the cross section and welded to 20 mm thick steel plates at the ends (Figure 3.2). All specimens are without confinement reinforcement. Some reference specimens were cast without longitudinal reinforcement to determine the response of plain concrete. The diameter of the longitudinal

reinforcement bar is varied so that the reinforcement ratio ($\rho = A_s/A$) is equal to 0%, 0.5%, 0.9%, 2.3% and 4%. These values cover a wide range of practical cases, typically representing light, medium and high reinforcement ratios of columns and compression zones. The tests are performed with different loading rates, leading to failures occurring between approximately 2 minutes and 8 hours. Details on the specimen are given in Table 3.3 (named according to the diameter of the bar and target loading duration). All tests were performed in the Structural Laboratory of École Polytechnique Fédérale de Lausanne (EPFL), Switzerland.

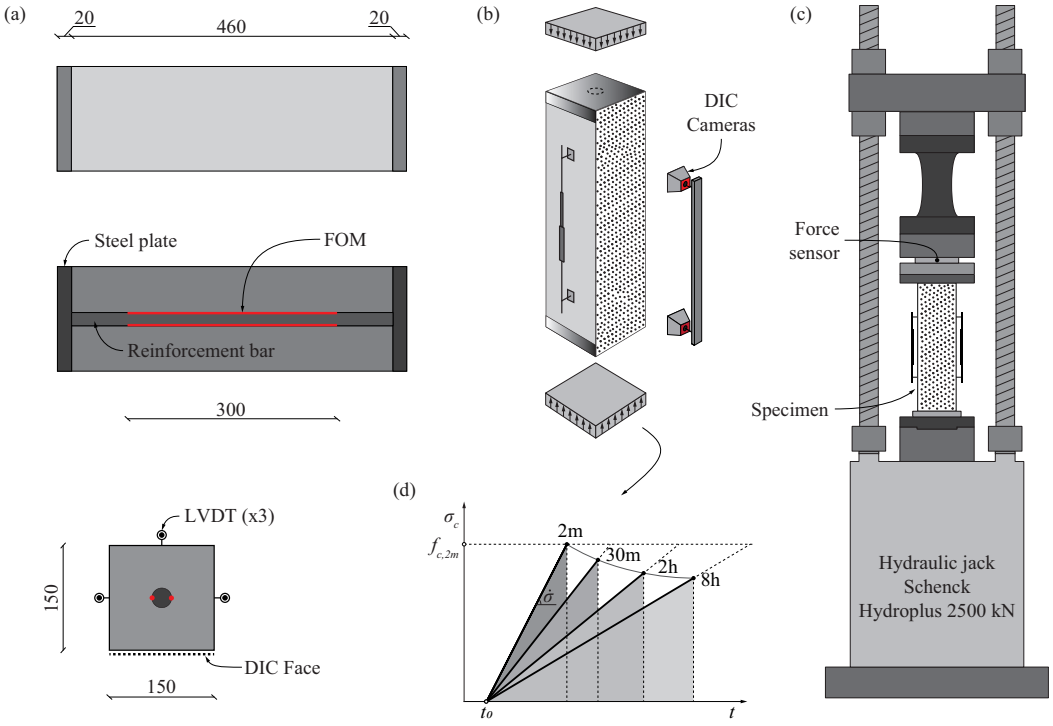

Figure 3.2: Test setup: (a) view and sections of the specimen; (b) 3D view of the specimen and of the performed measurements; (c) test setup; (d) applied loading patterns

3.2.1 Material properties

The specimens were produced using normal strength concrete with a maximum aggregate size of 16 mm provided by an external supplier. The cement was CEM-II 42.5R and the water-to-cement ratio was equal to 0.56. Twenty-one cylinders ($Ø \times h$ = 160 × 320 mm) were cast to characterize the concrete mechanical properties. Standard compression tests were performed with a strain rate of 0.02‰ s^{-1} (failure reached within approximately 120 seconds). An overview of the results in compression is given in Table 3.1 and in Figure 3.3b. The average modulus of elasticity at 28 days E_c was 35.5 GPa (secant stiffness between $0.03 \cdot f_c$ and $0.3 \cdot f_c$ in the loading phase after three loading and unloading cycles).

The development of the concrete compressive strength with time is estimated with the expression provided in MC2010 [FIB13] as in Eq. (3.1) with t representing the concrete age in days.

$$f_c(t) = f_{c,28} \cdot e^{s\cdot\left(1-\sqrt{\frac{28}{t}}\right)} \tag{3.1}$$

Table 3.1: Concrete cylinders compression tests

Name	Age [days]	f_c [MPa]	Avg [MPa]
C1	7	36.5	34.3
C2		32.0	
C3	14	34.9	35.9
C4		37.1	
C5	21	40.2	37.9
C6		35.6	
C7	28	39.1	37.5
C8		34.9	
C9		38.4	
C10	28	37.6	38.1
C11		38.6	
C12	31	40.9	41.4
C13		41.9	
C14	37	40.7	41.5
C15		42.3	
C16	38	42.4	42.4
C17		42.4	
C18	44	41.5	42.3
C19		43.0	
C20	51	41.3	42.2
C21		43.2	

The parameters $f_{c,28}$ (reference strength at 28 days measured in concrete cylinders with diameter 160 mm and a height of 320 mm) and s (coefficient defining the early-age evolution of the compressive strength) are determined by least-square fitting of the test results, leading eventually to s = 0.189 and $f_{c,28}$ = 39.6 MPa with a coefficient of variation of 4.4% (experimental results and Eq. (3.1) are compared in Figure 3.3a). Figure 3.3b shows the measured short-term stress-strain response (failure occurring in about 2 minutes) of 4 representative concrete cylinders (2 tests performed at 28 days and 2 performed at 38 days).

Shrinkage and linear creep strains were measured on a total of 6 cylinders stored under standard laboratory conditions (temperature equal to 21±0.5°C and relative humidity (RH) equal to 55±1%). Three cylinders were placed within a shrinkage rig after demoulding, performed at

14 days for all specimens of the programme, and measurements were performed during the following 3 months covering the testing programme duration. The remaining 3 cylinders were used to perform linear creep measurements in a standard creep rig. The applied load was equal to 30% of the short-term concrete strength. The expressions provided in MC2010 [FIB13] for predicting shrinkage and linear creep development are calibrated to best fit the experimental results, as shown in Eq. (3.2) and Eq. (3.3), respectively. The time of evaluation is indicated with t (in days) while t_s and t_0 are the age at demoulding and loading, respectively. The calibrated coefficients result $\varepsilon_{cs,1}$ = -0.0609‰; $\varepsilon_{cs,2}$ = -0.804‰; t_c = 61.2 days; φ_1 = 2.73; φ_2 = 0.477; k_φ = 0.357 and t_{cr} = 476 days. Test results and the analytical expressions are compared in Figure 3.3c and Figure 3.3d.

$$\varepsilon_{cs}\left(t,t_s\right)=\varepsilon_{cs,1}\cdot\left(1-e^{-0.2\sqrt{t}}\right)+\varepsilon_{cs,2}\cdot\frac{t-t_s}{\sqrt{t_c+t-t_s}} \tag{3.2}$$

$$\varphi\left(t,t_0\right)=\frac{\varphi_1}{0.1+t_0^{0.2}}\cdot\left[\frac{t-t_0}{476+t-t_0}\right]^{\frac{1}{2.3+\frac{3.5}{\sqrt{t_o}}}}+\varphi_2\cdot\log\left(k_\varphi\cdot\left(t-t_0+1\right)\right) \tag{3.3}$$

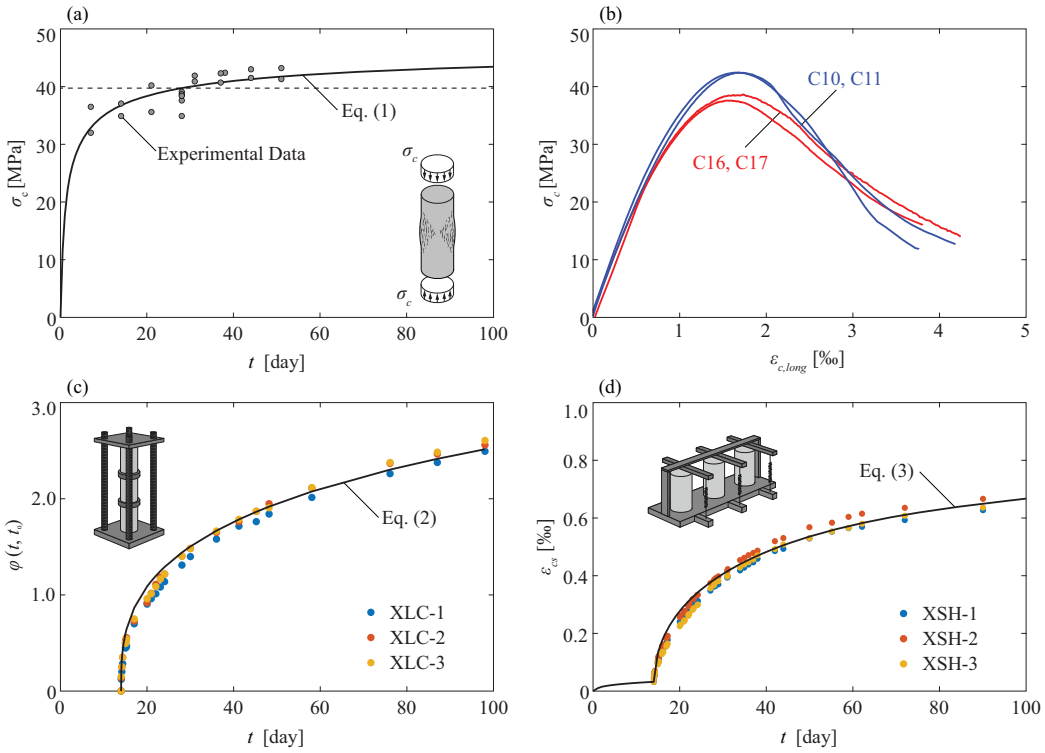

Figure 3.3: Time-dependent concrete properties: (a) compressive strength with respect to time; (b) concrete monotonic compressive curves; (c) linear creep coefficient; (d) longitudinal shrinkage strain (positive strains refer to shortening)

With respect to the reinforcement, steel B500B according to [EN105] was used (specified characteristic yield strength f_{yk} = 500 MPa, ductility class B). The bars with diameter 12 and 16 mm were cold-worked whereas the bars with diameter 26 and 34 mm were hot-rolled. For each bar diameter, at least 2 tests in compression and 2 in tension were performed. For the tension tests, reinforcement bars of one meter were instrumented with extensometers. For the compression tests, the length of the bars was limited to five times the bar diameter to limit second-order effects and steel plates were welded at both ends to ensure a uniform stress distribution. In addition, DIC was used to obtain accurate strain measurements and to track lateral displacements. Figure 3.4 shows the stress-strain curves in tension and compression while details are given in Table 3.2.

Table 3.2: Main results from rebars testing (average values)

Ø [mm]	$f_{y,tens}$ [MPa]	$f_{y,comp}$ [MPa]	$f_{y,comp} / f_{y,tens}$	$f_{t,tens}$ [MPa]	$\varepsilon_{lim,tens}$
12	500	479	0.958	567	0.030
16	525	487	0.928	582	0.063
26	535	527	0.985	626	0.096
34	512	533	1.041	654	0.121

One can observe that for the cold-worked steel, the yield strength in compression is 4-7% lower than in tension, while for the hot-rolled steel, the ratio $f_{y,comp}/f_{y,tens}$ varies between 0.985 and 1.041 (in all cases, the yield strength is defined as the stress with 2‰ irreversible strain).

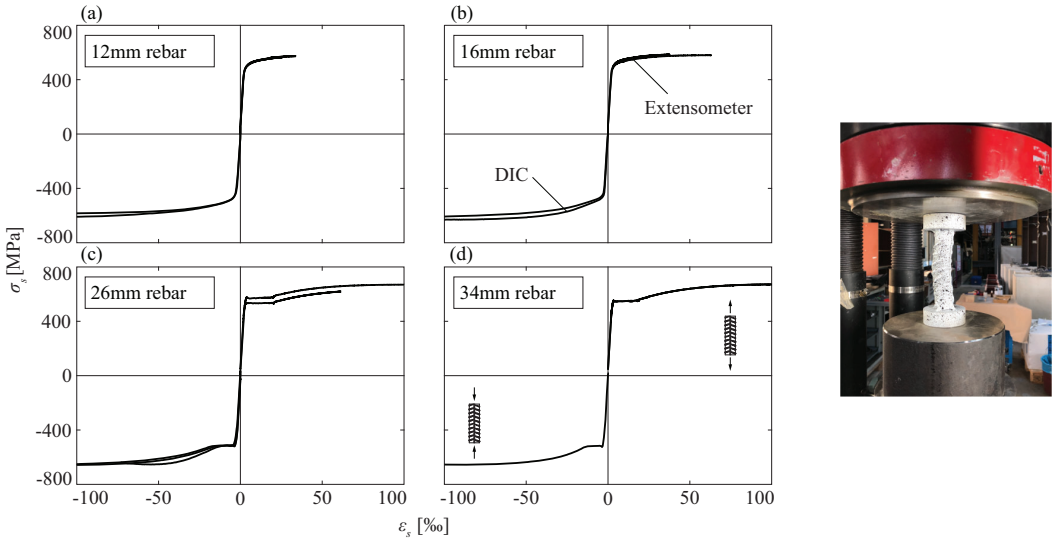

Figure 3.4: Reinforcement bars: (a) stress-strain curves from experimental tests; (b) detail of a rebar being tested in compression (tensile stresses and strains positive)

3.2.2 Test setup and measurements

Demoulding of all specimens was performed at 14 days. Thereafter, the specimens were stored and tested under standard laboratory conditions. All tests were performed between 28 and 37 days (details are given in Table 3.3) using a Schenck Hydroplus servo-hydraulic testing machine with a capacity of 2.5 MN. A load cell positioned between the steel frame and the specimen measured the force, while the longitudinal strain $\varepsilon_{c,long}$ was tracked by means of three LVDTs (Linear Variable Differential Transformers) placed on three faces of the specimen and with a measurement length of 300 mm. Figure 3.3 presents an overview of the test setup.

To accurately investigate the interaction between concrete and the reinforcement, Digital Image Correlation (DIC) was used on the concrete surface and Fibre Optic Measurements (FOM) on the reinforcement bar. For the DIC measurements (Figure 3.2d), a pair of CMOS IMX304 sensor cameras (12 Mpx) in combination with controlled lighting conditions were used. Cameras were calibrated before the test and lighting conditions were controlled to avoid temperature variations and reduce the displacement noise in the measurements. The front face of the specimens was painted with a random speckle pattern (spray painting with a size of 1 ± 0.5 mm) to increase the contrast of the pixels in the acquired pictures. Based on the calibration images acquired before the tests (zero displacement), a displacement noise below 1/50 times the size of the pixel (pixel size ≈ 0.5 mm) was observed. The displacement analysis is performed with Vic3D software [Cor10] by adopting a subset size of 27 × 27 pixels. Pictures were generally acquired with a frequency up to 1 Hz but it was increased close to the failure load to better investigate the development of cracking.

In addition, to accurately measure the reinforcement strain, FOM were performed on two opposite sides of the bars. A cutting disc was used to generate two 1×1 mm^2 grooves on the sides of the rebar to embed and glue the fibres as shown in Figure 3.5 (further details on the adopted technique can be consulted in [Can20]). For the acquisition of data, the Odisi–B version by Luna Innovations [Lun13] was used. Odisi–B allows extracting strain profiles at relatively high sampling rates and refined spatial resolution (around 1mm). The rebar region covered by FOM is shown in Figure 3.2a.

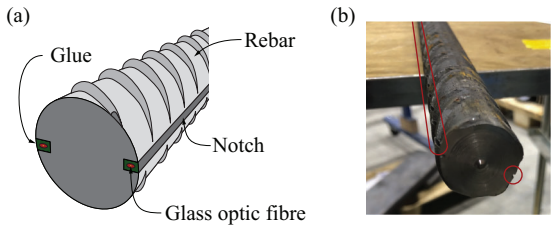

Figure 3.5: Detail of FOM in rebars

3.2.3 Loading patterns

The response of the specimens was investigated for decreasing stress rates. Such loading pattern allows investigating efficiently the time-dependent response of concrete, both in terms of the strength and deformation capacity (Figure 3.2d), as shown by Tasevski et al. [Tas18].

Table 3.3: Overview of the main experimental results (positive strains refer to shortening, A refers to the toal area of the specimen)

Specimen	$\emptyset$ [mm]	$\dot{\sigma}$ [MPa/s]	Concrete age [days]	Test duration	N_{max}/A [MPa]	$\varepsilon_{c,long}$ [‰]
CX-0-2m	-	3.46E-01	34	1.9 min.	39.7	1.92
CX-0-30m	-	2.10E-02	28	31.0 min.	40.4	2.45
CX-0-2h	-	5.63E-03	29	1.9 hour	38.1	2.68
CX-0-8h	-	1.47E-03	38	7.6 hour	37.5	2.92
CX-12-2m	12	3.16E-01	35	2.1 min.	40.9	1.94
CX-16-2m	16	3.04E-01	35	2.2 min.	42.6	2.01
CX-16-30m	16	1.98E-02	29	33.0 min.	41.8	2.38
CX-16-2h	16	5.01 E-03	28	2.2 hour	40.3	2.72
CX-16-8h	16	1.33E-03	37	8.4 hour	39.3	3.07
CX-26-2m	26	2.83E-01	35	2.4 min.	44.7	2.10
CX-26-30m	26	1.67E-02	28	39.0 min.	44.3	2.61
CX-26-2h	26	4.41E-03	29	2.5 hour	42.2	2.74
CX-26-8h	26	1.13E-03	36	9.8 hour	43.3	3.06
CX-34-2m	34	2.61E-01	34	2.5 min.	47.4	2.15

3.2.4 Experimental results

Table 3.3 presents for each specimen the actual stress rate, the test duration, the maximum average stress N_{max}/A (maximum compression force attained divided by the gross cross-sectional area) and the longitudinal strain at peak load (shortening positive). Figure 3.6 shows the longitudinal stress-strain response and Figure 3.7 the Poisson's coefficient ($\nu = -\varepsilon_{c,trans} / \varepsilon_{c,long}$) as a function of the stress in concrete calculated on the basis of the measured total force and the reinforcement force calculated from the strain measurements.

The longitudinal strain $\varepsilon_{c,long}$ presented in Table 3.3 is calculated as the average value of the LVDTs placed in the two opposite lateral faces. In addition to the average strain measured with the lateral LVDTs (continuous lines), Figure 3.6 shows the FOM of the strains integrated on a total length of 100 mm at selected load levels (dots). Sound agreement is observed between LVDTs measurements and FOM. Some limited scatter is observed for specimens CX-26-2m,

CX-34-2m and CX-16-30m. This might be due to the initial calibration of the fibres. Overall, experimental data confirms a decreasing trend of the failure load with decreasing stress rate (increasing load duration) and an increasing value of the Poisson's coefficient for lower stress rates.

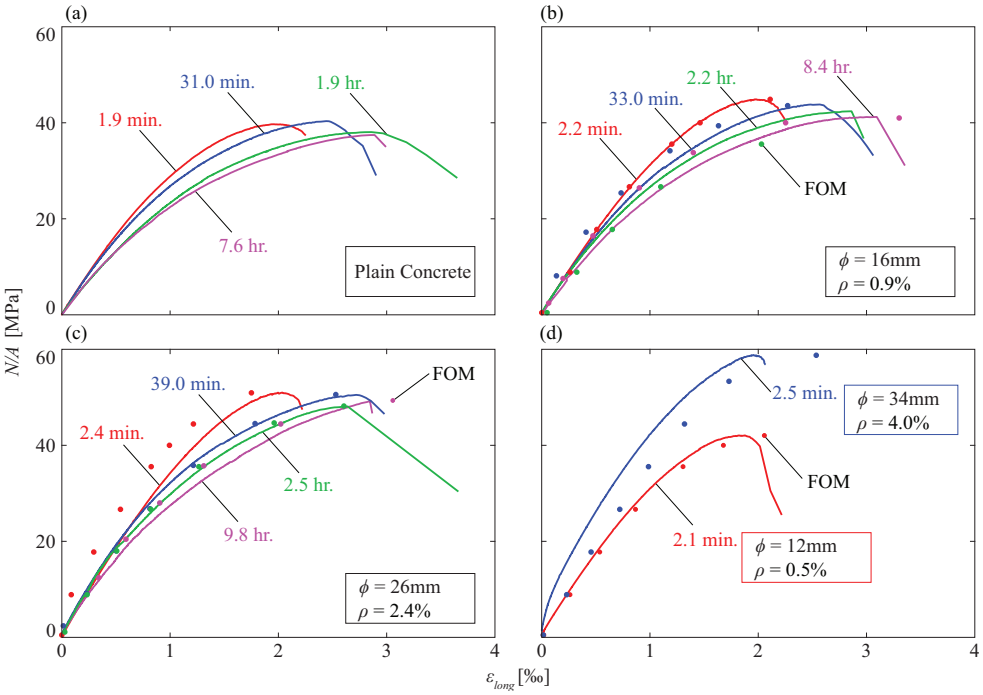

Figure 3.6: Axial force (N) divided by total area (A) as a function of strain (ε_{long})

3.3 Analysis of the response of concrete under variable loading rates

Several approaches have been developed in the past to analyse the time-dependent response of concrete accounting for its linear and nonlinear response [Zho92,El-04, Tas18]. In this Chapter, the approach proposed by Fernández Ruiz et al. [Fer07] is adopted, consistently with the methodology applied by Tasevski et al. [Tas18, Tas19] for failures in plain concrete specimens under variable loading rates. According to this approach, concrete micro-cracking and its associated damage are considered as the source of nonlinear creep strains. Such damage starts developing when the applied stress exceeds 40% of the uniaxial compressive strength $f_c(t)$. Above this threshold, the nonlinear creep strains are assumed to be affine to the linear creep strains (according to a ratio η [Fer07]) and ensure up to 2/3 of the creep strains at failure, as shown in Figure 3.8a. For stress levels above 75% of $f_c(t)$, micro-cracking leads to crack coalescence [Tas18] along with a rapid increase of nonlinear creep strains (Figure 3.8a). Eventually, such rapid increase of creep strains leads to failure under sustained compression.

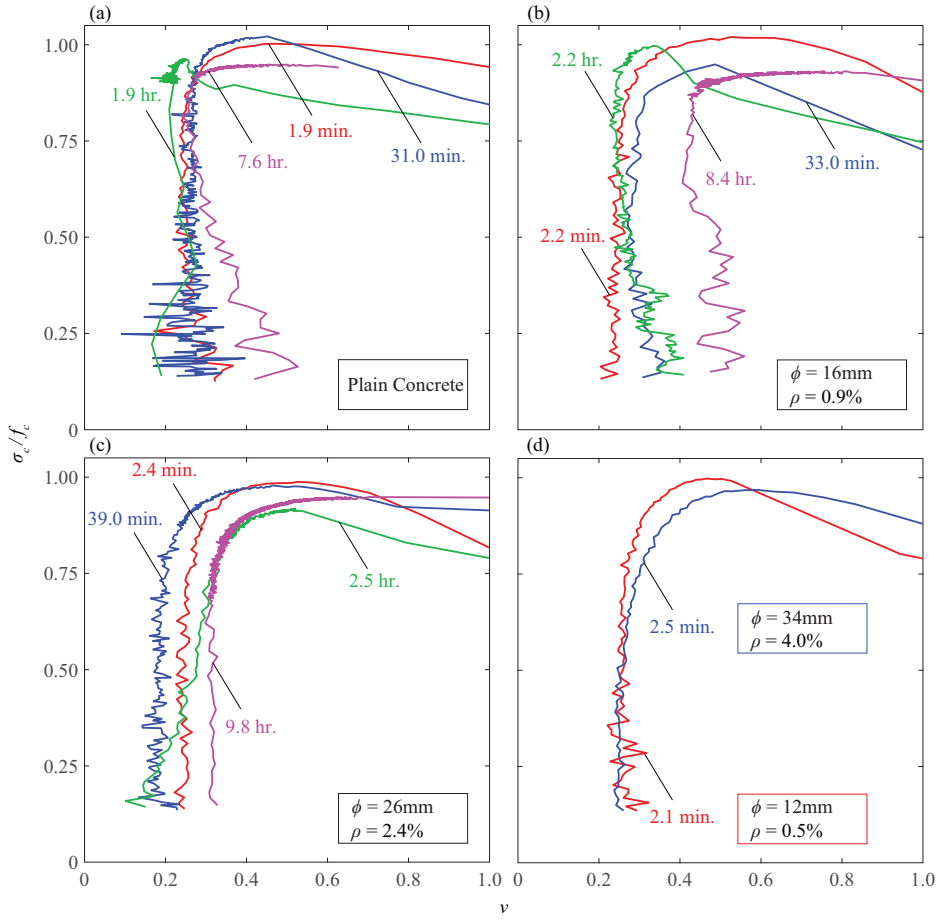

Figure 3.7: Resulting Poisson's coefficients as a function of the concrete stress

3.3.1 Failure criterion

As assumed by Fernández Ruiz et al. [Fer07], concrete failure occurs when the total inelastic strain associated to micro-cracking is equal to the available inelastic strain capacity ($\varepsilon_{cc,in,av}$). The inelastic strain capacity is defined as the difference between the strain in the softening branch (post-peak) and the strain in its ascending branch (pre-peak) for a fixed level of applied stress (Figure 3.8b). The reference stress-strain diagram is obtained by using a strain rate of 0.02‰ s^{-1} (rapid loading conditions) with the peak strength reached approximately after two minutes of loading.

Such approach has been experimentally verified for a large number of cases by Tasevski et al. [Tas18]. Another advantage of this approach is that the inelastic strain capacity, which determines the failure criterion, allows calculating not only the resistance, but also the deformation capacity of concrete as shown in Figure 3.8c.

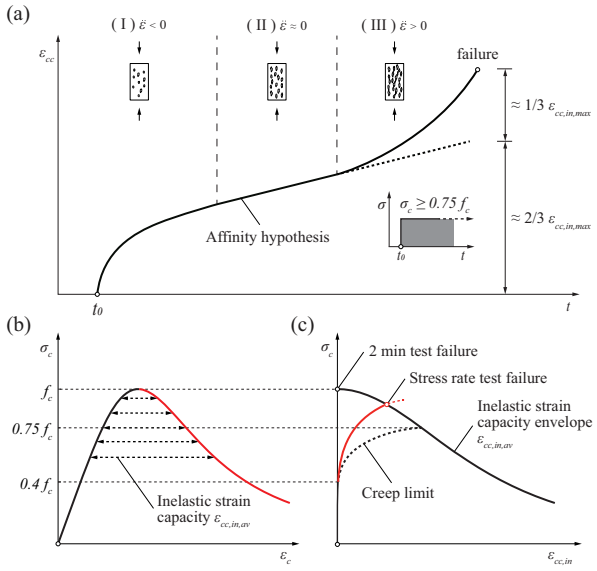

Figure 3.8: Inelastic creep strain development: (a) evolution of creep with time for low and high sustained loads (primary, secondary and tertiary); (b) $\varepsilon_{cc,in,av}$ calculation for different levels of stress; (c) failure criterion according to the development of the inelastic strains ($\varepsilon_{cc,in}$)

3.3.2 Inelastic strain development in concrete

The total strain of concrete ε_c for a time t is expressed in a general manner as the sum of the instantaneous strains $\varepsilon_{c,0}$, the shrinkage strains ε_{cs} and the creep strains ε_{cc} as in Eq. (3.4). The time t_0 corresponds to the application of the load, t_s to the demoulding time (start of hygrometric shrinkage) and σ_c/f_c to the level of applied concrete stress.

$$\varepsilon_c\left(t,t_0,\frac{\sigma_c}{f_c(t)}\right)=\varepsilon_{c,0}\left(t_0,\frac{\sigma_c}{f_c(t)}\right)+\Delta\varepsilon_{cs}\left(t,t_s\right)+\Delta\varepsilon_{cc}\left(t,t_0,\frac{\sigma_c}{f_c(t)}\right) \tag{3.4}$$

In this Chapter, the shrinkage strain is assumed to be independent from creep effects. With respect to creep strains, they are generally divided into 3 main components [Mae04, Tas18] named primary ($\varepsilon_{cc,1}$), secondary ($\varepsilon_{cc,2}$) and tertiary ($\varepsilon_{cc,3}$) as shown in Eq. (3.5).

$$\varepsilon_{cc}\left(t,t_0,\frac{\sigma_c}{f_c}\right)=\varepsilon_{cc,1}\left(t,t_0\right)+\varepsilon_{cc,2}\left(t,t_0,\frac{\sigma_c}{f_c}\right)+\varepsilon_{cc,3}\left(t,t_0,\frac{\sigma_c}{f_c},\frac{\varepsilon_{in}}{\varepsilon_{in,av}}\right) \tag{3.5}$$

Primary creep strains $\varepsilon_{cc,1}(t,t_0)$ (see for instance Eq. (3.3)) are related to the response of the undamaged material, i.e. when the stress level is lower than approximately 40% than its uniaxial strength and micro-cracking is negligible. Its value is linearly related to the instantaneous strain $\varepsilon_{c,0}$ through the linear creep coefficient φ_{lin} as in Eq. (3.6).

$$\varepsilon_{cc,1}\left(t,t_0\right)=\varphi_{lin}\left(t,t_0\right)\cdot\varepsilon_{c,0} \tag{3.6}$$

For higher levels of load, the correlation between the instantaneous and creep strains is no longer linear. A reasonable estimate is obtained by assuming the affinity hypothesis [Fer07], which relates the nonlinear and linear creep strain through the parameter η as in Eq. (3.7):

$$\varepsilon_{cc,2}\left(t,t_0,\frac{\sigma_c}{f_c}\right)=\left(\eta-1\right)\cdot\varepsilon_{cc,1}\left(t,t_0\right) \tag{3.7}$$

This parameter accounts for micro-crack propagation and depends on the stress level as expressed in Eq. (3.8):

$$\eta\left(t,t_0,\frac{\sigma_c}{f_c}\right)=1+2\cdot\eta_\tau\left(t,t_0\right)\cdot\left(\frac{\sigma_c}{f_c\left(t\right)}\right)^4 \tag{3.8}$$

The parameter $\eta_\tau(t,t_0)$ in this Equation is estimated using Eq. (3.9), where $t_m = 100$ days and $n = 0.75$ [Tas18] (for large values of t, the parameter is approximated as 1).

$$\begin{cases}\eta_\tau\left(t,t_0\right)=\left(1-\log\dfrac{t-t_0}{t_m+t-t_0}\right)^n\\ \eta_\tau\left(t,t_0\right)\approx 1 \quad \text{for} \quad t\to\infty\end{cases} \tag{3.9}$$

Tertiary creep, associated to micro-cracks coalescence, develops for stress levels larger than approximately 75% of $f_c(t)$. Unlike primary and secondary creep, tertiary creep strains can lead to failure of concrete in compression. In this Chapter, the tertiary creep is estimated using the general formulation in Eq. (3.10) which was proposed by Tasevski et al [Tas18].

$$\varepsilon_{cc,3}\left(t,t_0,\frac{\sigma_c}{f_c\left(t\right)},\frac{\varepsilon_{cc,in}}{\varepsilon_{cc,in,av}}\right)=\gamma\left(\frac{\sigma_c}{f_c\left(t\right)},\frac{\varepsilon_{cc,in}}{\varepsilon_{cc,in,av}}\right)\cdot\varepsilon_{cc,2}\left(t,t_0,\frac{\sigma_c}{f_c}\right) \tag{3.10}$$

$$\gamma\left(\frac{\sigma_c}{f_c\left(t\right)},\frac{\varepsilon_{cc,in}}{\varepsilon_{cc,in,av}}\right)=\frac{1}{2}\cdot\left(\frac{\varepsilon_{cc,in}}{\varepsilon_{cc,in,av}}\right)^\alpha \qquad for \qquad \sigma_c/f_c\left(t\right)\geq 0.75 \tag{3.11}$$

For levels of stress higher than 75% of the short-term concrete strength, the parameter γ is calculated as in Eq. (3.11) with $\alpha = 4$ according to [Tas18]. Figure 3.8c shows failure occurring when $\varepsilon_{cc,in}$ equals $\varepsilon_{cc,in,av}$. Since the model is strain based, the amount of material damage as well as its associated deformation capacity is estimated independently from the loading history.

3.3.3 Application to reinforced concrete elements

The above presented model has been extensively checked for unreinforced concrete [Fer07, Tas18]. However, for reinforced concrete members, there is an interaction between concrete and the longitudinal reinforcement [Tas19]. In general, when nonlinear strains develop in concrete, a fraction of its load is transferred to the reinforcement (stiffer component) if the latter is still in its elastic domain. In some cases, this process can lead to yielding of the reinforcement and to failure of the member. Such response and its structural implications will be investigated hereafter under the following assumptions:

- Concrete is modelled according to the response described in Section 3.3. Also, concrete ageing is considered consistently with [Tas18];
- Steel reinforcement is considered to have a bilinear response, characterized by the modulus of elasticity (E_s) and the yield strength (f_y) as in Figure 3.9. Strain hardening in the reinforcement is not considered (although this would be possible).
- Compatibility of deformations and perfect bond is assumed ($\varepsilon_s = \varepsilon_c$).

When the load is applied, pre-existing strains due to shrinkage (which develops before application of the load (Figure 3.3d)) and the related stresses are calculated by imposing the compatibility of the deformations between concrete and the reinforcement. After applying the load, for every increment of time the general analysis procedure is described above:

1. Determination of initial strains and stresses in each material (time t_i). Concrete and reinforcement are uncoupled and concrete is left to develop freely its delayed strains (shrinkage and creep), accounting for previous history of loading [Tas19]:

$$\Delta\varepsilon_c(t) = \sum_{i=1}^{n} \left[\varepsilon_{c0}(\sigma_{c,i}) \cdot \left[\eta\left(\frac{\sigma_{c,i}}{f_{c,i}}\right) + \gamma\left(\frac{\sigma_{c,i}}{f_{c,i}}, \frac{\sigma_{\varepsilon_{cc,in,i}}}{\varepsilon_{cc,in,av}}\right) \cdot \left(\eta\left(\frac{\sigma_{c,i}}{f_{c,i}}\right) - 1 \right) \right] \cdot \varphi\left(t, t_i\right) - \right.$$
$$+ \varepsilon_{c0}\left(\sigma_{c,i-1}\right) \cdot \left[\eta\left(\frac{\sigma_{c,i-1}}{f_{c,i-1}}\right) + \gamma\left(\frac{\sigma_{c,i-1}}{f_{c,i-1}}, \frac{\sigma_{\varepsilon_{cc,in,i-1}}}{\varepsilon_{cc,in,av}}\right) \cdot \left(\eta\left(\frac{\sigma_{c,i-1}}{f_{c,i-1}}\right) - 1 \right) \right] \cdot \varphi\left(t, t_i\right) \Bigg] + \tag{3.12}$$
$$+ \left(\varepsilon_{cs}\left(t, t_s\right) - \varepsilon_{cs}\left(t_1, t_s\right)\right)$$

2. Compatibility is reinstalled by applying a set of self-equilibrated forces in concrete and in the reinforcement, considering the instantaneous response of concrete to that aim.

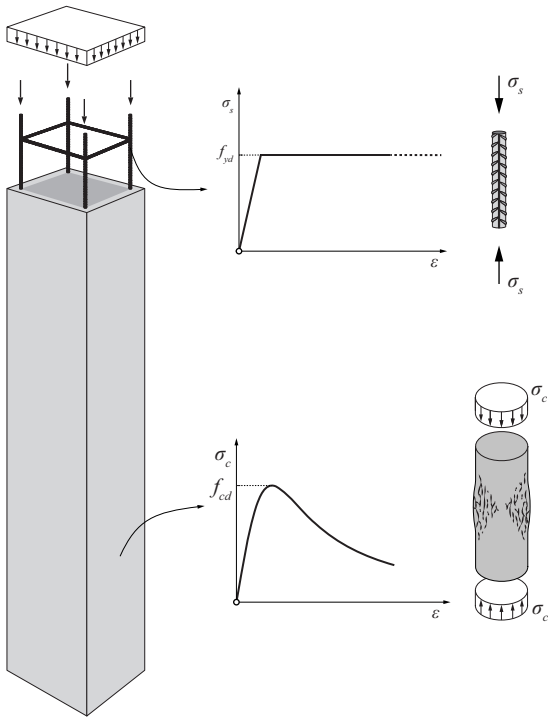

Figure 3.9: Stresses in the column and adopted materials constitutive laws

3.4 Comparisons to test results

To validate the failure criterion, the response of plain concrete specimens (series CX-0) is first investigated. The inelastic strain development is calculated according to Eq. (3.13) and consistently with the previous section.

$$\varepsilon_{cc,in}(t) = \varepsilon(t) - \varepsilon_{c0}(t) - \varepsilon_{cc,1}(t) - \varepsilon_{cs}(t) \tag{3.13}$$

In Figure 3.10, the continuous curves refer to the experimental results, while the black dashed curve represents the calculated failure criterion $\varepsilon_{cc,in,av}$ (Tasevski et al. [Tas18]). The comparison shows the consistency of the failure criterion, confirming the trend of decreasing strength for increasing deformation capacity (as loading rates are lower).

Table 3.4: Comparison of measured-to-predicted strain and stress values at peak load

Specimen	σ_{peak} [MPa]		$\frac{\sigma_{peak,test}}{\sigma_{peak,mod}}$	ε_{peak} [‰]		$\frac{\varepsilon_{peak,test}}{\varepsilon_{peak,mod}}$
	Test	**Model**		**Test**	**Model**	
CX-0-2m	39.7	39.9	0.99	1.93	2.09	0.92
CX-0-30m	40.4	37.1	1.08	2.46	2.43	1.01
CX-0-2h	38.1	36.0	1.06	2.86	2.59	1.10
CX-0-8h	37.5	36.1	1.04	2.89	2.78	1.04
CX-12-2m	42.1	42.7	0.99	1.88	1.71	1.09
CX-16-2m	44.9	44.2	1.02	1.98	1.74	1.14
CX-16-30m	43.8	42.1	1.04	2.57	2.26	1.14
CX-16-2h	42.4	41.2	1.03	2.86	2.49	1.15
CX-16-8h	41.2	41.1	1.00	3.10	2.66	1.16
CX-26-2m	51.0	50.2	1.02	2.04	1.84	1.11
CX-26-30m	50.5	49.3	1.02	2.72	2.45	1.11
CX-26-2h	48.1	48.6	0.99	2.64	2.64	1.00
CX-26-8h	49.3	48.5	1.02	2.84	2.84	1.00
CX-34-2m	58.8	58	1.01	1.95	2.09	0.93
		Avg	1.022		**Avg**	1.065
		StDev	0.027		**StDev**	0.080
		CoV	0.027		**CoV**	0.075

Figure 3.11 presents a comparison of the predicted stress-strain response (accounting also for shrinkage strains) and the experimental results of the reinforced specimens (details are given in Table 3.4). The model shows fine agreement for both strength and deformation capacity independently on the reinforcement ratio and the loading pattern. Also, strain values are consistent with those observed by Hognestad [Hog51]. Such good agreement is based on the fact that the failure criterion reproduces accurately the maximum strain capacity as well as its development in time (Figures 3.12a-c). Figures 3.12a-c show that for low loading rates, larger strains develop due to a significant level of linear and nonlinear creep strains in concrete. Also, for low loading rates, larger strains develop, activating more the reinforcement and leading to an overall increase of strength of the member. However, the contribution of the reinforcement is eventually limited by its yield strength (if strain-hardening effects in the reinforcement are neglected).

More details on the response of the tests, and particularly on the reinforcement contribution are presented in Figures 3.12d-e. The x-axis refers to the time (normalized with respect to the load duration at failure) while the y-axis refers to the total force carried by each material. It can be observed that the reinforcement ratio and the loading rate influence significantly the redistribution of internal forces. For failures observed between 2 minutes and 1 hour, the limited

development of linear and nonlinear creep strains in concrete does not allow for significant stress redistributions and the reinforcement does not yield at peak load (refer to red and blue curves in Figures 3.12d-e). For failures occurring after more than 2 hours, the reinforcement yields before the peak load is reached (refer to green and magenta curves in Figures 3.12d-e). It is important to note that cold-worked steel might show some additional hardening that is not considered in Figures 3.12d-e.

If the load rate is kept constant, once the reinforcement yields and does not carry additional force, concrete is subjected to a higher stress rate and develops additional non-linear creep strain. This transition is more visible in members with higher reinforcement ratio as it can be observed in Figures 3.12d-e. Shrinkage also influences the response of the reinforcement which is compressed before the application of the load (refer to Figures 3.12d-e where the force carried by the reinforcement is higher than zero at $\Delta t / \Delta t_{\text{failure}} = 0$; it is assumed that the concrete tensile strength is sufficient to prevent shrinkage cracks).

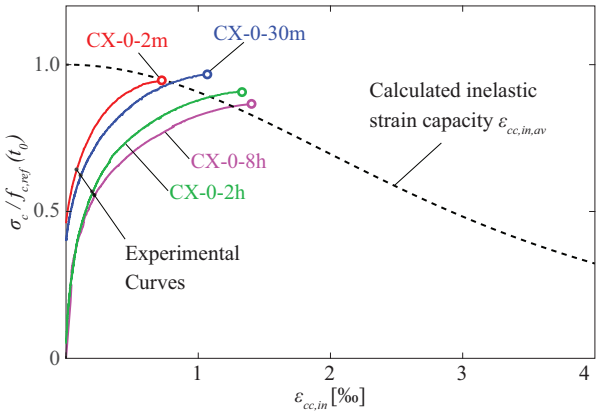

Figure 3.10: Comparison of the failure criterion ($\varepsilon_{cc,in,av}$) to experimental results ($\varepsilon_{cc,in}$) for plain concrete specimens

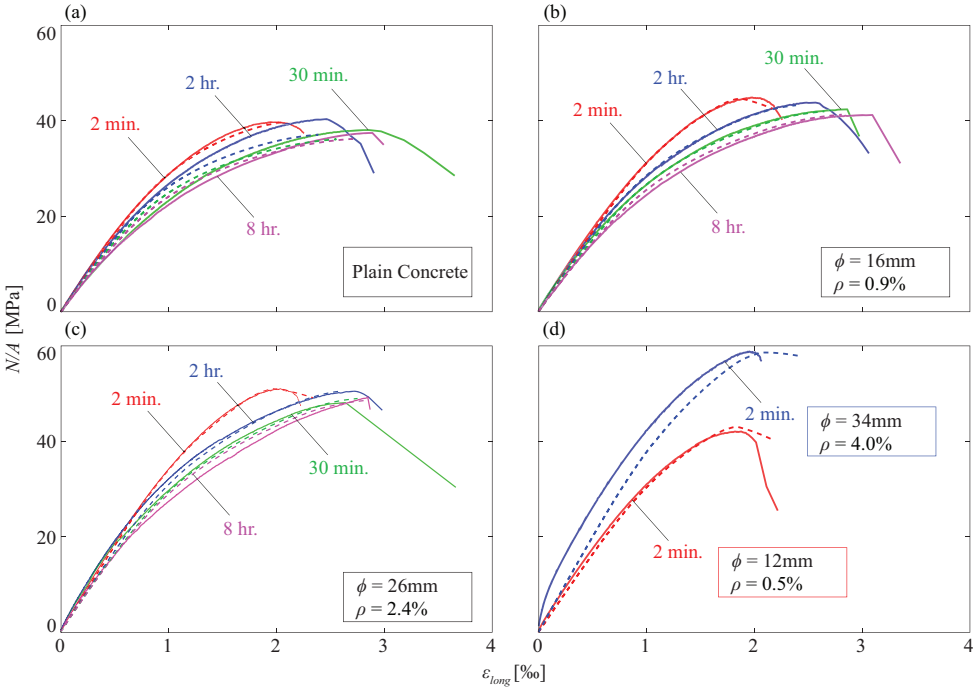

Figure 3.11: Comparison of the proposed model (dashed lines) and experimental results (continous lines) in terms of stress-strain response: (a) PC; (b) ρ = 0.9%; (c) ρ = 2.4%; (d) ρ = 0.5% and ρ = 4.0%

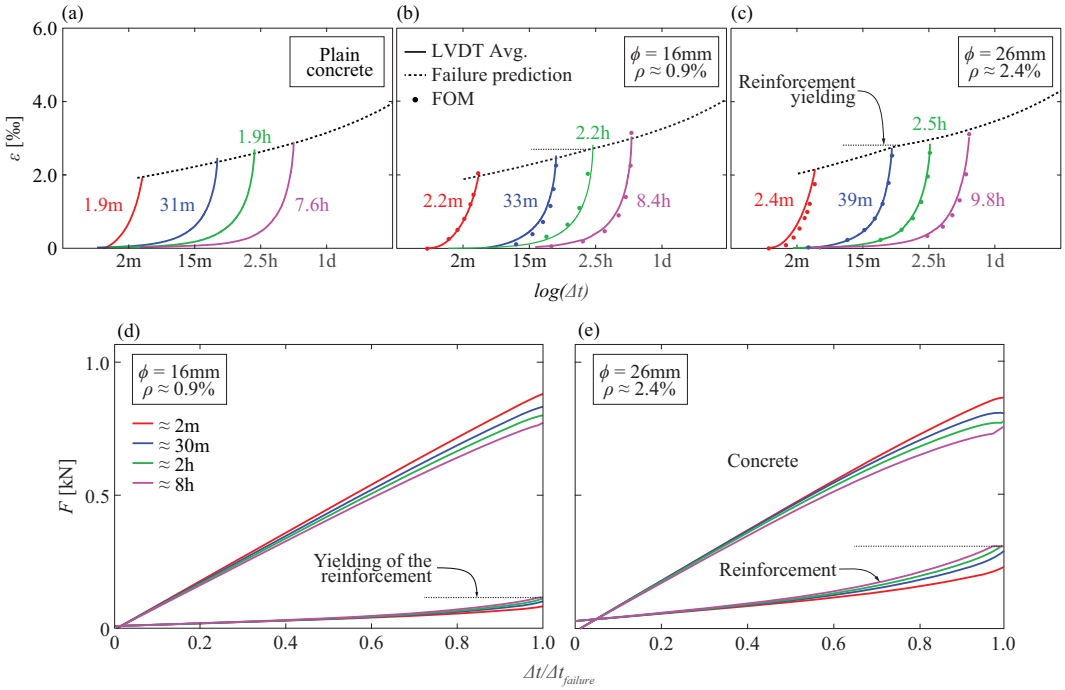

Figure 3.12: (a-c) Strain development in time with predicted failure: (a) plain concrete; (b) ρ = 0.9%; (c) ρ = 2.4%; (d-e) Distribution of internal forces using the above described model: (d) ρ = 0.9%; (e) ρ = 2.4%

3.5 Parametric analysis and practical implications

After validation of the proposed approach, the model presented in Section 3.3 is used to investigate the response of some selected cases and their practical implications. Other than the longitudinal reinforcement ratio (varied between 0.5 and 4%, as for the presented tests) and the loading rate (failure occurring between 2 minutes and 1.5 years), the influence of the concrete age is analysed (28, 91 and 365 days) along with the early-age evolution of the compressive strength (characterized by the dimensionless parameter *s*, refer to Eq. (3.1)).

3.5.1 Influence of the loading rate on members loaded at different ages

The concrete age is a key parameter influencing the long-term response of structures. Although the concrete strength increases with time due to continued cement hydration, the rate of such increase reduces for older concretes (i.e. a concrete loaded at early age can still significantly increase its strength while a fairly mature concrete shows very limited increase). As a result, for younger concretes, the strength reduction due to sustained loading is partly compensated while this does not hold for older concretes. Also, mature concretes show limited creep effects, having less influence on the global strain development.

The strength variation with respect to the loading rate is presented in Figures 3.13d-f, where the concrete strength $f_c(t)$ is estimated using Eq. (3.1) and, in absolute terms, is higher for older concretes (Figure 3.3a). For fast loading conditions, leading to failure between 2 minutes and 1.5 hours, a high reinforcement ratio is beneficial since its enhanced activation compensates for the decrease of strength due to sustained loading (green and magenta curves in Figures 3.13d-f, regime A). For failures occurring between 2 hours and 1.5 years, the reinforcement yields before concrete fails and the decrease of strength due to sustained loading is no longer compensated by the activation of the reinforcement (green and magenta curves in Figures 3.13d-f, regime B).

For younger concretes, the decrease of strength due to sustained loading is compensated by the continued cement hydration (Figures 3.13d, regime C). Since the rate of such increase reduces over time (as shown in Figure 3.3a), regime C does not develop in members loaded at older ages (Figure 3.13f).

For unreinforced or lightly reinforced members, the main difference with respect to highly reinforced members occurs in regime A. Due to the lower amount of force carried by the reinforcement, the latter cannot compensate for the decrease of strength due to sustained loading (black and red curves in Figures 3.13d-f, regime A).

Based on the model presented in Section 3.3, Figures 3.13a-c show an increase of deformation capacity with decreasing loading rate. Since shrinkage is considered with the strains calculated as in Eq. (3.12), the reinforcement yields at a lower value than the theoretical yielding strain.

This value depends of the reinforcement ratio. In fact, members with high reinforcement ratio show limited shrinkage deformation (magenta curve in Figures 3.13a-c) when compared to lightly reinforced members (red curve in Figures 3.13a-c).

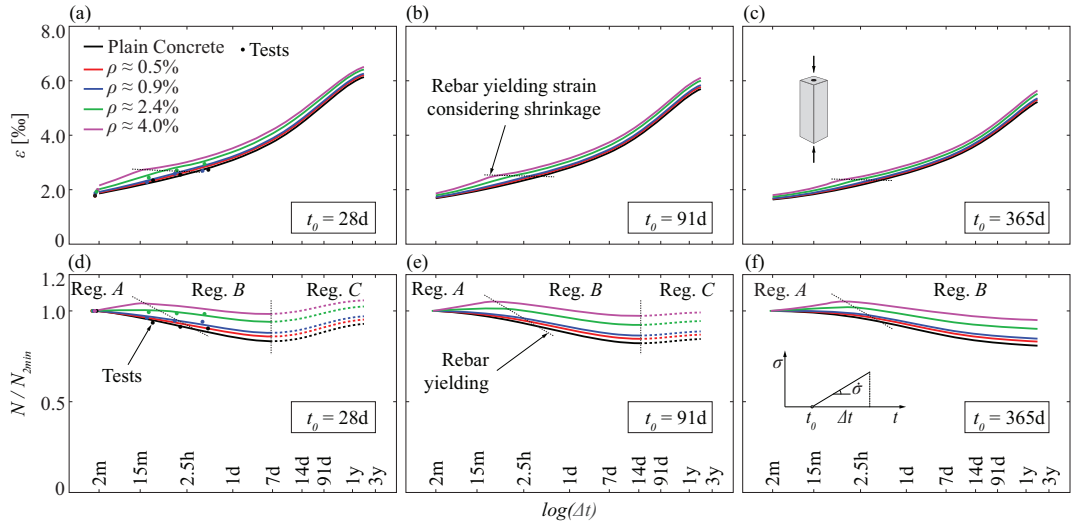

Figure 3.13: Influence of concrete age at loading; (a-c) strain development and (d-f) strength variation with respect to the 2 minutes test for: t_0 = 28 days, t_0 = 91 days and t_0 = 365 days

3.5.2 Influence of concrete and reinforcement properties

This section investigates the short-term concrete strength ($f_{c,28}$ measured at 28 days), its evolution in time characterized by the coefficient s in Eq. (3.1) and the yield strength of the reinforcement f_y. Figure 3.14 and Figure 3.15 present the results of the analyses performed for concrete loaded at 28 and 365 days. For low concrete strength (green line in Figures 3.14a-b), the longitudinal reinforcement (note that ρ = 0.9% for all members) provides a higher contribution to the overall resistance and increases the significance of regime A with respect to members with higher concrete strength (black line in Figures 3.14a-b). Thus, elements with higher concrete strengths are observed to be more sensitive to time-dependent effects.

Figures 3.14c-d show the influence of the cement hardening rate (considered as in Eq. (3.1) with the parameter s) on the variation of the members resistance. For younger concretes (Figure 3.14c), the difference is negligible for failures occurring in less than one week. For failures occurring after more than one week, members with low cement hardening rate can compensate partially or fully the decrease of concrete strength due to sustained loading (green and blue curve in Figure 3.14c).

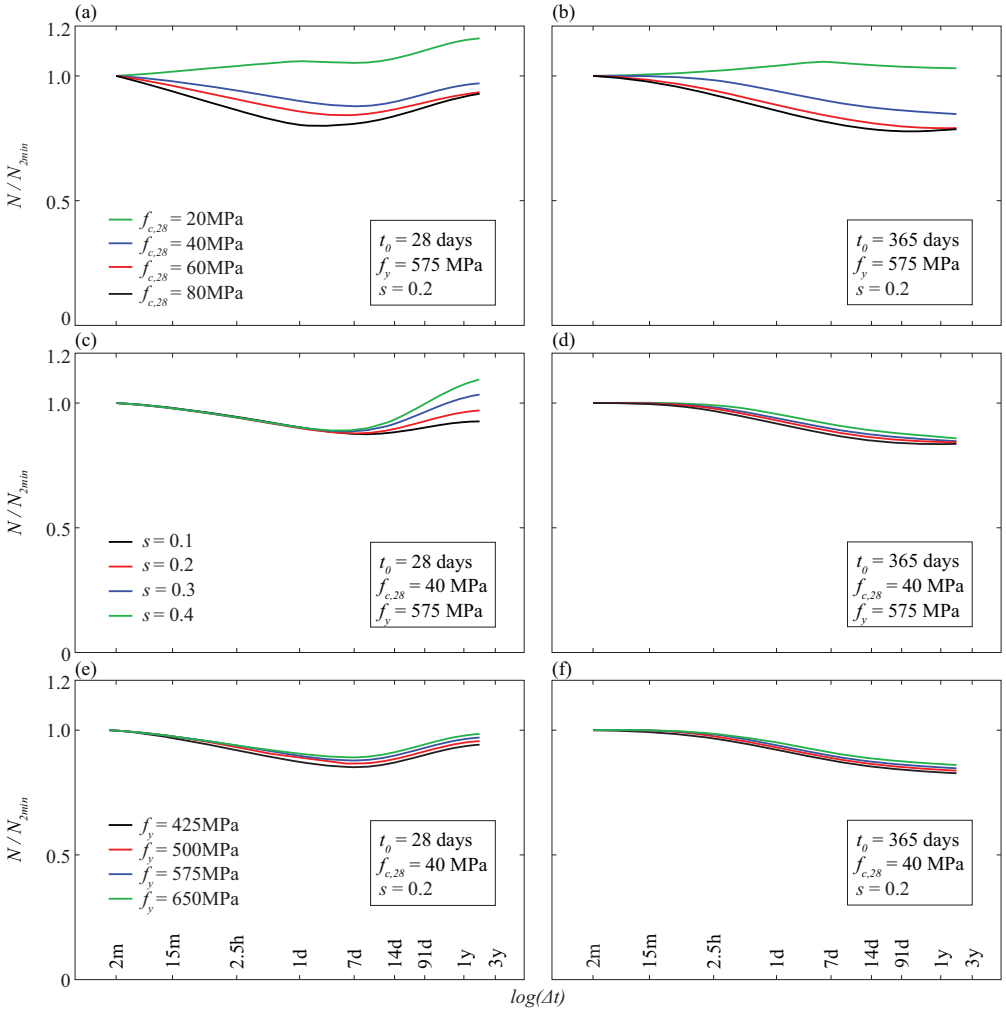

Figure 3.14: Influence of material properties on global strength for concretes loaded at different ages (E_c=33.5GPa and ρ = 0.9%): (a-b) concrete strength; (c-d) cement hardening; (e-f) reinforcement yielding

Such compensation does not occur in members with high cement hardening rate (where the cement hardening occurs at early stage, refer to black and red curve in Figure 3.14c). For members loaded at older ages (Figure 3.14d), since cement hardening is almost completed for all the concretes considered, no difference is observed. Figures 3.14e-f show the influence of the reinforcement yield strength. For failures occurring after yielding of the reinforcement, high reinforcement grades can compensate more the concrete decrease of strength (green curve in Figures 3.14e-f) if compared to low reinforcement grades (black curve in Figures 3.14e-f).

Figure 3.15 presents the results of the analyses in terms of deformation capacity. Concrete strength appears to have a significant influence as shown in Figures 3.15a-b. In fact, the total strain increases with increasing concrete strength (this result is a consequence of the failure criterion considered in the model, as described in Section 3.3). This finding needs however to

be further verified with additional experimental research. On the other hand, limited influence on the deformation capacity is shown by the cement hardening rate and the yield strength of the reinforcement (Figures 3.15c-f).

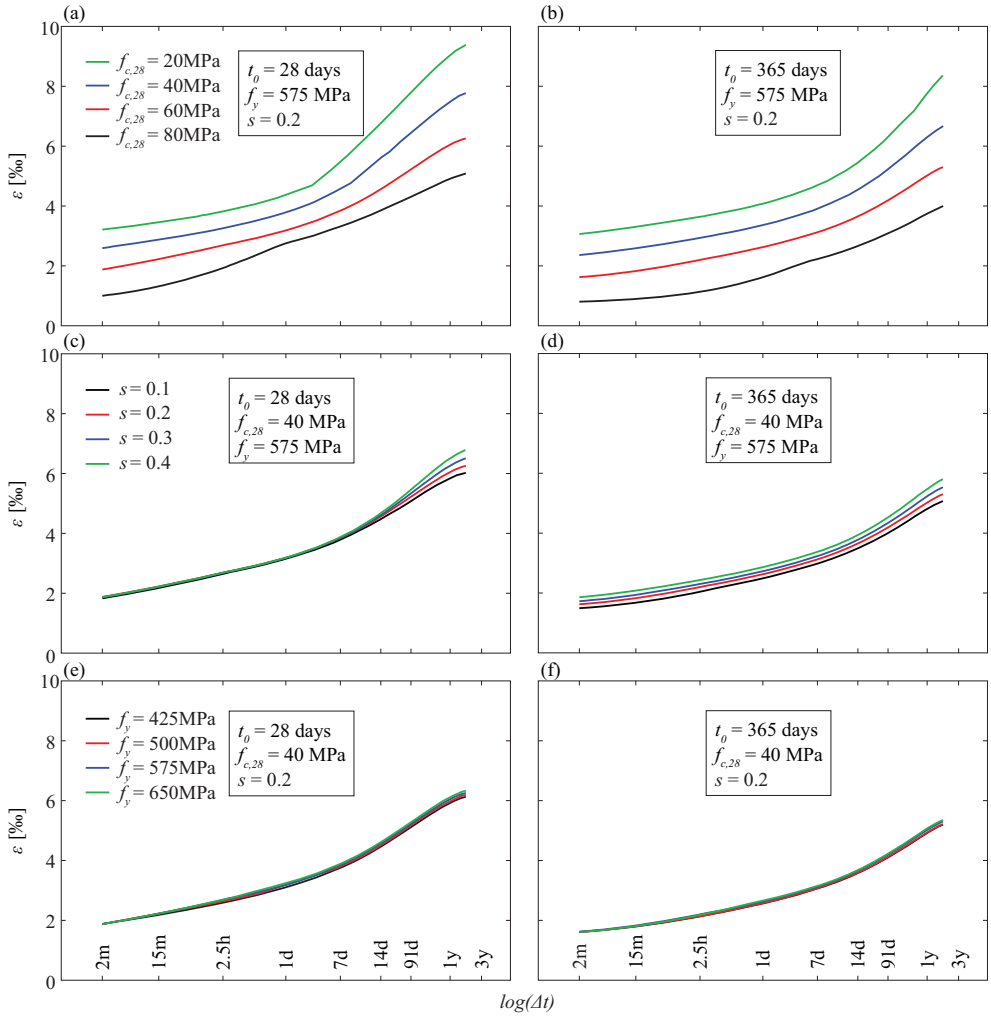

Figure 3.15: Influence of material properties on deformation capacity for concretes loaded at different ages (E_c=33.5GPa and ρ=0.9%): (a-b) concrete strength; (c-d) cement hardening; (e-f) reinforcement yielding

3.5.3 Practical implications

Following the previous findings, several practical implications are highlighted:

- The resistance and the deformation capacity of RC members is significantly influenced by several parameters as materials properties, age of concrete and the loading rate. Despite the reduction of concrete strength under sustained loading, it is shown that low loading rates (long loading durations) are beneficial in terms of overall resistance due

to an enhanced activation of the reinforcement. Structural concrete members loaded at early ages exhibit an enhanced performance due to the continuous cement hydration which leads to an increase of the concrete strength with time.

- For members loaded at early age, the minimum resistance is found for failures occurring after some weeks of loading. However, for members loaded after several years, the minimum resistance is attained after years of sustained loading.
- High-grade yield strength reinforcement is beneficial for the overall strength when sufficiently low loading rates are applied. This allows yielding of the reinforcement before failure occurs due to concrete crushing.
- Finally, an enhanced deformation capacity due to non-linear creep can lead to potential redistribution of stresses at structural level (between members).

3.6 Conclusions

This manuscript presents the results of an investigation on the strength and deformation capacity of reinforced concrete members failing in centric compression under variable loading rates. Differently to previous researches, which focused on the response only of concrete, this investigation addresses the response of systems composed by concrete and longitudinal reinforcement considering the redistributions of internal forces due to nonlinear behaviour. The main conclusions are listed below:

1. The long-term response of concrete (long loading time) is detrimental with respect to its strength, but enhances its deformation capacity. This allows redistributing stresses and can allow, provided that sufficient reinforcement is available, increasing the load-carrying capacity of a structural compressed member;
2. Columns with ordinary reinforcement centrically loaded under rapid loading conditions typically fail by concrete crushing prior to reinforcement yielding. However, when loading is applied slowly, higher levels of deformation allow increasing the reinforcement stresses up to yielding (typically occurring after one or two hours of loading);
3. For very low loading rates, the reinforcement can yield, but the reduction of the concrete strength under sustained loading reduces the resistance (maximum strength typically obtained after one or two hours of loading);
4. High reinforcement ratios and yield strengths are largely beneficial since the increase of deformation capacity allows yielding of the reinforcement, partly compensating for the loss of strength due to sustained loading;

5. Unlike concrete types with fast cement hardening, where the gain of strength occurs mostly in the first months, concretes with slower cement hardening have a better response under sustained loading (independently of the reinforcement ratio) compensating the loss of concrete strength under sustained loading even after years;
6. Consistent modelling and design for these phenomena are performed on the basis of a rheological model for concrete accounting for its linear and nonlinear creep strains. Such approach allows considering suitably the implications on the strength and deformation capacity as well as internal force redistributions;

Notation

***Acronyms*:**

RC:	Reinforced Concrete
PC:	Plain Concrete
FOM:	Fibre-Optics Measurements
DIC:	Digital Image Correlation
RH:	Relative Humidity
LVDT:	Linear Variable Differential Transformer

***Variables*:**

A	specimen gross cross-sectional area
A_s	reinforcement cross-sectional area
ρ	longitudinal reinforcement ratio
E_c	concrete modulus of elasticity
E_s	steel modulus of elasticity
f_c	concrete uniaxial compressive strength
f_{yk}	steel characteristic yield strength
$f_{y,tens}$	steel yield tensile strength
$f_{y,comp}$	steel yield compressive strength
$f_{t,tens}$	steel ultimate tensile strength
$\varepsilon_{lim,tens}$	steel maximum tensile strain
$Ø$	diameter
N_{max}	maximum compression force
$\dot{\sigma}$	stress rate
s	cement hardening rate parameter
t	generic time
t_0	time of load application
t_s	concrete age when drying starts
Δt	test duration

ε_{ud}	reinforcing steel tension strain
ε_{cu}	concrete compression strain limit
ε_{c2}	concrete pure compression strain limit
ε_{c}	concrete strain
ε_{s}	reinforcement strain
$\varepsilon_{c,0}$	instantaneous pre-peak strain
$\varepsilon_{c,trans}$	concrete transversal strain
$\varepsilon_{c,long}$	concrete longitudinal strain
ν	Poisson's ratio
η	affinity coefficient
γ	micro-crack coalescence parameter
σ_{c}	concrete stress
σ_{s}	steel stress
$\varepsilon_{cc,in}$	inelastic strain
$\varepsilon_{cc,in,av}$	inelastic strain capacity
$\varepsilon_{c,0}$	concrete instantaneous strain
ε_{cs}	concrete shrinkage strain
ε_{cc}	concrete creep strain
$\varepsilon_{cc,1}$	concrete primary creep strain
$\varepsilon_{cc,2}$	concrete secondary creep strain
$\varepsilon_{cc,3}$	concrete tertiary creep strain
φ_{lin}	linear creep coefficient

Chapter 4

Recalibration of partial safety factors for permanent loads in road bridges

This chapter is the pre-print version of the following paper to be submitted:

Malja X., Nussbaumer A., Muttoni A., *Recalibration of partial safety factors for permanent loads in road bridges.*

The work is performed by Xhemsi Malja under the supervision of Prof. Aurelio Muttoni and Prof. Alain Nussbaumer.

The main contributions of Xhemsi Malja are the following:

- comprehensive literature review,
- elaboration of available data,
- implementation of the mechanical models available in literature and codes of practice,
- implementation of an algorithm to perform parametric FE simulations,
- implementation of an algorithm to perform parametric reliability analyses,
- interpretation of the results,
- design recommendations,
- elaboration of the figures and tables,
- writing of the manuscript.

Abstract

For the dimensioning of structures, most current codes of practice adopt a semi-probabilistic design approach. Accordingly, structural safety is ensured by performing limit state verifications by means of design values determined with adequately calibrated Partial Safety Factors (PSFs). The calibration of the PSFs is generally performed to provide an acceptable level of safety for a wide range of design scenarios and each PSF covers well-defined uncertainties related to the variability of one or more basic random variables, such as actions, materials, geometry, and models. Besides clarifying the uncertainties covered by each partial safety factor, this work aims at updating the partial safety factor for permanent actions (structural and non-structural self-weight) in road bridges. To that aim, statistical distributions are updated using data collected on the Swiss road network and provided by institutions and private companies. Based on the updated statistics, parametric analyses are performed to investigate the sensitivity of the partial factors and to estimate their value. Accordingly, two partial factors are proposed for structural and non-structural self-weight, respectively. Finally, by means of case studies, it is demonstrated that a sufficient level of safety is ensured, both in absolute terms and when compared to current set of PSFs.

Keywords: structural reliability, reinforced concrete bridges, permanent load, pavement thickness variability, materials strength variability, traffic variability, failure modes;

4.1 Introduction

In this Chapter, the partial safety factors (PSFs) for permanent actions, used for designing new structures and for the assessment of existing ones, are updated for the case of reinforced concrete (RC) road bridges based on available statistical distributions of geometrical, material, traffic and model uncertainties. In road bridges, permanent loads result from the self-weight of structural and non-structural elements, which include the pavement, safety barriers and if present, non-structural curbs. In the latest available draft of FprEN1990:2022 [Eur22], the recommended partial safety factor for all permanent loads, denoted with γ_{Gi}, is equal to 1.35 and covers the uncertainty in the representative value of permanent loads and the model uncertainty in action effects calculation. For the model uncertainty in action effects calculation, the JCSS Probabilistic Model Code [JCS01] recommends a Log-Normal distribution with mean 1.0 and CoV between 0.05 and 0.20, but no clear background is provided. These values are confirmed in Chapter 2 of this thesis (additional references on this topic can be found in [Yu21] and in Chapter 2). As mentioned above, the recommended values of PSFs for structural and non-structural self-weight FprEN1990:2022 [Eur22] are the same. However, the latest available draft of prEN1991-1-1:2023 [Eur23] recommends to assume a deviation of the pavement thickness of

[-20%, +20%] or [-20%, +40%] depending on whether the pavement has already been replaced or not. In order to clarify whether these values are reasonable, data collected from measurements on various bridges in Switzerland will be analysed and it will be assessed whether there is a need to decouple the two partial safety factors for structural and non-structural self-weight, respectively. Traffic variability will also be considered using Weight In Motion (WIM) data collected in several locations in Switzerland. To estimate the partial safety factors, parametric reliability analyses, covering a wide range of scenarios, are performed based on the updated statistical distributions using the First Order Reliability Method (FORM). Finally, to investigate if a sufficient level of safety is achieved with the proposed partial safety factors, reliability analyses are performed using more refined methods on selected case studies.

4.2 Statistical uncertainties influencing structural self-weight

The self-weight of structural members in concrete bridges is affected by three main variables: (1) the specific weight of concrete, (2) the dimensions of concrete and (3) the reinforcement content (typically expressed in kg/m^3 and calculated on the basis of nominal dimensions). The bar diameter, the geometry and the specific weight of the reinforcement show also some variability affecting the self-weight, but these are negligible since the production is highly optimized and standardized. The same considerations apply also to composite bridges, where the largest source of variability for the structural self-weight is generally related to the reinforced concrete deck. Figure 4.1a shows the probability-plot of the specific weight of concrete obtained from around 3'500 samples (150×150×150 mm) collected in Western Switzerland between 2014 and 2021 (courtesy by TFB SA, only samples with an air content smaller than 2.5% are included in the analysis). The resulting CoV, neglecting the lowest part of the distribution, is 1.4%, significantly smaller than the value recommended by the JCSS report of 4% [JCS01] (which is based on the publication 115 of the CIB report [CIB89]). It is also much smaller than the value proposed by Ellingwood of 10% [Ell80], however, this value also included the geometric and reinforcement content variability, therefore, not directly comparable. It must be noted that the values shown in Figure 4.1a refer to the production of concrete in a limited area, thus, different statistical values could be found in similar studies in different locations where several aggregate types and petrography's can be found.

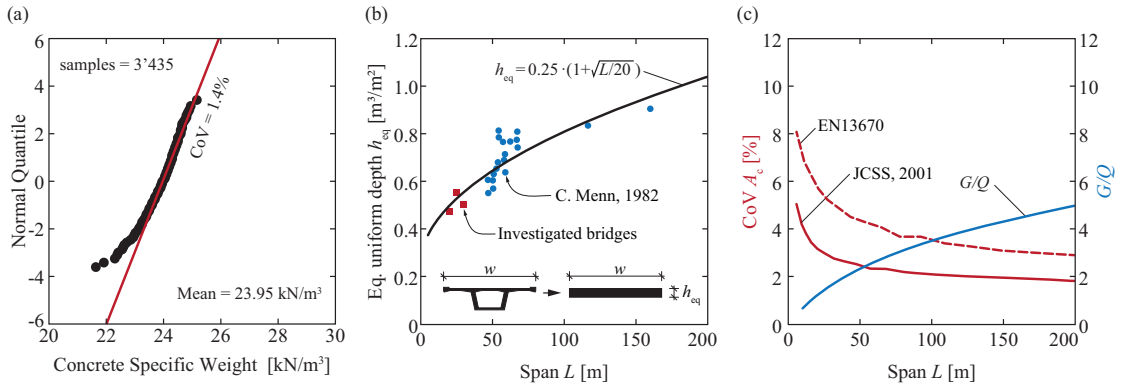

Figure 4.1: *(a) Normal probability-plot of concrete specific weight; (b) equivalent bridge deck thickness as a function of the span (values from Menn, 1982 [Men82] in blue circles and some investigated bridges of Table 4.1 in red squares); (c) CoV of the sectional area (A_c) variability assuming that tolerances correspond to standard deviations [ISO13] (dashed red) and statistical distributions according to the JCSS report [JCS01] (contionuous red); ratio of permanent load over traffic load (G/Q) for varying span (in blue).*

Figure 4.1c shows the coefficient of variation of the sectional area for increasing span of the bridge assuming that tolerances according to [ISO13] correspond to standard deviations (dashed red line) and using the statistical distributions recommended by the JCSS report [JCS01] (continuous red line). It can be observed that the importance of the geometric variability decreases with increasing cross-sectional dimensions. In fact, tolerances do not increase linearly and are limited for elements larger than a fixed threshold (e.g. 30 mm for cross-sectional dimensions larger than 2'500 mm [ISO13]). Thus, the geometrical variability has a relatively small influence on bridges with spans larger than 30 m.

Although geometric variability has a stronger influence on the structural self-weight of short span bridges, in these cases permanent loads are generally less significant compared to traffic loads. This is illustrated in Figure 4.1c (continuous blue curve), where the ratio between permanent load (obtained from the empirical relationship plotted in Figure 4.1b) and characteristic traffic loads (according to SIA 261:2020 [SIA20]) is presented as a function of the span length L. One can observe that the ratio G/Q varies between 0.5 for bridges with a short span (~10 m) and 4 for bridges with longer spans (~50-100 m).

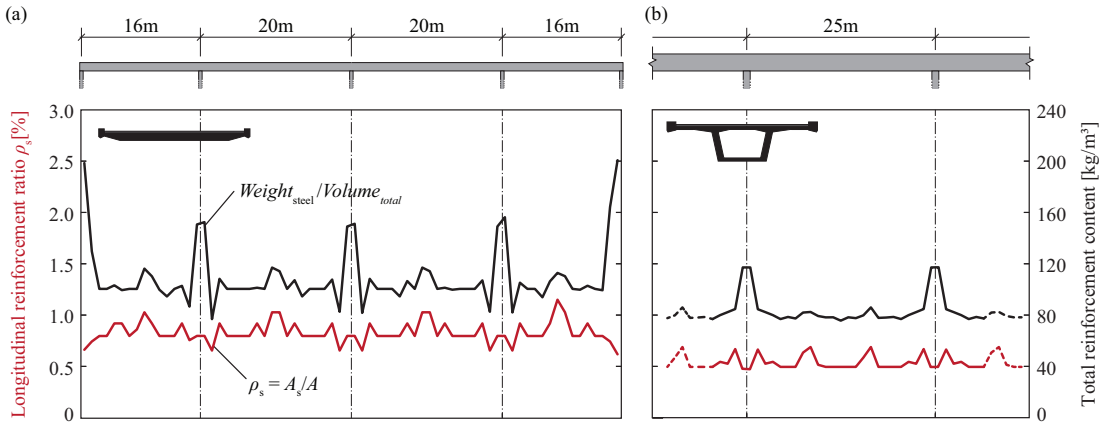

Figure 4.2: Longitudinal reinforcement ratio (red) and reinforcement content expressed in kg/m³ (black): (a) bridge Haute-Rive built in 1972 and (b) bridge Brocard built in 1964, see Table 4.1

Figures 4.2a,b show the reinforcement content in two reinforced concrete bridges calculated using the original drawings considering both prestressing and passive reinforcement. While the longitudinal reinforcement ratio (red line) is almost constant along the longitudinal axis of the bridge, the reinforcement content expressed in kg/m^3 increases close to the supports due to increased shear reinforcement and the more heavily reinforced transversal elements. However, close to the supports, as the load is directly transmitted to the latter, the reinforcement weight is less significant for the action effects. It must be noted that the reinforcement content in a bridge depends on several factors, such as the amount of prestressing, the structural system and the year of construction (generally, the reinforcement ratio of new structures being larger compared to older structures due to current more stringent requirements in terms of durability and serviceability as well as a reduced amount of prestressing).

4.3 Statistical uncertainties influencing non-structural self-weight

In addition to the structural self-weight, other non-structural loads contribute to the permanent load in road bridges. These include pavement, safety barriers and, if present, non-structural curbs. The same considerations made in the previous section for reinforced concrete elements apply also to reinforced concrete curbs while lane separation elements and safety barriers should be considered according to the corresponding specifications. In this work, the self-weight variability of the pavement is investigated whereas the variability of the other permanent actions is neglected. In particular, since the variability of the pavement thickness has a larger impact than the specific weight variability, the focus will be put on the former while the pavement

specific weight variability is assumed based on available literature [Hua89, Lyt93, Dal15]. Specifically, in this work, a mean value of 24.0 kN/m^3 and a CoV = 4% is assumed, as found by Hugenschmidt on bridges that were demolished in Switzerland [Hug06].

Figure 4.3a shows some typical cases of pavement thickness variability in the transversal and longitudinal direction. In particular, in the transversal direction, thickness variations occur mostly due to pre-existing deformations of the deck before surfacing which are generally caused by self-weight, transversal prestressing or imperfections during construction. In the longitudinal direction, two main scenarios can occur as illustrated qualitatively in Figure 4.3a: if the precamber and the deformations caused by prestressing exceed those caused by self-weight, the pavement will be typically thicker close to the supports while in case of non-prestressed bridges or if precamber and prestressing are not sufficient to compensate deformations caused by self-weight, the pavement is typically thicker at midspan. In addition, the imperfections of the concrete surface just after casting add an aleatory component to the variability of the pavement thickness. An additional source of uncertainty is related to the resurfacing of the pavement with partial replacement and correction of the deflections/settlements after some decades. The effects described above can be more or less significant and are generally combined in actual bridges.

Figure 4.3c shows the pavement thickness for one of the analysed bridges as part of this work using the Ground-Penetrating-Radar (GPR) technique. GPR measurements are performed by emitting electromagnetic waves which are reflected differently by the materials composing the different layers (i.e. bituminous pavement, concrete substrate). The propagation time of the electromagnetic waves is then recorded and converted to a dimension by determining the propagation speed of the wave in each layer. In all the analysed bridges, including this example, the propagation speed in the pavement is calibrated by means of control cores extracted at various locations along the bridge (red dots in Figure 4.3c). For details about GPR measurements and calibration see [Hug06, Hug10, Kal13]. The plot in Figure 4.3c shows that, in this case, in the transversal direction, the pavement is up to 50% thicker close to the edges. Also, the mean value of the thickness is significantly larger than the specified nominal value defined in the original drawings, suggesting that the pavement thickness was probably increased during resurfacing. Figure 4.3b shows the ratio between the mean of the measured thickness and the specified nominal value for 7 bridges build between 1963 and 1994 which were investigated as part of this research (raw data provided by Bridgology SA), see Table 4.1 for details.

Table 4.1: Details of the bridges where pavement thickness measurements are performed, raw data provided by Bridgology SA

Bridge	Location	Constr. year	Typology	Span [m]	Nominal thickness [m]	μ*	CoV [%]
Viaduc du Brocard	A21 Martigny - G. St. Bernard (km. 60.060)	1964	Box-girder	19.6-25.0	0.050	1.3-1.7	17.0-20.0
Pont de Rive-Haute	A21 Martigny - G. St. Bernard (km. 250.875)	1972	H-Core Slab	16.0-20.0	0.050	2.3-2.4	16.3-19.3
Jonction de Vennes	N9 Lausanne (km. 7.039)	1963	H-Core Slab	39.0	0.070	2.0-2.2	19.0-21.6
P. Supérieur Le Daillet	N9 Sion-Sierre (km. 105.161)	1992	Multi-beam	33.5	0.060	1.4	9.4-10.8
P. Supérieur Sierre-Ouest	N9 Sion-Sierre (km. 113.392)	1992	Slab	36.0	0.075	1.3-1.4	11.1-13.9
Viaduc des Îles Falcon-Nord	N9 Sion-Sierre (km. 116.104)	1994	Box-girder	27.4-73.0	0.075	1.1-1.4	10.8-13.8
Viaduc des Îles Falcon - Sud	N9 Sion-Sierre (km. 116.104)	1994	Box-girder	27.4-73.1	0.075	1.1-1.3	8.4-9.9

*The bias is defined as the mean of the measured thickness in each span over the nominal thickness:
$\mu = t_{pav,mean} / t_{pav,nomina}$

It can be observed that the bias factor μ, defined as the ratio between the measurements mean and the nominal thickness for each span, is generally between 1.1 and 1.7, which justifies the increase of the nominal value recommended by [Eur23] of 20 or 40%. The mean measured thickness is never found to be smaller than the nominal value. Also, it can be observed that for smaller spans, the bias ratio increases. This could be related to the fact that for short span bridges, the pavement thickness can depend mainly from requirement related to the level of the approaching road.

Considering the equivalent thickness of the concrete section, h_{eq}, as shown in Figure 4.1b and a standard pavement thickness of 100 mm, the pavement weight is relatively more significant for smaller spans than for larger ones, accounting up to 25% of the total permanent load for spans between 8 and 12 m. Since the bias is also larger in those cases, potentially unsafe scenarios are more likely to occur. Considering all the measurements within each span, the CoV of the pavement thickness ranges between 8.4 and 21.6%, see Table 4.1. Despite a slightly larger upper limit, these values are in line with previous researches which presented a CoV between 8 and 15% [Lyt93, Dal15].

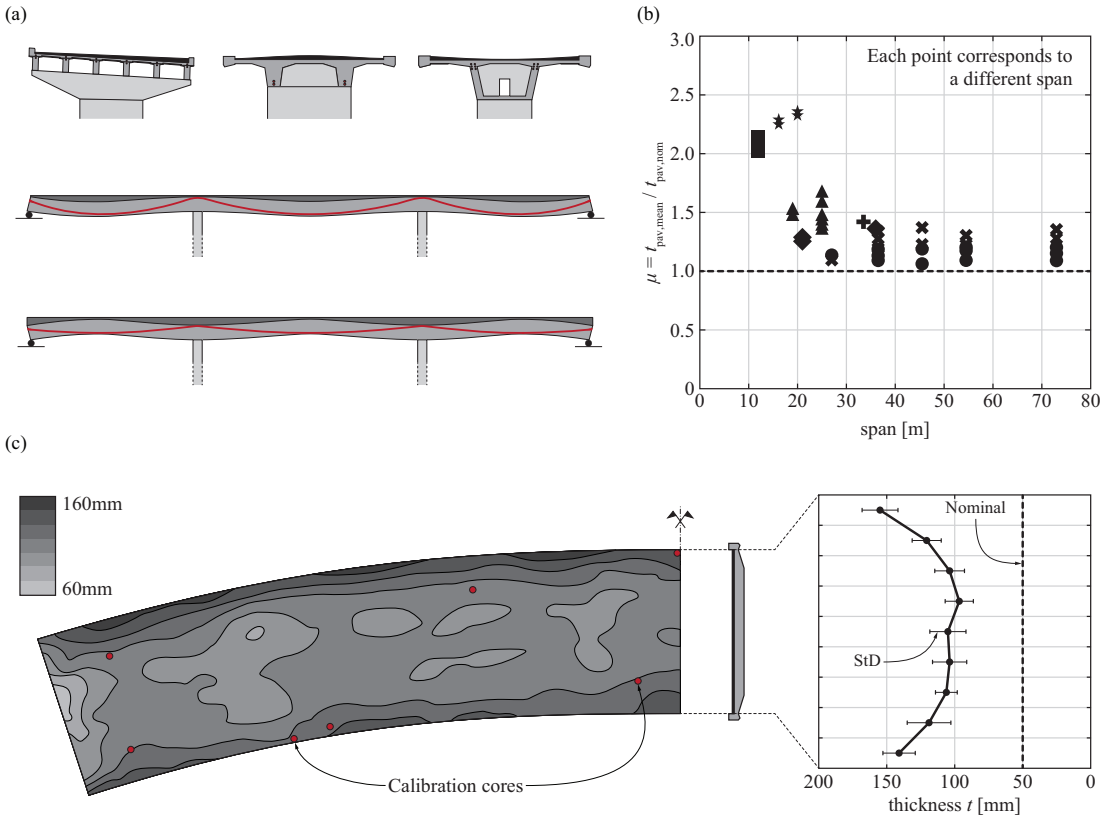

Figure 4.3: Typical pavement thickness variability in road bridges (a) qualitative transversal and longitudinal distributions; (b) ratio between the actual mean and the nominal pavement thickness as a function of the span for the investigated bridges; (c) greyscale map of the measured pavement thickness of the Rive-Haute bridge as an example, see Table 4.1 (raw data provided by Bridgology SA and analysed as part of this research)

4.4 Updating of other statistical uncertainties

In addition to the variability of the permanent loads in road bridges described above, an accurate estimation of the variability on the resistance side and of the traffic loads is necessary to calibrate the PSFs. In fact, all variabilities contribute to the limit function, which separates the safe structural domain from the unsafe one. In the First Order Reliability Method (FORM) analysis, the relative contribution of the single variabilities is represented by the sensitivity factors, α, which is the partial derivative of the limit state function with respect to the investigated variable. Per definition, the sum of the squares of all sensitivity factors corresponds to 1.0. Thus, if the weight of one variable increases, the weight of all the others must decrease (see [Sch17] for further details on the meaning of the sensitivity factors and FORM analysis). Therefore, to

accurately estimate the sensitivity factor of the permanent loads, in the following sections, the variability of the materials parameters, traffic loads and resistance models will be investigated.

4.4.1 Materials strength

Regarding the reinforcement yield strength, f_y, assumptions made in Annex A of prEN1992-1-1:2023 [Eur23] are assumed for new structures. For existing structures, these assumptions are verified on the basis of an existing database referring to steel produced in Switzerland [Ken15]. The data of more than 2'500 tests conducted between 1960 and 1994 for steel classes IIIa and IIIb according to SIA 162 [SIA68] (specified 5% characteristic value $f_{yk} \approx 451$MPa) are considered in this evaluation. Figures 4.4a and 4.4b show the mean and the CoV of the reinforcement yield strength, f_y, as a function of the year of production and of the bar diameter.

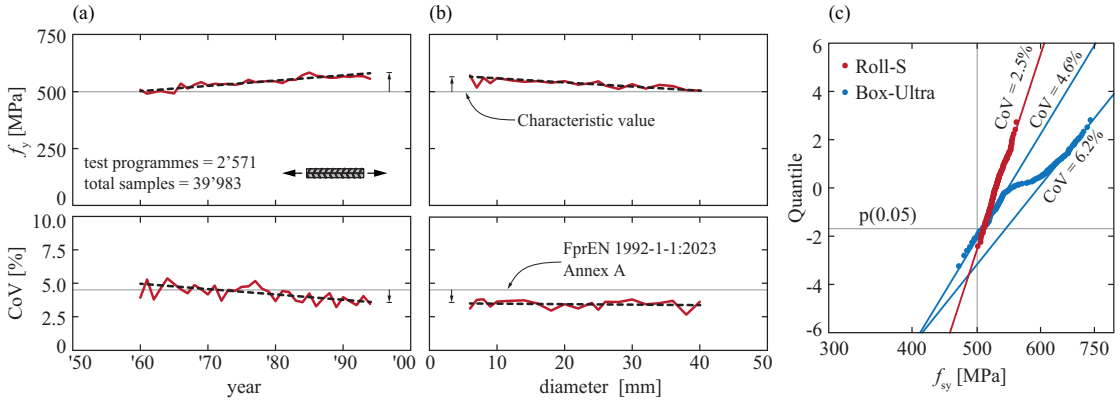

Figure 4.4: Mean and coefficient of variation of steel yield strength, respectively top and bottom: (a) as a function of time; (b) as a function of the bar diameter; (c) log-normal probability plot of two common steel products available in Switzerland

The mean value increased with time, associated also with a decrease of the CoV. This was most likely due to the optimization of the industrial production processes over time. For bars with larger diameters, the yield strength shows a decreasing trend. In some cases, when products are categorized by steel type (based on the producer), the distribution deviates from the typical Log-Normal (LN) distribution, see difference between Roll-S and Box-Ultra in Figure 4.4c. This was perhaps the result of two different products grouped under the same designation. In fact, the two distributions can clearly be identified and show similar CoV. Overall, the CoV resulting from the analysed data for existing structures is in line with Annex A of prEN1992-1-1:2023 [Eur23] where a CoV = 4.5% has been assumed for new structures. These values are also confirmed by other publications [Now03, Bee16]. Previous researches [Mir79, Ell80] report larger CoV, up to 10-12%, however, they are based on a more limited amount of

data and different steel grades. With respect to the variability of the actual cross-section of the reinforcement bars, it is implicitly accounted for in the evaluation of the yield strength since the latter is calculated on the basis of the nominal cross-sectional area.

Figure 4.5a shows the log-normal probability-plot of the yield strength (proof-stress at 0.1% irreversible strain) and the tensile strength of prestressing strands, respectively. The probability-plot of the Young's modulus is presented in Figure 4.5b. Data refer to tests carried out in Switzerland in the period between 1968 and 1979 (see [Kre79]). In particular, Figure 4.5a shows that the CoV of the yield strength of prestressing strands is similar to that of passive reinforcement, confirming the assumptions made in Annex A of prEN1992-1-1:2023 [Eur23], namely CoV = 4.5% and is consistent with value reported by other researches [Mir80, Ell80, Bas98, Now03, Fos16]. In addition, the mean value of the Young's modulus is equal to 195 GPa with a CoV of 2.8%. This value is also consistent with results published by other researchers [Mir80].

*Table 4.2: Distribution parameters of the concrete compressive strength variability at 28 days, data provided by TFB SA for samples with void content lower than 2.5%, collected in Western Switzerland between 2014 and 2021. The columns on the right refer to the concrete classification on the basis of the exposure (defined as concrete type according to the Swiss national annex to EN 206 [*SIA21*].)*

Strength Class	Number of tests	Mean $f_{c,cube,28}$ [MPa]	CoV [%]	$P(0.05)$ [MPa]	Type	Number of tests	Exposure Class	Mean $f_{c,cube,28}$ [MPa]	CoV [%]	$P(0.05)$ [MPa]
C20/25	86	35.5	14.1	27.9	A	86	XC1, XC2	35.5	14.1	27.9
C25/30	737	43.8	18.9	31.6	A	227	XC1, XC2	40.0	17.2	29.8
					B	347	XC3	41.3	14.4	32.3
					D	120	XC4, XD1, XF2, XF3, XD2a	53.2	10.4	44.6
					P2	43	ND	50.8	9.9	43
C30/37	2470	51.7	14.2	40.6	A	75	XC1/XC2	44.8	13.6	35.8
					B	121	XC3	56.9	9.2	48.7
					C	1583	XC4/XF1	51.1	11.8	41.8
					F	173	XC4, XD3, XF2, XD2b, XAA	52.1	15.2	40.2
					G	438	XC4, XD3, XF4, XD2b	56.1	15.9	42.7
					P2	80	ND	62.5	13.3	49.8
C35/45	167	59.2	10.9	49.2	C	83	XC4, XF1	56.7	8.7	48.9
					F	40	XC4, XD3, XF2, XD2b, XAA	63.5	11.3	52.4
					G	44	XC4, XD3, XF4, XD2b	62.6	8.0	54.7

Figure 4.5c shows the probability-plot of the concrete compressive strength at 28 days ($f_{c,cube,28}$) of various concrete strength classes (C20/25, C25/30, C30/37, C35/45). Distributions are obtained from ~3'500 compression tests performed on concrete cubes with an edge size of 150 mm in Western Switzerland between 2014 and 2021. Tests include concretes used in residential buildings and engineering works with a void content lower than 2.5% and various exposure classes, see Table 4.2 for details.

Data follows a log-normal distribution (see Figure 4.5) which is in line with recommendations of [JCS01] and [Eur22]. As it can be observed, the actual characteristic value of each concrete class (defined as the 5th percentile of the distribution) is generally slightly higher than the specified value (difference from 1.6 to 4.2 MPa). Also, the difference between mean value and 5th percentile varies between 7.6 and 12.2 MPa, which is more or less in line with the typical assumption (between 8 and 10 MPa, see [Eur23]). Besides the strength class, on the right-hand side of Table 4.2, concrete samples are classified based also on their exposure class, see [SIA21]. Table 4.2 shows that a larger mean compressive strength is generally obtained for concretes with more stringent exposure requirements (e.g. for a C30/37 strength class, $f_{c,cube,28}$ of Type G concrete typically used in engineering works is 56.1 MPa while that of Type A typically used in buildings is 44.8 MPa). This over-strength is related to the minimal cement content requirements and to the fact that exposure requirements are often governing in the mix design. This justifies also the large mean compressive strength of concretes used for underwater piles and slurry walls (Type P2). Overall, the resulting CoV for the concrete compressive strength is located in the upper range of results published in the literature, see Annex A of prEN1992-1-1:2023 [Eur23] and Torrenti & Dehn [Tor19]. The empirical rule: $f_{cm} - f_{ck} = 8$ MPa, provided in prEN1992-1-1:2023 [Eur23] is generally confirmed, although, slightly higher values are obtained. However, it must be noted that these values are specific to the current Swiss concrete production situation which will probably evolve due to environmental requirements.

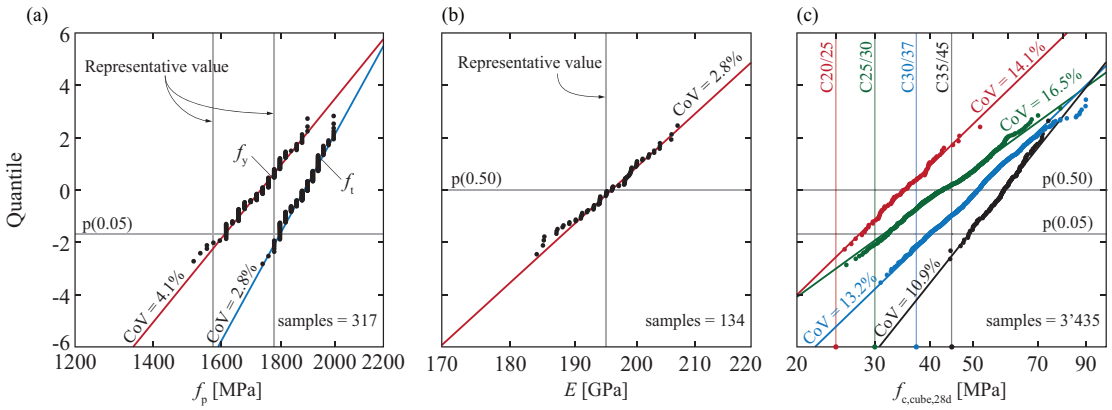

Figure 4.5: Log-normal probability plot of: (a) yield strength (red) and tensile strength (blue) of prestressing strands; (b) elastic modulus of prestressing strands; (c) concrete compressive strength at 28 days ($f_{c,cube,28}$) for various concrete strength classes (all exposure classes included in the analysis), see Table 4.2.

4.4.2 Traffic loads

The aim of this investigation is not to reproduce a realistic scenario from the structural point of view but to quantify the variability of the traffic loads without considering the uncertainties related to the calculation of action effects and the transversal load distribution. To this purpose, a simply supported bridge with a width of 3 m (single lane) and span varying between 6 and 24 m is used, as shown in Figure 4.6a.

Traffic load is simulated using Weight In Motion (WIM) measurements which were performed during more than 20 years at 14 stations located in Switzerland. After being classified considering the vehicle type, the measurements are combined and directly applied on the structure (this simulation procedure is denoted as "direct WIM" in the following, for details regarding WIM data classification and generation of direct-WIM loads, see [Sja20]). Action effects calculated from direct WIM simulations are then compared with those obtained using a representative load model, assumed according to the SIA 261:2020 [SIA20], which is derived from EN1991-2:2003 [Eur03]. As already mentioned, the aim of this investigation is to quantify the variability of the traffic load in terms of CoV of the action effects. Since the investigated bridge is not representative of a real case (single lane), the bias of the action effects (E_{WIM}/E_{REP}) is not significant for this investigation. For this reason, the adjustment factors $\alpha_{act,Q,i}$ and $\alpha_{act,q,i}$ are set equal to 1.0 (not in accordance with SIA 261:2020 [SIA20]).

Direct WIM simulations are performed using both the weekly maxima traffic loads distribution, obtained from WIM measurements, and the 50-year maxima traffic loads distribution, derived from the weekly maxima as explained further on. To determine the 50-year maxima distribution, the weekly maxima events are considered as Independent-Identically-Distributed (IID) variables. Based on this assumption, if $F_X(x)$ is the common Cumulative Distribution Function (CDF) of the weekly maxima traffic load, and $F_N(y)$ is the CDF of the 50-year maxima traffic loads, with $Y = \max\{X_1, X_2, \ldots, X_N\}$, $F_N(y)$ is obtained from Eq. (4.1), with N equal to the number of weeks in 50 years (~2'607). Thus, the CDF of Y, the 50-year maxima distribution is obtained by taking the N^{th} power of the CDF of X, the weekly maxima distribution.

$$F_N(y) = P\left[(X_1 < y) \cap (X_2 < y) \cap \ldots \cap (X_N < y)\right] = \left\{F_X(y)\right\}^N \tag{4.1}$$

If N is a large number, the 50-year maxima distribution is either a Gumbel Extreme Values (GEV) Type-I or a Type-II depending on the tail approximation of the IID variable. In particular, if the tail of the Probability Density Function (PDF) of the weekly maxima distribution follows a Log-Normal (LN) or a GEV Type-I distribution, the 50-year maxima distribution will be a GEV Type- I (for additional details about the theoretical derivation and sample maxima distributions, see [Ric06]).

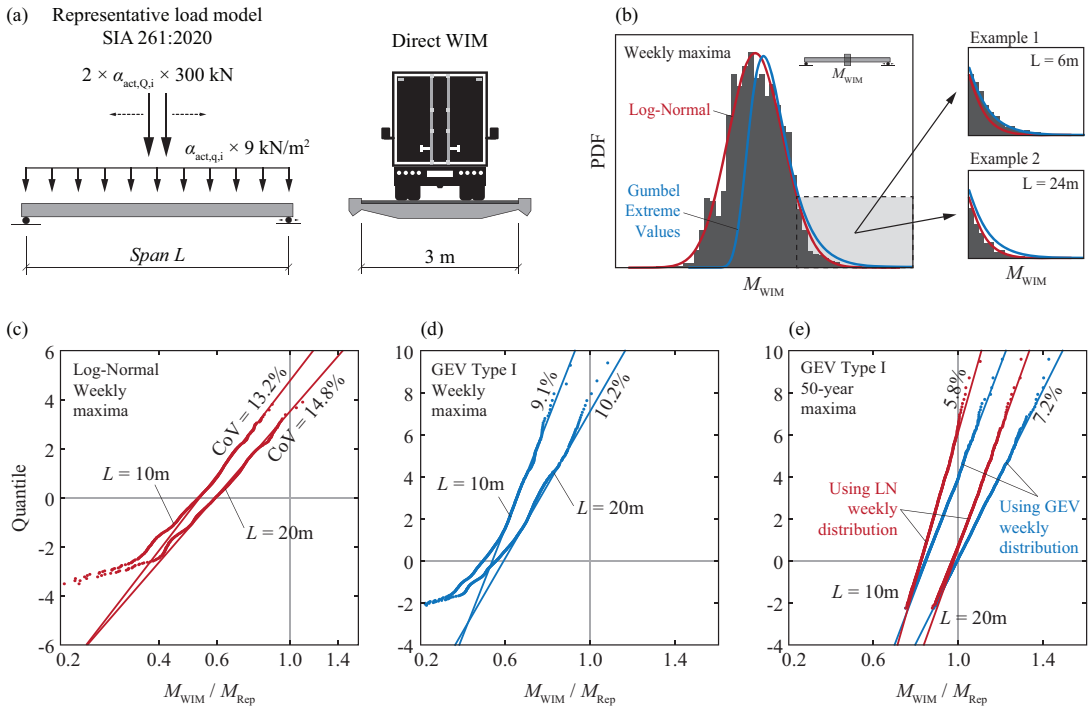

Figure 4.6: *(a) Investigated structural system and representative load model according to [SIA20] with the adjustment factors $\alpha_{act,Q,i} = \alpha_{act,q,i} = 1.0$; (b) typical histogram of the bending moment at midspan obtained from the weekly maxima direct WIM simulation (E_{WIM}) and tail fitting using a LN (red line) and a GEV Type-I distribution (blue line) with tail fitting details; (c) ratio between the bending moment at midspan obtained from direct WIM simulation with weekly maxima distribution and the bending moment at midspan obtained with the representative load model (M_{WIM}/M_{Rep}), tail fitted using a LN distribution for a span of 10 m and 20 m; (d) same data presented in (c) but tail fitted using a GEV Type-I distribution; (e) 50-year maxima distributions resulting from the weekly maxima distributions presented in (c) and (d)*

Figure 4.6b shows a typical histogram obtained for the bending moment at midspan using the weekly maxima traffic distribution and the tail fitting using both a LN and a GEV Type-I distribution presented respectively in red and blue. As presented in the tail fitting details of Figure 4.6b, with example 1 and 2 corresponding respectively to a span of 6 and 24 m, the most suitable distribution type depends on the specific case. Since the accuracy in approximating the tail fitting of the weekly maxima distribution influences significantly the distribution of the 50-year maxima and it is not possible to know a priori the best tail fitting distribution, both, a LN and a GEV Type-I distributions are used in the following to fit the tail of the weekly maxima distribution for each span L. Figure 4.6c shows the probability-plot of the ratio between the bending moment at midspan obtained using the traffic weekly maxima distribution (M_{WIM}) and

the bending moment obtained with the representative load model (M_{REP}) fitted using a LN distribution for a span L = 10 m and L = 20 m. The same cases are presented also in Figures 4.6d but using a GEV Type-I distribution. In Figures 4.6c and 4.6d, the fitting is performed considering only points on the upper part of the distribution ($P > 0.5$). Figure 4.6e shows the resulting 50-year maxima distribution using the weekly distributions of Figure 4.6c and 4.6d. Since the PDF tail of the GEV Type-I distribution shows a slower decrease than the LN distribution, it leads to larger bias and CoV. Based on the analysed spans, the CoV of the traffic load effects is found between 10% and 18% for the weekly maxima traffic load distribution and between 6% and 10% for the 50-year maxima traffic load distribution.

4.4.3 Variability of resistance calculation

The variability of the sectional resistance calculation is quantified by means of Monte-Carlo simulations performed considering the variability of the materials strength, the calculation models and the geometry. More specifically, this work focuses in quantifying the variability of the resisting bending moment calculation and the variability of the shear resistance calculation for members with shear reinforcement. To this purpose, the models provided in Section 8 of Fpr EN1992-1-1:2023 [Eur23] are implemented (provisions 8.1.1 and 8.1.2(1) for bending and 8.2.3(1-3,5,7,8) for shear). In addition, to investigate the influence of the cross-sectional dimensions (see Figure 4.1c), a concrete section with constant width and depth, h, varying between 0.35 m and 1.4 m is investigated.

Table 4.3: Statistical distributions assumed for performing Monte-Carlo analyses to quantify the variability of shear resistance for members with shear reinforcement and bending moment resistance for RC members

Random variable	CoV – V [%]	Bias - μ	Reference
f_c	10.0	1.18	Annex A of prEN1992 1 1:2023 [Eur23]
η_{is}	12.0	0.95	Annex A of prEN1992 1 1:2023 [Eur23]
f_y	4.50	1.08	Annex A of prEN1992 1 1:2023 [Eur23] and Section 4.4.1
d	$5\cdot(200/d)^{2/3}$	$1 - 0.05\cdot(200/d)^{2/3}$	Annex A of prEN1992 1 1:2023 [Eur23]
A_c	2.0 – 6.0	1.00	JCSS report, 2001 [JCS01]
$\theta_{R,Flex,steel}$	4.50	1.09	Annex A of prEN1992 1 1:2023 [Eur23]
$\theta_{R,Shear}$	19.4	1.11	Pejatovic et al. [Pej22]

The variability of the materials strength is assumed according to Annex A of prEN1992-1-1:2023 [Eur23] while the geometric variability is assumed according to [JCS01],

except for the effective depth which is assumed according to Annex A, see Table 4.3. With regard to the model uncertainty for the calculation of the resisting bending moment, with failure occurring on the steel side, the value proposed in Annex A is assumed while the model uncertainty for the calculation of the shear resistance in members with shear reinforcement is assumed according to [Pej22]. Table 4.3 gives an overview of the statistical parameters used to perform the Monte-Carlo simulations. For details on the implemented models, see Fpr EN1992-1-1:2023 [Eur23].

Figures 4.7a and 4.7b show the resulting CoV (V_R) and the bias factor (μ) for the calculated resistances as a function of the section depth h. For each section depth, 10'000 simulations are performed for both shear resistance and bending moment resistance to determine the coefficient of variation and the bias factor. Figure 4.7c shows the probability plot for the case of h = 0.35 m.

Figure 4.7a shows that for the calculation of the bending moment, the CoV decreases with increasing depth, h. This is due to the fact that the relative variability of the effective depth (d) is less significant for larger members. In fact, according to the formula in Table 4.3, an effective depth d = 1.2 m leads to μ =0.985 and V = 1.51% whereas for d = 0.2 m, μ =0.95 and V = 5%. On the other hand, for the calculation of the shear resistance, the variability of the effective depth is less significant, leading to a less pronounced reduction of CoV for larger members. Figure 4.7b shows that for the shear resistance calculation, the bias varies between 1.20 and 1.25 while for the calculation of the bending moment, the bias varies between 1.14 and 1.16.

It can be noted that, regardless of the beam depth, the coefficient of variation V_R is much larger for the calculation of the shear resistance than for the calculation of the resisting bending moment. This is mainly due to the large model uncertainty for shear resistance calculation, see Table 4.3. Figure 4.7c shows also that a Log-Normal (LN) distribution is a good fit for the resistance variability both for the calculation of shear and bending moment resistance, in line with the recommendations of [JCS01] and Annex A of prEN1992-1-1:2023 [Eur23].

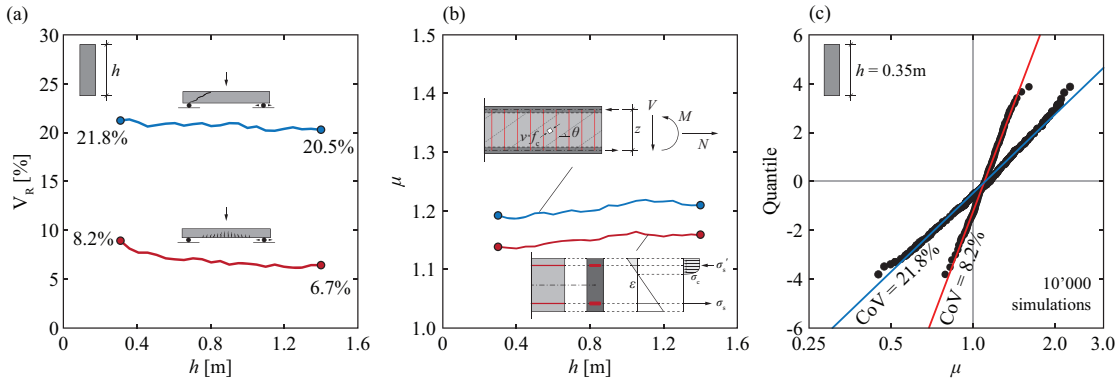

Figure 4.7: Variability of bending moment and shear resistance calculation for a beam with fixed width and varying depth between 0.35 m and 1.4 m: (a) coefficient of variation V_R and (b) bias factor μ; (c) LN probability-plot of sectional resistance calculation for a beam with h = 0.35 m

4.5 Calibration of γ_{G1} and γ_{G2} using FORM

As already discussed in the previous sections, the variability of the structural and non-structural self-weight is significantly different in road bridges. Therefore, the partial safety factor for permanent loads, γ_{Gi}, is treated separately for structural and non-structural self-weight, denoted with γ_{G1} and γ_{G2}, respectively. To estimate their values, parametric FORM analyses are performed covering a wide range of scenarios. The statistical distribution parameters of action effects (E), sectional resistance (R) and model uncertainty in action effects calculation (θ_E) are presented in Table 4.4.

The statistical distributions of the actions effects due to the structural and non-structural self-weight, respectively E_{G1} and E_{G2}, are obtained on the basis of the considerations made in the previous sections which are resumed in Tables 4.5 and 4.6. To account for the large uncertainty related to the traffic loads, a wide range of CoVs is considered on the action effects due to the latter (V_{EQ}). Also, since the variability of the sectional resistance calculation varies largely depending on the failure mode, the latter is investigated considering a wide range of the CoV (V_R). Finally, the statistical distribution parameters of the uncertainty in action effects calculation are assumed according to Chapter 2 of this thesis. In particular, for a Linear Elastic model with uncracked sectional stiffness, a CoV of 6.5% is assumed as shown in Table 4.4.

Regarding the representative values of the actions, the self-weight for reinforced concrete members is calculated using the nominal dimensions and the specific weight equal to 25 kN/m^3 [Eur23], including the reinforcement. The pavement load is calculated considering a representative thickness of the pavement of 100 mm (i.e., not accounting for the increase of 20-40% recommended in [Eur23]) and the specific weight equal to 24 kN/m^3 [Eur23]. Finally, the representative value of the traffic load (Q) is considered as a function of the permanent loads ($G = G_1+G_2$). Specifically, the ratio of the action effect due to permanent loads over the action effects due to traffic loads E_G/E_Q, is assumed equal to 4 and 0.5, which correspond respectively to a long and a short span bridge.

$$g(R,E) = R - E = R - (E_{G1} + E_{G2} + E_Q) \cdot \theta_E \tag{4.2}$$

$$\gamma_{Gi} = \mu_{Gi} \cdot exp(\alpha_{Gi} \cdot \beta_{tgt} \cdot V_{Gi}) \tag{4.3}$$

$$\alpha_{Gi} = \sqrt{\alpha_{gi}^2 + \alpha_{\theta E}^2} \qquad V_{Gi} = \sqrt{V_{gi}^2 + V_{\theta E}^2} \qquad \mu_{Gi} = \mu_{gi} \cdot \mu_{\theta E} \tag{4.4}$$

The limit state function is formulated in the classical form as in Eq. (4.2) while γ_{Gi} is calculated according to Eq. (4.3) with the sensitivity factors, α, obtained from the FORM analyses. Besides the uncertainty related to the representative value of the permanent loads, γ_{Gi} covers also the model uncertainty in the action effects calculation, denoted with θ_E. Thus, to account for this uncertainty, α_{Gi}, V_{Gi} and μ_{Gi} are calculated as in Eq. (4.4). The value of $\beta_{tgt,50y}$ is assumed

according to [Eur22], equal to 3.8. Indeed, the choice of β_{tgt} depends on the risk acceptance at a societal level and is not treated in this work.

Table 4.4: Distribution type and parameters of random variables used for the parametric analyses

Var.	Distribution	μ	V [%]
E_{G1}	Normal	1.00	3-6
E_{G2}	Normal	1.10-1.30	15-25
E_Q	Log-normal	0.7-1.0	4-26
R	Log-normal	1.09-1.12	4-24
θ_E	Log-normal	1.00	6.5

Figure 4.8 shows the sensitivity factors α, smaller than 1 by definition, and the partial safety factors γ, larger than 1, obtained from the parametric analysis as a function of the coefficients of variation V_R and V_Q. As already mentioned, two ratios of E_G/E_Q are investigated, namely 4 and 0.5, which correspond respectively to a long and short span bridge (the ratio total permanent load / total live load (G/Q) for bridges with increasing span is shown in Figure 4.1c). For a long-span bridge, Figures 4.8a and 4.8c show that V_Q does not influence γ_{G1} and γ_{G2} while an increase of V_R leads to smaller values of γ_{G1} and γ_{G2}. In fact, since traffic loads are less significant compared to permanent loads, their variability does not lead to a remarkable change of the sensitivity factor (α), and consequently on the partial factors (γ). On the other hand, for short span bridges, an increase of both V_Q and V_R leads to a decrease of γ_{G1} and γ_{G2}. Overall, for the investigated scenarios, the required value of γ_{G1} varies between 1.1 and 1.2, whereas γ_{G2} varies between 1.3 and 1.8.

Based on the results of the parametric analysis, the proposed values for γ_{G1} and γ_{G2} are 1.2 and 1.5, respectively. To cover the cases where γ_{G2} is larger than 1.5, an increase of the representative value of the pavement thickness as required in [Eur02] and in [Eur23] is justified (an increase of the nominal value by 20% covers the cases where γ_{G2} is larger than 1.5: $1.2 \times 1.5 = 1.8$).

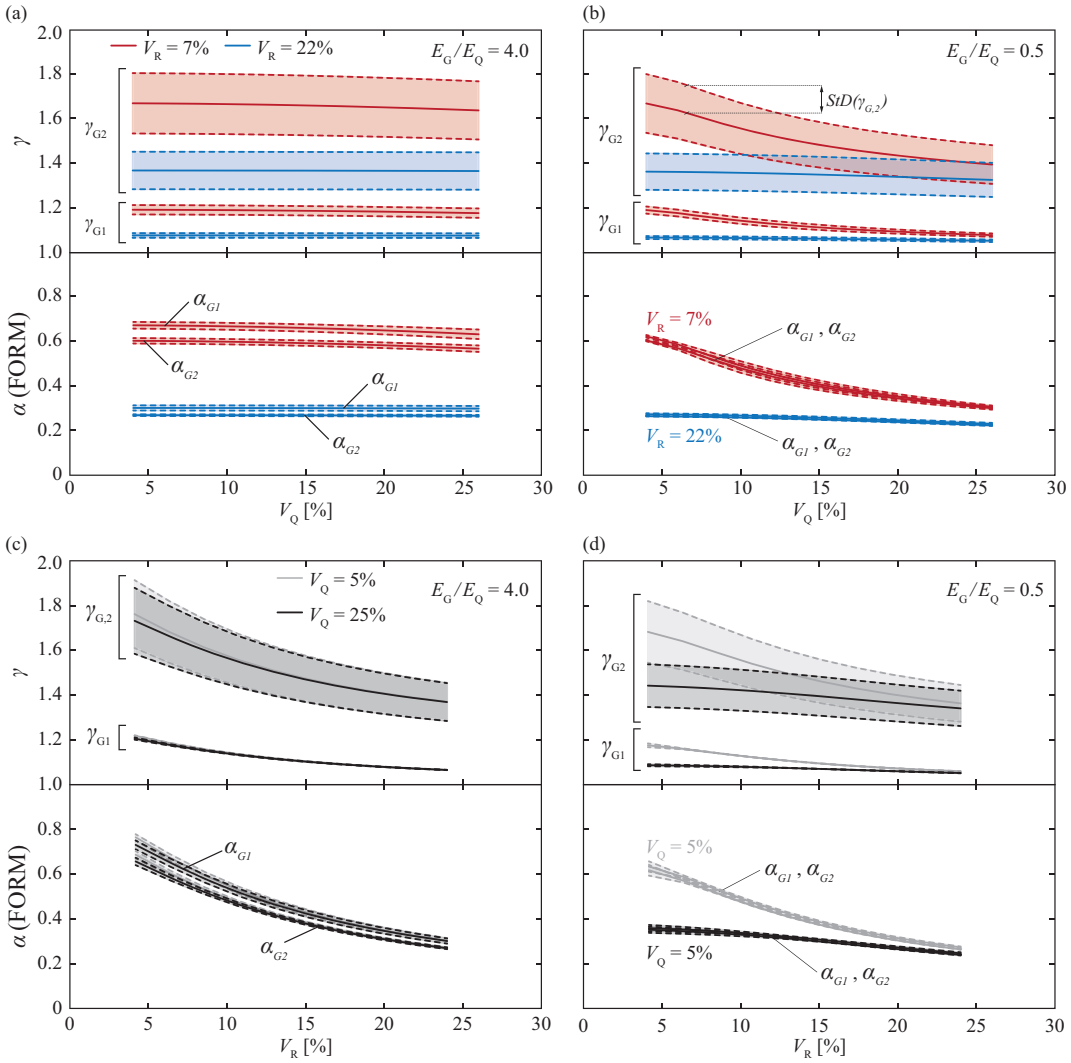

Figure 4.8: α_{G1} , α_{G2} *[0,1] and* γ_{G1} , γ_{G2} *(>1) as a function of* V_Q *and* V_R *for a road bridge with* E_G/E_Q *equal to 4 and 0.5, which correspond respectively to a long and short span bridge.*

4.6 Validation of the proposed partial factors for a particular case

To investigate if a sufficient level of safety is achieved with the proposed partial safety factors, more refined reliability analyses are performed on two bridges with a maximum span of 20 and 30 m, respectively. Figure 4.11a shows the longitudinal scheme and the transversal cross-section of the investigated bridges.

Both bridges are designed to fulfil the requirements of traffic loads for new bridges, according to [SIA20], and for existing bridges according to [SIA11], while representative permanent loads are calculated according to [Eur23] (but no increase of the nominal pavement thickness is considered). Dimensioning is performed according to Section 8 of Fpr EN1992-1-1:2023 [Eur23] with a reinforcement ratio in the tension zones ranging between 0.4 and 0.8% and the posttensioning tendons designed to carry the remaining required tension force at ULS (the average compressive concrete stress due to prestressing P/A_c is 1.75 and 2.05 MPa for the bridge with maximum span of 20 m and 30 m, respectively). The considered partial factors for the dimensioning are $\gamma_S = 1.15$ and $\gamma_C = 1.50$ whereas the currently recommended partial factors for the permanent actions $\gamma_{G1} = \gamma_{G2} = 1.35$ as well as the proposed combination $\gamma_{G1} = 1.20$ and $\gamma_{G2} = 1.50$ are considered. The strain difference in the prestressing steel and the hyperstatic moments due to prestressing are calculated considering: (i) an initial prestressing stress of $0.7 \cdot f_{pk}$, (ii) the tendon's geometry shown in Figure 4.10c, (iii) the friction losses according to Fpr EN1992-1-1:2023, and (iv) 15% losses due to relaxation, shrinkage and creep.

For the refined reliability analyses, the variability of the geometry and the specific weight is modelled considering that a certain correlation exists between two points in the same element. This correlation is expressed by the Pearson correlation coefficient, which is denoted with ρ_{cc} and is calculated according to [JCS01] as shown by Eq. (4.5), where δ is the correlation length, characteristic of the member type (e.g. equal to 6 m for slabs and walls and 10 m for reinforced concrete beam) and Δr is the distance between the points. The parameter ρ_{cc0} represents the correlation between two far away points in the same element.

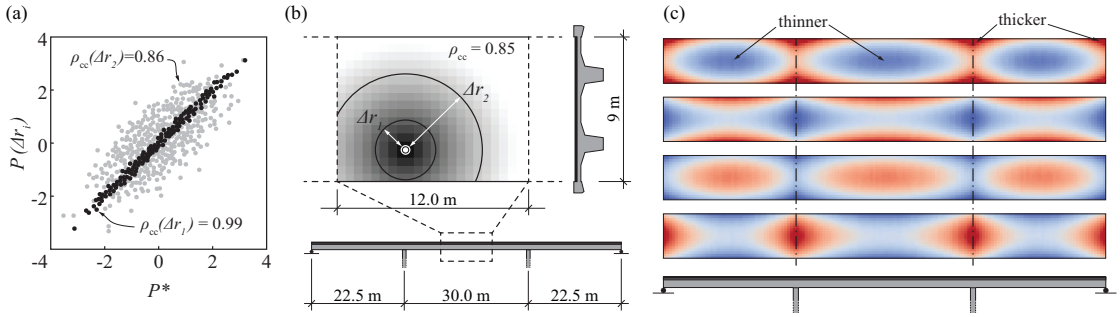

Figure 4.9: (a) Property of a reference point P and property of a point at a distance Δr_1 and Δr_2 considering the Pearson correlation coefficient ρ_{cc}; (b) decrease of ρ_{cc} from a reference point; (c) typical simulations of pavement thickness variability in road bridges.*

Figure 4.9a illustrates the correlation between the property of a reference point, P^*, and the property of two different points, $P(\Delta R_1)$ and $P(\Delta R_2)$, part of the same structural element, respectively at a distance Δr_1 and Δr_2 from the reference point, see Figure 4.9b. Figure 4.9b shows the decrease of ρ_{cc} as a function of the distance Δr. For a distance between the points larger than the characteristic length (δ), $\rho_{cc} = \rho_{cc0}$, with $\rho_{cc0} = 0.85$ in this particular case, assumed according to [JCS01]. If multiple points are involved, instead of a single coefficient, the

correlation is represented by a symmetric matrix [$n \times n$] with n equal to the number of investigated points. The symmetry of the matrix is due to the fact that ρ_{cc} is calculated considering only the distance between points and not the direction.

$$\rho_{cc}(\Delta r) = \rho_{cc} + (1 - \rho_{cc0}) \cdot \exp\left(-(\Delta r / \delta)^2\right) \quad with \quad \rho_{cc0} = 0.85 \tag{4.5}$$

Correlation of the pavement thickness and specific weight in different points of the same bridge is modelled using the same procedure and the characteristic length δ = 6 m.

Figure 4.9c presents the resulting pavement thickness modelled by discretizing the surface of the bridge deck and implementing the longitudinal, the transversal and the aleatoric variability (see Section 4.3). The correlation is implemented using the methodology described above. The longitudinal and transversal thickness variabilities, which account for the pre-existing deformations, are modelled assuming a parabolic profile in both directions with the ratio $t_{long,support} / t_{long,midspan}$ and $t_{transv,center} / t_{transv,edge}$ defined by the distribution presented in Table 4.6. Table 4.5 presents the distribution parameters assumed for modelling the variability of the structural self-weight. The geometric variability is modelled according to [JCS01] as shown in Figure 4.1c. For the reinforcement content, the statistical parameters presented in Table 4.5 are assumed, see also Figure 4.2.

Table 4.5: Statistical parameters for modelling of the structural self-weight

Random variable	CoV – V [%]	Bias factor – μ	Mean value
A_c	2.0 – 5.0	1.00	-
$\rho_{concrete}$ [kN/m^3]	4.0	-	24.0
Reinforcement content [kg/m^3]	15.0	-	130.0

Table 4.6: Statistical parameters for modelling of the pavement load

Random variable	CoV – V [%]	Bias factor - μ	Mean value
$t_{long,support} / t_{long,midspan}$	20.0	1.00	-
$t_{transv,center} / t_{transv,edge}$	20.0	1.00	-
$t / t_{nominal}$	4.0	1.00	-
$Vol / Vol_{nominal}$	22.0	1.25	-
ρ_{pav} [kN/m^3]	4.0	-	24.0

The aleatoric variability, $t / t_{nominal}$ is not related to pre-existing deformations but to imperfections of the concrete substrate and paving placing precision. The variability of the total volume of the pavement is defined by a distribution with mean 1.25 and CoV of 22%, in line with previous researches and the findings of this work. It is important to note that cases where the nominal thickness is increased as a maintenance strategy are not considered as variability.

To obtain the variability of the action effect at a given position for both structural and non-structural load, a Monte-Carlo simulation is performed using the statistical distributions in Tables 4.6 and 4.5. For each draw, the load pattern (load of each discretized element) is defined accounting also for the correlation and the action effect at a given position is calculated using a finite element (FE) model with 2D elements as shown in Figure 4.10a.

Due to the large number of simulations, the influence surfaces / lines are calculated for each investigated cross-section and internal force (i.e. shear and bending moment). Subsequently, the action effect (E), is calculated by performing fast matrix operations. As an example, Figure 4.10b shows the influence surface of the bending moment at midspan for one beam of the half-section.

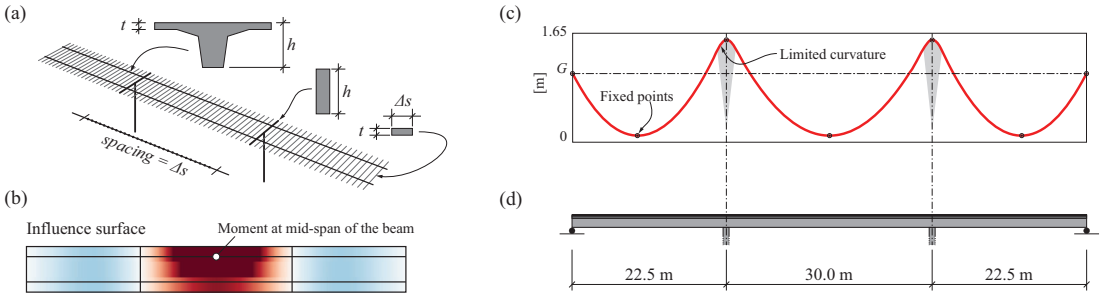

Figure 4.10: (a) FE model for calculation of influence lines/surfaces; (b) influence surface of the moment at midspan of the beam; (c) automatically determined profile of the prestressing tendon given the constraints on the curvature and the mandatory passing points; (d) longitudinal profile of the investigated bridge.

For both investigated bridges (maximum spans of 20 and 30 m, respectively), 2×2×2 = 8 different scenarios are investigated, as presented in Table 4.7. Specifically, they include two different traffic configurations (unidirectional and bidirectional), two vehicle typologies (up to 42 t or 96 t, i.e., without and with mobile cranes) and two distribution types for fitting the tail of the WIM weekly maxima traffic loads (LN and GEV Type-I). For each scenario, reliability analyses are performed at the support and midspan section, denoted respectively with S1 and S2 in Figure 4.11a. The following failure modes are considered: (1) shear failure for sections S1, (2) flexural failure with failure occurring on the steel side for both sections S1 and S2 (3) flexural failure with failure occurring on the concrete side for section S1. For the bridge with maximum span of 20 m and 30 m the ratio between the neutral axis depth and the effective depth in section S1, is respectively $x/d = 0.36$ ($x = 469$ mm) and $x/d = 0.40$ ($x = 625$ mm), justifying such a failure mode. As a comparison with the parametric reliability analysis, the ratio E_G / E_Q for the sections of the investigated bridges ranges between 0.55 and 1.25, thus, covered by the limit cases of 0.5 and 4.0 considered for the FORM calibration of γ_{G1} and γ_{G2} shown in the previous subsection.

Table 4.7: Scenarios considered for calculation of the reliability index β_{50y}

Scenario	Traffic configuration	Vehicles class	Weekly maxima tail-fitting
1	Unidirectional	Including mobile cranes	GEV
2	Unidirectional	Including mobile cranes	LN
3	Unidirectional	Without mobile cranes	GEV
4	Unidirectional	Without mobile cranes	LN
5	Bidirectional	Including mobile cranes	GEV
6	Bidirectional	Including mobile cranes	LN
7	Bidirectional	Without mobile cranes	GEV
8	Bidirectional	Without mobile cranes	LN

The traffic load variability is considered using the WIM measurements introduced in Section 4.3.2 while the variability of the structural and non-structural self-weight is modelled using the methodology presented above. The variability of the resistance calculation is calculated as in Section 4.3.3 while the variability of the model for calculation of action effects is assumed according to the results presented in Chapter 2 of this thesis, as for the parametric analysis.

To reduce the time needed to perform the crude Monte-Carlo (MC) reliability analyses, the Importance Sampling technique (MC-IS) is adopted. Accordingly, a FORM analysis is first performed to determine the design point and subsequently, the Monte-Carlo simulations are then performed around that point. This technique requires a smaller number of simulations to determine the reliability index β (see [Mel18] for details about Monte-Carlo analysis and the Importance Sampling technique).

The limit state function is formulated in the classical form as for the parametric reliability analyses in Eq. (4.2). For each analysis, the limit state function is evaluated ~100'000 times to calculate the reliability index β. Overall, for all the investigated scenarios, sections and failure modes, ~5'000'000 simulations were performed.

Figures 4.11b and 4.11c show the β_{50y} obtained from the MC-IS reliability analyses. The points corresponding to the same scenario refer to the different sections, failure modes, partial factors for permanent loads and different spans investigated. It can be observed that the β_{50y} obtained with the proposed partial factors γ_{G1} and γ_{G2} is similar to the one obtained with the current partial safety factors. Thus, the overall structural safety remains unchanged. However, the partial safety factors reflect better the uncertainties they are supposed to cover. This observation is further supported by the fact that β_{50y} is generally less dispersed with the newly proposed values. Figure 4.11b shows that for new bridges, regardless of the scenario, β_{50y} is generally larger than 4.5, indicating that a safety margin is present if compared to the target value $\beta_{tgt,50y} = 3.8$. On the other hand, β_{50y} calculated using reduced traffic loads for existing bridges shown in Figure 4.11c, is much closer to $\beta_{tgt,50y}$ (however, it must be noted that for existing structures, the value of $\beta_{tgt,50y}$ may be reduced).

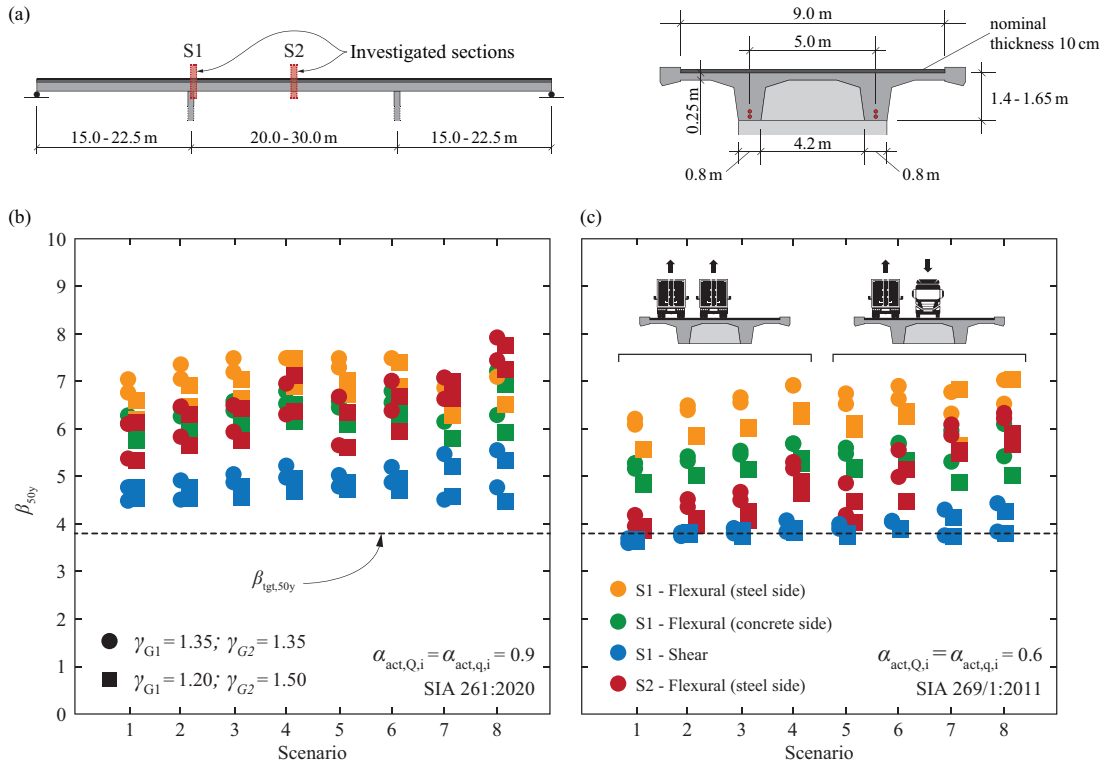

Figure 4.11: (a) Longitudinal scheme and cross-section of the investigated bridges, resulting β_{50y} calculated with the current (circles) and the proposed partial safety factors (squares): (b) considering adjustment factors $\alpha_{act,q,i}$ and $\alpha_{act,Q,i}$ according to [SIA20] for new structures and (c) according to [SIA11] for existing structures.

4.7 Modelling of the structure, evolutions of structural system and designer's choices

It has to be noted that the proposed values for the partial safety factors γ_{G1} and γ_{G2} are based on the model uncertainties for the action effects presented in Chapter 2. As already mentioned, the model uncertainty related to the action effects significantly depends on the complexity and the level of statical indeterminacy of the structure. In fact, in statically determinate structures, where the internal forces depend almost only on the actions and on equilibrium, the model uncertainty related to the internal forces is very small and only depends on the geometrical uncertainties which has an almost negligible effect. In these cases, the assumed values for the model uncertainties of the action effects calculation can be considered as overly conservative. At the other side, for highly indeterminate complex structures, the model uncertainties can be significant, particularly in the case of system changes during construction. With this respect, the

exact construction sequence is not necessarily known during the design, the creep deformations which affect the redistributions of internal forces are also affected by significant uncertainties, and above all, these effects are usually not accounted for in a detailed manner. In this context, the deformation capacity of the critical cross sections associated to the governing failure modes plays also a significant role. In case of ductile behaviour, all these types of uncertainties have little influence on the load-bearing capacity since plastic redistributions of the internal forces can adjust a difference between calculated and actual internal forces (see Chapter 2 of this thesis) On the other side, for brittle behaviour, the possibility of a redistribution of internal forces is limited, so that the model uncertainties in the actions affect calculation can play a major role. In addition, for complex structures, additional uncertainties can be expected with respect to the models implemented in commercial analysis software tools and the choices by the designer in modelling the structures. This applies for linear elastic calculations, but also to an even larger extent for nonlinear analyses. These considerations, which were not the aim of the present work, deserve to be investigated in the future also accounting for the increasing complexity of the analysis tools used nowadays which can give to the designer the impression of a precision which cannot be reached for the reasons explained above.

To solve these problems, an increase of the complexity in the analysis, the consideration of a larger number of load combinations and scenarios, as well as a detailed analysis of the effects related to system changes during construction are not necessarily to be recommended. Also, designer's choices regarding structural modelling a complex structure in an apparently more detailed manner can lead to further uncertainties in calculating action effects. In fact, the increasing complexity of commercially available software makes it more difficult to verify the assumptions. For instance, the modelling of the load, the selection of the finite element, the interaction between different finite elements, the definition of the reference axis, the modelling of prestressing, the modelling of the system changes etc. are more or less conscious choices whose influences should be evaluated by the designers. In addition, an analysis with increasing complexity can even be counterproductive since it would increase the probability of human errors. According to the authors, it is more reasonable to invest time in thinking which is the most suitable and reasonably safe modelling, trying to evaluate qualitatively the potential uncertainties and interpret correctly the results.

These considerations are not the aim of this Chapter and further effort should be put in investigating this topic.

4.8 Conclusions

This Chapter investigates the sources of structural and non-structural self-weight variability in road bridges along with other variabilities influencing structural safety in reinforced concrete structures. Based on the presented work, the main findings are:

1. Structural self-weight variability in bridges is mainly caused by geometrical, reinforcement content and concrete specific weight variability. Geometrical variabilities are less significant for large members. The CoV for structural self-weight of common members is generally between 3 and 6%;
2. Variability of the pavement thickness in a road bridge can be significant. For each span of the investigated bridges, the ratio between the measurements mean and the nominal thickness is generally located between 1.1 and 1.7 (larger for smaller spans). Considering all the measurements within each span, the CoV of the pavement thickness ranges between 8.4 and 21.6%. In some cases, the ratio between the measurements mean and the nominal thickness is larger than 2 suggesting an increase of the nominal value during resurfacing.
3. Distribution parameters of materials strength based on Swiss measurement are generally in line with values specified in Section 1. However, the CoV and bias factor of concrete strength for the analysed data are larger than data found in international literature. This over-strength is probably to be attributed to an increase in cement content to meet durability and workability criteria by producers;
4. The variability of the traffic load for the weekly-maxima events is found between 10 and 18%. Extrapolation of 50-year maxima distributions depends significantly on the tail fitting accuracy of the starting distribution. Considering log-normal and Gumbel distributions for the tail fitting leads to CoV of the traffic load variability between 6 and 10%;
5. According to the parametric reliability analyses, the required value of γ_{G1} for self-weight to reach the target value of the reliability index $\beta_{tgt,50y} = 3.8$ lies between 1.1 and 1.2 while γ_{G2} for other permanent actions is between 1.3 and 1.8 in case the nominal pavement thickness is considered as reference value. Reliability analyses performed on selected case studies including various failure modes confirm that $\gamma_{G1} = 1.2$ and $\gamma_{G2} = 1.5$ lead in general to sufficiently safe results for the design of new and the assessment of existing structures. With respect to the reference value of the pavement thickness, an increase of 20% of the nominal value as recommended in Eurocode 1 is justified;
6. Structural system changes during construction and significant differences between modelling of complex structures and actual behaviour are not accounted for in the partial safety factors on the load side described above. If relevant for the structural system, depending on its complexity and particularly in case of governing brittle failure modes, if the behaviour cannot be improved with sound detailing during the design process, the structure should be modelled in a reasonably conservative manner and the results interpreted accordingly.

Notation

***Acronyms*:**

RC:	Reinforced Concrete
WIM:	Weight In Motion
FORM:	First Order Reliability Method
MCIS:	Monte-Carlo Importance-Sampling
IID:	Independent-Identically-Distributed
CDF:	Cumulative Distribution Function
PDF:	Probability Density Function
GEV:	Gumbel Extreme Values
LN:	Log-Normal
CoV:	Coefficient of Variation
GPR:	Ground Penetrating Radar Measurements
PSF:	Partial Safety Factor
PSFF:	Partial Safety Factor Format

***Variables*:**

β:	Reliability index
f_c:	Concrete strength
f_y:	Steel yield strength
f_{pk}:	Characteristic value of the tensile strength of prestressing steel
ρ_s:	Sectional reinforcement ratio
A_c:	Concrete area
h_{eq}:	Equivalent depth of concrete deck
w:	Width of concrete element
G:	Permanent load
G_1:	Structural self-weight
G_2:	Non-structural self-weight
Q:	Live load

θ_E: Model uncertainty in action effect calculation

Vol: Volume

α: Sensitivity factor

α_{act}: Actualisation factors for the traffic load model

V: Coefficient of Variation of the resistance

μ: Bias factor

Chapter 5

Conclusions and Outlook

5.1 Conclusions

This thesis addresses the current research gaps within the main method used by designers to ensure structural safety, namely, the partial safety factor format (PSFF). While this method simplifies considerably the process for determining if an acceptable level of structural safety is achieved, the underlying methods and simplifications are still not clear. In this context, three main topics are investigated: (1) the model uncertainty in action effects and load bearing capacity calculation, (2) the influence of high-intensity sustained loading on the compressive strength and deformation capacity of reinforced concrete members in compression and (3) the suitability of the currently recommended sensitivity factors on the load and resistance side followed by the recalibration of the partial factors for permanent loads. In the following sections the conclusions of the previous chapters are summarised.

Chapter 2 investigates the model uncertainty in action effects and load-bearing capacity calculations in statically indeterminate concrete structures. In addition to the type of mechanical model, various failure modes are considered. Based on the outcome of the investigation the main conclusions can be resumed as follows:

- compared to more refined models, the Linear Elastic Uncracked model, typically used by the majority of designers, leads to larger CoV of model uncertainty in load bearing capacity calculation, however, the mean of the distribution is larger (safer results), leading to similar tail's distribution approximations, thus, similar safety margin,
- for Linear Elastic Uncracked models, an over design of one or more components of a statically indeterminate system influences the CoV of the model uncertainty in action effects calculation, if one member is largely over-designed, the CoV is generally larger;
- refined calculation models lead to more accurate results and generally to lower CoV of the internal forces ratio and the load bearing capacity ratio,
- the failure mode influences the model uncertainty in load bearing capacity calculation but it does not influence the model uncertainty in action effects calculation. Larger CoVs are observed for brittle systems, independently of the calculation model,
- plastic calculation models with unlimited deformation capacity, if performed without ductility requirements lead to very large CoV and unsafe results. Limiting the deformation capacity, or verifying that ductility requirements are met reduces considerably the CoV,
- considering supports deformability allows larger redistribution of forces and leads to slightly smaller CoV.
- parametric analyses and investigated case studies show that the partial factor γ_{Sd} which covers the uncertainties of the internal force calculation ranges between 1.05 and 1.15. It must be noted that the estimated γ_{Sd} factor does not account for uncertainties related to structural system variations during construction or structural modelling of complex

structures. These additional uncertainties, which deserve to be investigated more in detail, significantly depend on the complexity of the structure, the construction method, the tools used tools and the experience of the designer.

Chapter 3 presents the results of an investigation on the strength and deformation capacity of reinforced concrete members failing in centric compression under variable loading rates. In this work the redistributions of internal forces due to nonlinear deformations are investigated by means of experimental results and a mechanical model. The main conclusions can be resumed as follows:

- the long-term response of concrete (long loading duration) is detrimental with respect to its strength, but enhances its deformation capacity. This allows redistributing stresses and can allow, provided that sufficient reinforcement is available, increasing the load carrying capacity of a structural compressed member,
- columns with ordinary reinforcement centrically loaded under rapid loading conditions typically fail by concrete crushing prior to reinforcement yielding. However, when loading is applied slowly, higher levels of deformation allow increasing the reinforcement stresses up to yielding (typically occurring after one or two hours of loading),
- for very low loading rates, the reinforcement can yield, but the reduction of the concrete strength under sustained loading reduces the resistance (maximum strength typically obtained after one or two hours of loading),
- high reinforcement ratios and yield strengths are largely beneficial since the increase of deformation capacity allows yielding of the reinforcement, partly compensating for the loss of strength due to sustained loading,
- unlike concrete types with fast cement hardening, where the gain of strength occurs mostly in the first months, concretes with slower cement hardening have a better response under sustained loading (independently of the reinforcement ratio) compensating the loss of concrete strength under sustained loading even after years,
- consistent modelling and design for these phenomena are performed on the basis of a rheological model for concrete accounting for its linear and nonlinear creep strains. Such approach allows considering suitably the implications on the strength and deformation capacity as well as internal force redistributions.

Chapter 4 investigates the sources of structural and non-structural self-weight variability in road bridges along with other variabilities influencing structural safety in reinforced concrete structures. Based on the presented work, the main findings can be resumed as follows:

- structural self-weight variability in bridges is mainly caused by geometrical, reinforcement content and concrete specific weight variability. Geometrical variabilities are less significant for large members. The CoV for structural self-weight of common members is generally between 3 and 6%,

- variability of the pavement thickness in a road bridge can be significant. For each span of the investigated bridges, the ratio between the measurements mean and the nominal thickness is generally located between 1.1 and 1.7 (larger for smaller spans). Considering all the measurements within each span, the CoV of the pavement thickness ranges between 8.4 and 21.6%. In some cases, the ratio between the measurements mean and the nominal thickness is larger than 2 suggesting an increase of the nominal value during resurfacing,
- distribution parameters of materials strength based on Swiss measurement are generally in line with values specified in Section 1. However, the CoV and bias factor of concrete strength for the analysed data are larger than data found in international literature. This over strength is probably to be attributed to an increase in cement content to meet durability and workability criteria by producers,
- the variability of the traffic load for the weekly maxima events is found between 10 and 18%. Extrapolation of 50-year maxima distributions depends significantly on the tail fitting accuracy of the starting distribution. Considering log-normal and Gumbel distributions for the tail fitting leads to CoV of the traffic load variability between 6 and 10%,
- according to the parametric reliability analyses, the required value of γ_{G1} for self-weight to reach the target value of the reliability index $\beta_{tgt,50y} = 3.8$ lies between 1.1 and 1.2 while γ_{G2} for other permanent actions is between 1.3 and 1.8 in case the nominal pavement thickness is considered as reference value. Reliability analyses performed on selected case studies including various failure modes confirm that $\gamma_{G1} = 1.2$ and $\gamma_{G2} = 1.5$ lead in general to sufficiently safe results for the design of new and the assessment of existing structures. With respect to the reference value of the pavement thickness, an increase of 20% of the nominal value as recommended in Eurocode 1 is justified,
- structural system changes during construction and significant differences between modelling of complex structures and actual behaviour are not accounted for in the partial safety factors on the load side described above. If relevant for the structural system, depending on its complexity and particularly in case of governing brittle failure modes, if the behaviour cannot be improved with sound detailing during the design process, the structure should be modelled in a reasonably conservative manner and the results interpreted accordingly.

5.2 Outlook and future works

Although the notions discussed in this thesis were already introduced early in the 20th century [May26]. Most of the scientific advances to date have been made starting at the end of the century. Nowadays, with the available tools and technological advancement, many of the still open questions can have an answer. However, other question arises due to the introduction of new tools and techniques to determine structural safety. A non-exhaustive list of significant topics for future researches in this domain is presented below.

- The work of the designer is closely tied to that on the construction site, which usually takes place remotely both temporally and spatially. Currently, the variability of the geometry related to the manufacture of reinforced concrete elements does not consider technological advancements generally integrated in modern construction sites. In fact, the statistical parameters of geometric variability are typically assumed based on the recommendations of [JCS01] which are in turn, are based on the publication 115 of the CIB report [CIB89]. Therefore, these data refer to measurements made almost 50 years ago, in different parts of the world with, usually, different construction practices. Also, it is currently unclear which relationship exists between these commonly assumed statistics and tolerances of the codes of practice, see [ISO13, SIA13]
- In the structural design process, one of the initial challenges the engineer faces is the modelling of the actual structure, which does not exist yet. Thus, to represent the actual behaviour as closely as possible, choices and hypotheses are constantly made. These choices depend on several factors, for instance, the complexity of the structure, the phase of the project, the experience of the engineer and the tools used. In a finite element calculation some of these choices can be related to the reference line chosen to model each element, the modelling of inclined elements, the modelling of variable cross sections, etc. Other choices specific to the finite element models are the dimensions of the finite elements, the link between different elements, and the simplification of some cross sections. To this should be added the modelling of the boundary conditions which can widely depend on the designer. The result of the choices mentioned above will be different structures that will inevitably have different levels of security, however, it is important to note that all these choices are rightful to the designer and human error is not included.
- For complex structures, if the exact construction sequence is not known during the design, uncertainties related to the calculation of the action effects or the load bearing capacity can be very large. To avoid extremely safe-sided partial safety factors, those cases are typically not covered by the standard partial safety factors, i.e. γ_{Sd} in [CEN02]. In addition, the creep deformations which can affect the redistributions of internal forces are also affected by significant uncertainties (cross-section, temperature, relative

humidity, material properties etc.). In a standard design scenario, these uncertainties are usually not accounted for in a detailed manner and might lead to unsafe scenarios if the structural system includes members with brittle behaviour.

- Nowadays concrete is the most widely used material for construction. Many factors contribute to this dominance: availability of raw materials, durability, structural performance etc. Nonetheless, in terms of environmental impact, this material is a major source of greenhouse gas emissions. This has motivated many researchers to focus on the development of concretes with a lower environmental impact achieving extremely promising results. However, to build up confidence in designers regarding these materials, thorough studies must be performed to assess whether the current framework for safety assessment is suitable.
- Most of the existing infrastructure in Europe and North America was built in the second half of the 20th century, meaning that in the next decades engineers will face a major challenge in assessing the safety of these structures. In order to improve the decision-making process, it is necessary for the currently used partial safety factor format, which greatly simplifies the work of the designers, to be consistent and allow adjusting the factors according to the specific knowledge concerning a structure. In this context, a framework for performing probabilistic analyses with consistent and well-defined boundaries can be developed to determine the level of safety compared to the current requirements. This becomes even more important in a context where an increasing number of civil engineering works are considered part of the artistic and cultural heritage.

Bibliography

[Adh15] **Adhikary S. D., Li B., Fujikake K.**, *Residual resistance of impact-damaged reinforced concrete beams*, Magazine of Concrete Research, 67 (7), 364-378, 2015.

[Ang99] **Angelakos D.**, *The Influence of Concrete Strength and Longitudinal Reinforcement Ratio on the Shear Strength of Large-Size Reinforced Concrete Beams With and Without Transverse Reinforcement*, MSc thesis, Department of Civil Engineering, University of Toronto, 181 pp., 1999.

[Bas98] **Bassetti A., Bailey S. F., Banz A.**, *Lastfaktoren für Eigenlast und Auflast zur Beurteilung der Tragsicherheit bestehender Strassenbrücken*, Rapport OFROU, 530, 63 p., Zürich, Switzerland, German, 1998.

[Bee16] **Beeby A., Jackson P.**, *Partial safety factor for reinforcement*, Structures, 5, pp. 101-111, 2016.

[Big93] **Bigaj A., Walraven J. C.**, *Size effect on rotational capacity of plastic hinges in reinforced concrete beams*, CEB Bulletin d'Information, 218, 7-23, 1993.

[Bos93] **Bosco C., Debernadi G.**, *Influence of some basic parameters on the plastic rotation of reinforced concrete elements*, CEB Bulletin d'Information, 218, 25-44, 1993.

[Can20] **Cantone R., Fernández Ruiz M., Muttoni A.**, *A detailed view on the rebar-to-concrete interaction based on refined measurement techniques*, Engineering Structures, Vol. 226, 19 p., 2020.

[Can22] **Cantone R., Setiawan A., Fernández Ruiz M., Muttoni A.**, *Characterization of shear deformations in reinforced concrete members without shear reinforcement*, Engineering Structures, Vol. 257, 113910, 16 p., 2022.

[Cav15] **Cavagnis F., Fernández Ruiz M., Muttoni A.**, *Shear failures in reinforced concrete members without transverse reinforcement: An analysis of the critical shear crack development on the basis of test results*, Engineering structures, Vol. 103, pp. 157-173, UK, 2015.

[CEB74] **CEB**, *Manuel "sécurite des structures" concepts généraux, charges et actions*, Paris, 1974.

[CEB64] **CEB**, *Practical unified recommendations for the design and execution of structures in reinforced concrete (in French: Recomemndations pratiques unifiées pour le calcul et l'éxécution des ouvrages en béton armé*, 257, Paris, 1964.

[CEB59] **CEB**, *Bulletin 19: Technical conclusions of the 5th CEB meeting in Vienna*, Comité Européen du Béton Bulletin: Section on Structural Safety, 94, Paris, France, 1959.

[CEN22] **CEN**, *FprEN 1990:2022: Eurocode - Basis of structural and geotechnical design*, CEN European committee for standardization, Draft E, 171, Brussels, 2022.

[CEN02] **CEN**, *EN 1990:2002: Eurocode: Basis of Structural Design*, European Committee for Standardization (CEN), Brussels, Anglais, 2002.

[CIB89] **CIB Report**, *Publication 115, Actions On Structures - Self-weight Loads*, CIB Commission W81, 1989.

[Col78] **Collins M. P.**, *Towards a Rational Theory for RC Members in Shear*, ASCE, Journal of the Structural Division, Vol.104, No 4, pp. 219-231, Reston, USA, 1978.

[Cor69] **Cornell C. A.**, *A Probability-Based Structural Code*, ACI Journal, 12, 66, 974-985, 1969.

[Cor10] **Correlated Solutions**, *Vic-3D 7 Reference Manual*, 108 p., 2010.

[Dal15] **Dalla Valle P., Thom N.**, *Variability In Pavement Design*, The International Journal of Pavement Engineering and Asphalt Technology, 16, 50-67, 2015.

[Dav31] **Davis R. E., Davis H.E.**, *Flow of Concrete Under the Action of Sustained Loads*, ACI Journal, vol. 24, pp. 303-326, 1931.

[Der91] **Der Kiureghian Armen, De Stefano M.**, *Efficient algorithm for second-order reliability analysis*, Journal of Engineering Mechanics, 117.12, pp.2904-2923, 1991.

[Dia71] **Diaz S. I.**, *Fracture Mechanisms of Concrete Under Static, Sustained, and Repeated Compressive Loads*, University of Illinois at Urbana-Champaign, 1971.

[Dit94] **Ditlevsen O.**, *Distribution arbitrariness in structural reliability*, Structural Safety and Reliability, Schuëller, Shinozuka and Yao (eds), 1241-1247, Rotterdam, 1994.

[Dry71] **Drysdale R. G., Huggins M. W.**, *Sustained biaxial load on slender concrete columns*, Journal of the Structural Division, 97.5, pp. 1423–1443, 1971.

[Du17] **Du M., Du X., Li D.**, *Size effect tests of stocky reinforced concrete columns confined by stirrups*, Structural Concrete, 18, 454-465, 2017.

[El-04] **El-Kashif K. F., Maekawa K.**, *Time-dependent nonlinearity of compression softening in concrete*, Journal of Advanced Concrete Technology, 2.2, pp. 233-247, Japan, 2004.

[Ell80] **Ellingwood B.**, *Development of a probability based load criterion for American national standard A58: building code requirements for minimum design loads in buildings and other structures*, NBS SPECIAL PUBLICATION 577, 222, Washington, 1980.

[EN105] **EN10080:2005**, *Steel for the reinforcement of concrete. Weldable reinforcing steel - General*, European Committee for Standardization (CEN), Brussels, Belgium, 2005.

[EN104] **EN1992-1-1:2004**, *Eurocode 2*, European Committee for Standardization (CEN), Brussels, Belgium, 2004.

[Eur22] **Eurocode 0**, *Basis of structural and geotechnical design*, Draft prEN 1990, European Committee for Standardization (CEN), Brussels, Belgium, 2022.

[Eur23] **Eurocode 1**, *Actions on structures - Part 1-1: General actions - Specific weight of materials, self-weight of construction works and imposed loads for buildings*, Draft prEN 1991-1-1, European Committee for Standardization (CEN), Brussels, Belgium, 2023.

[Eur03] **Eurocode 1**, *Actions on structures – Part 2: Traffic loads on bridges*, EN 1991-2, 2003.

[Eur02] **Eurocode 1**, *Actions on structures - Part 1-1: General actions*, CEN, 47, Brussels, 2002.

[Eur23] **Eurocode 2**, *Design of concrete structures - Part 1-1: General rules and rules for buildings, bridges and civil engineering structures*, Final draft FprEN 1992-1-1, European Committee for Standardization (CEN), 405 p., Brussels, Belgium, 2023.

[Fab28] **Faber O.**, *Plastic Yield, Shrinkage, and Other Problems of Concrete, and Their Effect on Design*, Institution of Civil Engineers, vol. 225, pp. 27-73, 1928.

[Fer07] **Fernández Ruiz M., Muttoni A., Gambarova P.**, *Relationship between nonlinear creep and cracking of concrete under uniaxial compression*, Journal of Advanced Concrete Technology, Vol. 5, No 3, pp. 383-393, Japan, 2007.

[FIB13] **FIB**, *fib Model Code for Concrete Structures 2010*, fib, First Edition, UK, 2013.

[Flu58] **Fluck P. G., Washa G. W.**, *Creep of Plain and Reinforced Concrete*, ACI Journal Proceedings, vol. 54, pp. 879-895, 1958.

[Fos16] **Foster S. J., Stewart M. G., Loo M., Ahammed M., Sirivivatnonon V.**, *Calibration of Australian Standard AS3600 Concrete Structures: part I statistical analysis of material properties and model error*, Australian journal of structural engineering, Taylor & Francis, 17, 242-253, 2016.

[Fuj14] **Fujikake K., Adhikary S. D., Li B.**, *Effects of high loading rate on reinforced concrete beams*, ACI Structural Journal, 111.3, 651-660, 2014.

[Fuj09] **Fujikake K., Li B., Soeun S.**, *Impact response of reinforced concrete beam and its analytical evaluation*, Journal of Structural Engineering, 135.8, 938-950, 2009.

[Gil91] **Gilbert R. I., Mickleborough N. C.**, *Creep Effects in Slender Reinforced and Prestressed Concrete Columns*, ACI Symposium Publication, vol. 129, pp. 77-100, 1991.

[Gui11] **Guidotti R., Fernández Ruiz M., Muttoni A.**, *Crushing and Flexural Strength of Slab-Column Joints*, Engineering structures, Vol. 33 n° 3, pp. 855-867, 2011.

[Has74] **Hasofer A. M., Lind N. C.**, *Exact and invariant second-moment code format*, Journal of the Engineering Mechanics Division, 111-121, 1974.

[Hog51] **Hognestad E.**, *Study of combined bending and axial load in reinforced concrete members*, University of Illinois. Engineering Experiment Station. Bulletin; , no. 399, 1951.

[Hua89] **Huang Y. H., Sharpe G. W.**, *Thickness Design of Concrete Pavements by Probabilistic Method*, Proceedings, Fourth International Conference on Concrete Pavement Design and Rehabilitation, 1989.

[Hug10] **Hugenschmidt J., Kalogeropoulos A., Soldovieri F., Prisco G.**, *Processing strategies for high-resolution GPR concrete inspections*, NDT & E International, 43, pp. 334-342, 2010.

[Hug06] **Hugenschmidt J., Mastrangelo R.**, *GPR inspection of concrete bridges*, Concrete and Cement Research, 28, 384-392, 2006.

[Hug82] **Hughes G., Speirs D. M.**, *An investigation of the beam impact problem*, Cement and Concrete Association, 42.546, 117, 1982.

[ISO13] **ISO**, *EN 13670 Execution of concrete structures*, International Organization for Standardization, 72 p., 2013.

[Jan97] **Jansen D. C., Shah S. P.**, *Effect of length on compressive strain softening of concrete*, J. Engng Mech., ASCE, 123, 25 p., 1997.

[JCS01] **JCSS**, *Probalistic Model Code*, Part III, 2001.

[Jin17] **Jin L., Du M., Li D., Du X., Xu H.**, *Effects of cross section size and transverse rebar on the behavior of short squared RC columns under axial compression*, Engineering Structures, 142, 223-239, 2017.

[Kal13] **Kalogeropoulos A., Van Der Kruk J., Hugenschmidt J., Bikowski J., Brühwiler E.**, *Full-waveform GPR inversion to assess chloride gradients in concrete*, NDT & e International, pp. 74-84, 2013.

[Ken15] **Kenel A., Stussi U., Ebschner P.**, *Central documentation of mechanical properties of existing reinforcements*, Rapport OFROU, 669, p. 183, Suisse, German, 2015.

[Kre79] **Kreis A., Rosli A.**, *Statistische Auswertung Von Spannstahlversuchen Der EMPA Aus Jahren 1968 - 1979*, EMPA 10820, 25703/4, p. 40, German, 1979.

[Lau10] **Lau D., Pam H. J.**, *Experimental study of hybrid FRP reinforced concrete beams*, Engineering Structures, 32.12, 3857-3865, 2010.

[Lee11] **Lee J.-Y., Kim S. W., Mansour M. Y.**, *Nonlinear analysis of shear-critical reinforced concrete beams using fixed angle theory*, Journal of Structural Engineering, 137.10, 1017-1029, 2011.

[Li16] **Li D., Jin L., Fu J., Lu A.**, *Size effect tests of normal-strength and high-strength RC columns subjected to axial compressive loading*, Engineering Structures, 109, 43-60, 2016.

[Lun13] **Luna Technologies Inc.**, *Optical Backscatter Reflectometer 4600 User Guide*, 227 p., Blacksburg, VA, 2013.

[Lyt93] **Lytton R. L., Zollinger D. G.**, *Modeling Reliability in Pavements*, 72nd Annual Meeting of the Transportation Research Board, p. 88, Washington D.C., 1993.

[Mad06] **Madsen H. O., Krenk S., Lind N. C.**, *Methods of Structural Safety*, Dover Publications, New York, 2006.

[Mae04] **Maekawa K., El-Kashif K. F.**, *Cyclic Cumulative Damaging of Reinforced Concrete in Post-Peak Regions*, Journal of Advanced Concrete Technology, 2.2, pp. 257-271, 2004.

[Mau63] **Mauch S., Holley M. J.**, *Creep buckling of reinforced concrete columns*, Journal of the Structural Division, 89.4, pp. 451–482, 1963.

[May26] **Mayer M.**, *The safety of structures and their calculation according to limit forces instead of allowable stresses (Die Sicherheit der Bauwerke und ihre Berechnung nach Grenzkräften anstatt nach zulässigen Spannungen)*, Julius Springer, Berlin, German, 1926.

[Mel18] **Melchers R. E., Beck A. T.**, *Structural reliability analysis and prediction*, John Wiley & Sons, 2018.

[Men82] **Menn C.**, *Comparison of costs and material quantities for some new highway bridges in Switzerland*, Prestressed Concrete of Switzerland, pp. 41-48, Wildegg, Switzerland, German/English, 1982.

[Mic92] **Mickleborough N. C.**, *Creep Buckling of Uniaxially Loaded Reinforced Concrete Columns*, American Concrete Institute, SP 129, pp. 39-55, 1992.

[Mir80] **Mirza S. A., Kikuchi D. K., MacGregor J. G.**, *Flexural Strength Reduction Factor for Bonded Prestressed Concrete Beams*, Journal Proceedings, 77, pp. 237-246, 1980.

[Mir79] **Mirza S. A., MacGregor J. G.**, *Variability of mechanical properties of reinforcing bars*, Journal of the Structural Division, American Society of Civil Engineers, 105, pp. 921--937, 1979.

[Mut23] **Muttoni A.**, *Background document to clause 4.3.3 and Annex A Partial safety factors for materials, Background Document for FprEN 1992-1-1*, CEN/TC 250/SC 2 N2087, 2023.

[Mut89] **Muttoni A.**, *Die Anwendbarkeit der Plastizitätstheorie in der Bemessung von Stahlbeton*, Dissertation ETHZ, 159 p., Zürich, Switzerland, German, 1989.

[Mut08] **Muttoni A., Fernández Ruiz M.**, *Shear strength of members without transverse reinforcement as function of critical shear crack width*, ACI Structural Journal, V. 105, No 2, pp. 163-172, Farmington Hills, USA, 2008.

[Nev55] **Neville A.**, *Theories of Creep in Concrete*, ACI Journal Proceedings, vol. 52, pp. 47-60, 1955.

[Nga80] **Ngab A. S.**, *Behavior of high-strength concrete under sustained compressive stress*, Dept. of Structural Engineering, School of Civil and Environmental Engineering, Cornell University, no. 80-2, 201 pages, 1980.

[Now03] **Nowak A. S., Szerszen M. M.**, *Calibration of design code for buildings (ACI 318): Part 1 - Statistical models for resistance*, ACI structural journal, 3, 100, 377-382, 2003.

[Pej22] **Pejatovic M., Fernández Ruiz M., Muttoni A.**, *Design of slender and squat reinforced concrete members with shear reinforcement*, Structural Concrete, 17 p., 2022.

[Ric06] **Rice J. A.**, *Mathematical statistics and data analysis*, Cengage Learning, 2006.

[Ric38] **Richart F. E., Heitman R. H.**, *Tests of Reinforced Concrete Columns Under Sustained Loading*, Journal of American Concrete Institute, Proceedings of the American Concrete Institute, 35, pp. 33-38, USA, 1938.

[Ric32] **Richart F. E., Staehle G. C.**, *Fourth Progress Report on the Column Tests made at the University of Illinois*, Journal of American Concrete Institute, 28, pp. 279-315, USA, 1932.

[Ric31] **Richart F. E., Staehle G. C.**, *Progress Report on Column Tests at the University of Illinois*, Journal of American Concrete Institute, 27, pp. 731-760, USA, 1931.

[Ric31] **Richart F. E., Staehle G. C.**, *Second Progress Report on Column Tests at the University of Illinois*, Journal of American Concrete Institute, 27, pp. 761-790, USA, 1931.

[Ric31] **Richart F. E., Staehle G. C.**, *Third Progress Report on Column Tests made at the University of Illinois*, Journal of American Concrete Institute, 28, pp. 167-175, USA, 1931.

[Rüs60] **Rüsch H.**, *Researches towards a general flexural theory for structural concrete*, Journal of ACI, 57, pp. 1-28, USA, 1960.

[Rüs56] **Rüsch H.**, *Experimental determination of the effect of the duration of loading on the resistance and deflection [versuche zur bestimmung des einflusses der zeit auf festigkeit und verformung]*, IABSE Kongressbericht 5, pp. 237–244, German, 1956.

[Saa09] **Saatci S., Vecchio F. J.**, *Effects of shear mechanisms on impact behavior of reinforced concrete beams*, ACI Structural Journal, 106.09, 2009.

[Sch17] **Schneider J., Vrouwenvelder T.**, *Introduction to Safety and Reliability of Structures*, IABSE Structural Engineering Documents, 5, 164 p., Zürich, Switzerland, 2017.

[Sel59] **Sell R.**, *Investigations into the strength of concrete under sustained load*, RILEM Bulletin, no. 5, pp. 5-13, 1959.

[Sha70] **Shah S. P., Chandra S.**, *Fracture of concrete subjected to cyclic and sustained loading*, ACI Journal Proceedings, vol. 67, pp. 816-827, 1970.

[Sha87] **Shah S. P., Sankar R.**, *Internal cracking and strain-softening response of concrete under uniaxial compression*, ACI Materials Journal, pp. 200-212, USA, 1987.

[Sha49] **Shank J. R.**, *Plastic flow of concrete at high overload*, ACI Journal Proceedings, vol. 45, pp. 493-498, 1949.

[She80] **Sheikh S. A., Uzumeri S. M.**, *Strength and ductility of tied concrete columns*, ASCE Journal of the Structural Division, Vol. 106, pp. 1079-1102, USA, 1980.

[Shi99] **Shin S.-W., Lee K.-S., Moon J.-I.**, *Shear Strength of Reinforced High-Strength Concrete Beams with Shear Span-to-Depth Ratios between 1.5 and 2.5*, ACI, Structural Journal, 96, pp. 549-556, Farmington Hills, USA, 1999.

[SIA21] **SIA**, *SIA 262.051+A2 - Béton - Spécification, performances, production et conformité*, Société Suisse des Ingénieurs et des Architectes, Norme suisse SN EN 206+A2:2021, pp. 148, 2021.

[SIA11] **SIA**, *SIA 269/1 - Existing structures - Actions*, Société Suisse des Ingénieurs et des Architectes, 2011.

[SIA68] **SIA**, *SIA 162 : Norme pour le calcul, la construction et l'exécution des ouvrages en béton, en béton armé et en béton précontraint*, Société Suisse des Ingénieurs et des Architectes, 84 p., Zürich, Switzerland, 1968.

[SIA20] **SIA 261**, *Actions sur les structures porteuses*, 136, 2020.

[SIA13] **SIA 262**, *Construction en béton*, 102, 2013.

[Sig95] **Sigrist V.**, *Zum Verformungsvermögen von Stahlbetonträgern*, Dissertation, No. 11169, ETHZ, 159 p., Zürich, Switzerland, German, 1995.

[Sja20] **Sjaarda M., Meystre T., Nussbaumer A., Hirt M. A.**, *A systematic approach to estimating traffic load effects on bridges using weigh-in-motion data*, Structural Concrete, 89, pp. 585-598, 2020.

[Sma85] **Smadi M. M., Slate F. O., Nilson A. H.**, *High-, Medium-, and Low-Strength Concretes Subject to Sustained Overloads-Strains, Strengths, and Failure Mechanisms*, ACI Journal Proceedings, vol. 82, pp. 657-664, 1985.

[Stu65] **Sturman G. M., Shah S. P., Winter G.**, *Microcracking and Inelastic Behavior of Concrete*, ACI Symposium Publication, vol. 12, 1965.

[Sur13] **Suryanto B., Maekawa K., Nagai K.**, *Predicting the Creep Strain of PVA-ECC at High Stress Levels based on the Evolution of Plasticity and Damage*, Journal of Advanced Concrete Technology, vol. 11, pp. 215-230, 2013.

[Tas19] **Tasevski D., Fernández Ruiz M., Muttoni A.**, *Assessing the compressive strength of concrete under sustained actions: from refined models to simple design expressions*, Structural Concrete, 20, 971-985, 2019.

[Tas18] **Tasevski D., Fernández Ruiz M., Muttoni A.**, *Compressive Strength and Deformation Capacity of Concrete under Sustained Loading and Low Stress Rates*, Journal of Advanced Concrete Technology, pp. 396-415, Japan, 2018.

[Tor19] **Torrenti J-M., Dehn F.**, *On the relation between the mean compressive strength and the characteristic one*, Structural Concrete, 21, pp. 409-412, 2019.

[Tro58] **Troxell G. E., Raphael J. M., Davis R. E.**, *Long-time creep and shrinkage tests of plain end reinforced concrete*, Proceedings ASTM, vol. 58, pp. 1101-1120, USA, 1958.

[Vec04] **Vecchio F. J., Shim W.**, *Experimental and Analytical Reexamination of Classic Concrete Beam Tests*, ASCE Journal of Structural Engineering, Vol.130, pp. 460-469, USA, Anglais, 2004.

[Vie56] **Viest I. M., Elstner R. C., Hognestad E.**, *Sustained Load Strength of Eccentrically Loaded Short Reinforced Concrete Columns*, ACI Journal Proceedings, vol. 52, pp. 727-755, 1956.

[Wil28] **Wilson M. F. G., Dixon S. M., Williams E. O., Lea F. C., Jackson H., Stroyer R. N.**, *Discussion. Plastic Yield, Shrinkage, and Other Problems of Concrete, and Their Effect on Design*, Institution of Civil Engineers, vol. 225, pp. 74-92, 1928.

[Yos00] **Yoshida Y.**, *Shear reinforcement for large lightly reinforced concrete members*, Master thesis, University of Toronto, 160 p., Toronto, Canada, 2000.

[Yu21] **Yu Q., Valeri P, Fernández Ruiz M., Muttoni A.**, *A consistent safety format and design approach for brittle systems and application to textile reinforced concrete structures*, Engineering Structures, 249, 2021.

[Zha17] **Zhao D. B., Yi W.-J., Kunnath S.K**, *Shear Mechanisms in Reinforced Concrete Beams under Impact Loading*, Journal of Structural Engineering, 143 (9), 2017.

[Zho92] **Zhou F. P.**, *Time-dependent crack growth and fracture in concrete*, PhD Thesis, pp. 148, Lund, Sweden, 1992.

Xhemsi Malja

xhemsi.malja@gmail.com
+41 77 529 99 52
Chemin de Montelly, 18, 1007 Lausanne
28.02.1994

Education

2019 - 2024 **PhD Candidate** – thesis: Influence of model uncertainty and long-term deformations in action effects calculation in reinforced concrete structures. *Structural Concrete Laboratory (IBETON), Swiss Federal Institute of Technology (EPFL), Lausanne, Switzerland.*

2016 - 2018 **MSc in Structural Engineering** – thesis: Shape optimization of a steel slit damper for precast post-tensioned concrete walls. *Department of Engineering Enzo Ferrari (DIEF), University of Modena and Reggio Emilia (UNIMORE), Italy.*

2013 - 2016 **BSc in Civil Engineering** – thesis: Water roof - an Innovative roof with variable thermal inertia. *Department of Engineering Enzo Ferrari (DIEF), University of Modena and Reggio Emilia (UNIMORE), Italy.*

2008 - 2013 **Liceo scientifico Ariosto/Spallanzani**
Reggio Emilia, Italy.

Employment

2019 - 2024 **PhD assistant**

Teaching assistant for the courses: *Structures I and II, Concrete structures, Conceptual design of bridges, Concrete bridges, Advanced design of concrete structures, Structure and architecture, Stress field.*

Supervision of master projects and the semester project *Conceptual design of a civil engineering structure.*

Structural Concrete Laboratory (IBETON), Swiss Federal Institute of Technology (EPFL), Lausanne, Switzerland.

2018 - 2019 **Bridge and Civil Structures Engineer**
Piacentini Ingegneri S.r.l., Bologna, Italy

2018 **Tutor, Research Internship**
Department of Engineering Enzo Ferrari, Modena, Italia.

Publications

2023 Malja X., Motlagh H.R.E., Fernández Ruiz M., Muttoni A., Influence of sustained loading on resistance and deformation capacity of reinforced concrete members in compression, Structural Concrete, Vol. 24.3, pp. 3656-3673, 2023. https://doi.org/10.1002/suco.202200571

2022 Malja X., Muttoni A., Evaluation of the model uncertainty of action effects in statically indeterminate systems, 14th fib International PhD Symposium in Civil Engineering, pp. 895-902, Rome, Italy, 2022.

Awards

2018 First place in photography competition*, Scientific and Technological University Library.*

2017 Award for Outstanding Academic Achievement*, Fondo Sostegno Giovani.*

2016, 2019 Award for Excellence*, University of Modena and Reggio Emilia.*

Associations and certifications

Membership Société pour l'art de l'ingénieur

Membership *fib* Student membership

Membership Chartered engineer, Italy

Certification First aid, generic provider SRC, BLS-AED

Languages

Albanian (native), Italian (native), English (fluent), French (fluent), German (notions)

Programming & software

Programming: Python, Matlab, C++

Structural calculation : Code_aster, Abaqus, Cubus suite

Drawing: Autocad, Rhino, Archicad